9-10-2015

Direct Synthesis of Layered Intercalation Compounds and Single Layer Nanosheets and Their Applications

Jingfang Yu
University of Connecticut - Storrs, jingfang.yu@uconn.edu

Direct Synthesis of Layered Intercalation Compounds and Single Layer Nanosheets and Their Applications

Jingfang Yu, Ph.D.

University of Connecticut, 2015

Layered materials have been extensively studied and have found a wide range of applications predominately in the form of intercalated layered hybrids, or as exfoliated single layer nanosheets. Previous investigations in layered materials mainly focused on the preparation of layered intercalation compounds and obtaining single layer nanosheets. The preparation of layered intercalation compounds and exfoliation to obtain single layer nanosheets typically consists of two steps, where a layered material is first synthesized and subsequently intercalated/exfoliated through different approaches. However, the two step process is time consuming and inefficient. Moreover, the desired intercalation and exfoliation may not proceed as planned. Thus, it is highly desirable to explore new methodologies for facile synthesis of layered intercalation compounds and single layer nanosheets.

This dissertation reports a novel approach to directly synthesize layered intercalation compounds and single layer nanosheets via a one-step process. Two model layered compounds: α-zirconium phosphate (α-ZrP) with negative layer charge and layered double hydroxide (LDH) with positive layer charge were selected for the one-step direct synthesis of layered intercalation compounds and single layer nanosheets, respectively. The introduction of a layer growth coordinator and inhibitor was proposed to guide or inhibit the growth of layered materials in the third dimension for the formation of layered intercalation compounds and single layer

nanosheets, respectively. Our results have proved that the proposed one-step direct synthesis process to obtain layered intercalation compounds and single layer nanosheets is feasible. Detailed reaction mechanisms and the factors that influence the direct synthesis of layered intercalation compounds and single layer nanosheets were studied in detail.

Based on the aforementioned fundamental investigation, another strategy involving both a complexing agent and a layer growth coordinator was further designed to promote the growth of layered compounds in the Z direction to form hexagonal prisms.

Applications of the α-ZrP based intercalation compounds and LDH single layer nanosheets prepared through the developed methods were also studied. The Biginelli reactions catalyzed by the heterogeneous α-ZrP/BMIMCl intercalation compound were explored where the yield was maintained at 93% even after 4 times of recycle. A dip coating method was adopted to align LDH single layer nanosheets on polymer film substrates to enhance their barrier properties, where both the oxygen and water vapor barrier properties were significantly improved.

Direct Synthesis of Layered Intercalation Compounds and Single Layer Nanosheets and Their Applications

Jingfang Yu

B.E., Xiangtan University, 2011

M.S., Texas State University, 2013

A Dissertation

Submitted in Partial Fulfillment of the

Requirements for the Degree of

Doctor of Philosophy

at the

University of Connecticut

2015

APPROVAL PAGE

Doctor of Philosophy Dissertation

Direct Synthesis of Layered Intercalation Compounds and Single Layer Nanosheets and Their Applications

Presented by

Jingfang Yu, B.E., M.S.

Major Advisor _____
Dr. Luyi Sun

Associate Advisor _____
Dr. Mu-Ping Nieh

Associate Advisor _____
Dr. Richard Parnas

Associate Advisor _____
Dr. Steven L. Suib

Associate Advisor _____
Dr. Julia Valla

University of Connecticut
2015

This work is dedicated to my beloved parents for their nonstop love and support.

Acknowledgement

I would like to express my sincere gratitude to my major advisor Dr. Luyi Sun for his guidance and support throughout my graduate study. I appreciate all his contributions of time, patience, enthusiasm and immense knowledge. This work is impossible without his encouragement and support. During the past four years, he has guided me to finish both my master degree and my Ph.D. degree. He provided generous freedom for me to fulfill my thoughts and insightful discussions and suggestions about the research. His advices in my life and future carrier offered me enormous help. I am grateful to him for being such a great mentor in both research and in my life.

I also wish to thank my advisory committee, Dr. Mu-Ping Nieh, Dr. Richard Parnas, Dr. Steve Suib and Dr. Julia Valla for their valuable time, support, suggestions and insightful comments.

I'm grateful to Ms. Leah Winterberger in the Department of Chemical and Biomolecular Engineering for her warm help and professional work that has been very supportive in numerous ways when I first came to Uconn and during years I spent at Uconn.

I acknowledge my undergraduate students, Johnathan E. Sims, Michael T. Spiegel, and John Lampron for their assistance in both materials synthesis and characterization. I thank all of my lab mates for all their help and supports.

Most of all, I would like to give my thanks to my beloved parents, Guosheng Yu and Guozhong Xu, for giving birth to me, for their love and care they devoted to me, and for their support and encouragement in my pursuits.

Table of Contents

List of Figures

List of Tables

CHAPTER 1

INTRODUCTION

Layered materials, ranging from clays, silicates, metal oxides to graphite, are abundant in nature. Applicability of layered materials has been extended to many aspects of human activities because of their unique chemical and physical properties. Among all of the structure modifications of layered materials, intercalation and exfoliation are the two most extensively studied areas. Intercalation to obtain sandwiched compounds to fulfill aimed applications, such as heavy metal absorption,[1] and battery,[2] has been achieved. Exfoliation to maximize the utility of individual layers as well as study the emerging superb properties (e.g., the superior mechanical, thermal, and electrical properties of graphene) has become a hot scientific topic.[3-5]

1.1 Intercalation

Intercalation chemistry has been advanced through many years of development since intercalation compounds were first identified at ca. 600-700 A.D. in China.[6] Intercalation compounds exhibit a combined property of solid host matrix and intercalated guests. For decades, interests to study intercalation compounds lie in the following aspects: (i) develop a preparation method for new hybrid materials not accessible through conventional synthetic methods; (ii) gain a deep understanding of intercalation mechanisms; (iii) develop applications in a wide range of fields including battery electrodes,[7] catalysis,[8-9] sensors[10] and fuel cells.[11-12]

1.1.1 Review of existing intercalation methods

Intercalation of layered materials has been well investigated for over a century.[13] Current intercalation methods are limited to direct intercalation,[14] multi-step intercalation,[15-16] and exfoliation-reassembly process,[17] which require multiple processes and sometimes tedious repetitions to achieve intercalation. The existing direct intercalation methods are achieved through ion-exchange, acid-base reaction, hydrogen bonding, redox reaction, and electrochemical reaction.[9, 18] Mechanical intercalation through solid-solid[19] and solid-liquid[20] interface by grinding the reaction mixture using a mortar and pestle has been reported. Such a mechanochemical process is very effective, possibly owing to the strong mechanical force directly applied to the samples, which drives the reaction.

In general, it is preferred to directly intercalate guest species into layered compounds. However, when the guest species are much larger than the interlayer distance, it is very hard to achieve direct intercalation. In such cases, the typical strategy is to pre-intercalate layered compounds with a relatively small guest species to increase the interlayer distance to certain level, then intercalate the target molecules/ions into the pre-intercalated layered compounds.[9, 21] Exfoliation and reassembly[22-24] method where the layered material was first exfoliated into single layer nanosheets and then the exfoliated nanosheets were reassembled with guest species to form an intercalation structure has also been explored.

All of the above methods are based on the pre-synthesis of layered compounds followed by the intercalation step. Herein, we aim to achieve a one-step growth of layered intercalation compounds without the need of the pre-formation of layered compounds.

1.1.2 Review of the existing methods to prepare α-Zirconium phosphate intercalation compounds

α-Zirconium phosphate (α-ZrP) was an amorphous gel obtained by mixing excessive phosphoric acid with a soluble zirconium salt. First crystalline α-ZrP was prepared by Clearfield et al.[25] in 1964 by refluxing the gel in phosphoric acid. Owning to the exchangeable acidic protons on layer surface, α-ZrP can be readily intercalated by a wide variety of guests such as amines and quaternary ammonium ions. Accommodating guest species into the interlayer space of layered materials involves electrostatic interaction, hydrogen bonding, and/or other interactions with the matrix. Small molecules and ions can be directly intercalated into α-ZrP through direct intercalation or ion exchange method. When the binding energy of the guest species is greater than the interlayer interaction energy, intercalation phenomenon is spontaneously initiated.[26] However, the narrow interlayer distance of α-ZrP exerts a kinetic barrier for the intercalation. For large guest species, direct intercalation is usually not possible. The layered α-ZrP usually has to be pre-intercalated to increase the interlayer distance to accommodate such large guest species. However, the multi-step intercalation method is time consuming, and hard to be achieved. Moreover, the pre-intercalants may be an issue for future applications.

Other methods such as exfoliation and reassembly can also accommodate large molecules such as proteins within layers.[27] In this method, α-ZrP was first exfoliated into single layer nanosheets. The re-assembly of the exfoliated α-ZrP nanosheets with protein molecules was achieved when mixing the protein solution and α-ZrP nanosheets dispersion at a volume ratio of 3:1.[28] The expanded interlayer spacing of the obtained α-ZrP/protein hybrids up to 66 Å as shown in Figure 1 suggests the successful intercalation of the proteins in the galleries.

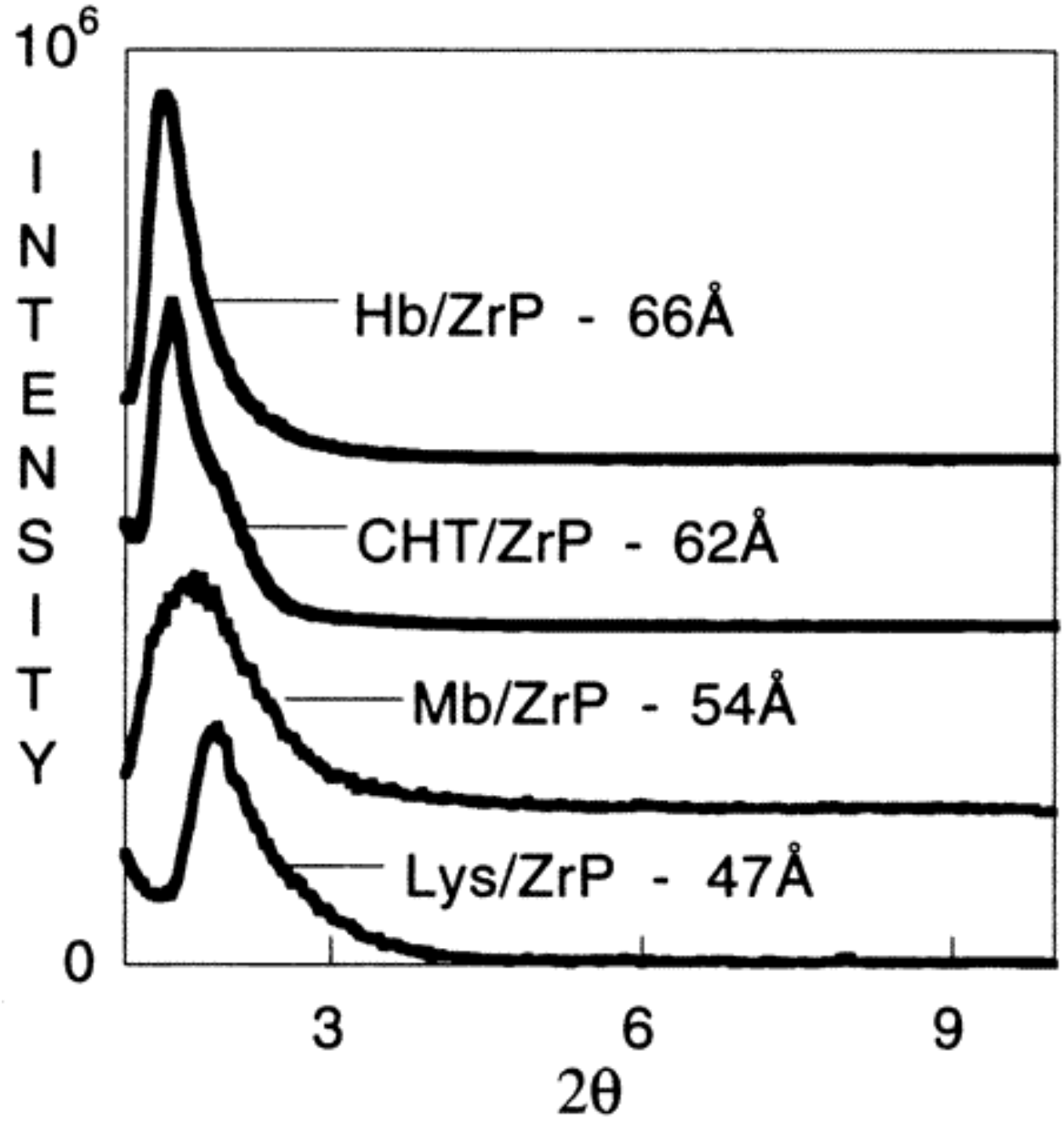

Figure 1. Powder X-ray diffraction patterns of α-ZrP/protein intercalation compounds (Mb: Myoglobin, Lys: lysozyme, Hb: hemoglobin, and CT: chymotrypsin).[27]

1.1.3 Problems and future objectives

Although several methods have been developed to intercalate large molecules, complicated procedures and long reaction time severely lowers the efficiency, and the resulting intercalation compounds may need post-treatment to exclude the pre-intercalated small molecules or exfoliation agents for further applications. Thus, new methods to prepared layered intercalation compounds, especially for handling large guest species, are highly desirable. In this dissertation, Chapter 2 reports a new method to directly prepare intercalation compounds through a one-step reaction.

1.2 Exfoliation

Exfoliation of layered materials into single layer nanosheets has been a research focus for the past two decades. Two dimensional (2D) graphene and graphene analogous materials such as transition metal dichalcogenides with a tunable band gap have received high research attention because they exhibit superior properties to their bulky counterparts. Applications of such 2D nanosheets have been well developed in sensors,[29-30] microelectronics,[31-32] thin films,[33-35] and energy storage devices.[36-39] Bulky molecules are usually used to first intercalate into a layered compound, which helps to expand the interlayer distance, facilitating the second step of sheet delamination.

1.2.1 Review of existing exfoliation methods

A wide variety of methods have been developed to exfoliate layered materials into single layer nanosheets. The most well-known one is the exfoliation of graphite developed by Geim and Novolosov, which was achieved essentially by mechanical tearing graphite apart with Scotch® tape.[40] Sonication of layered materials in surfactant, exfoliation solvents, as well as in polymers

is the most general method to prepare exfoliated single layer nanosheets in most layered materials including graphite,[41-46] boron nitride,[47-50] transition metal dichalcogenides,[3-4, 47, 51-52] metal oxides,[53-54] III-VI layered semiconductor,[55] layered double hydroxide (LDH),[5] α and γ ZrP,[56-57] and clays.[58] Other methods including pre-modifications, such as ion exchange, to first enlarge the interlayer distance and weaken the interlayer interactions and then exfoliation in different medias are also developed.[5, 40]

1.2.2 Review of the existing methods to exfoliate LDH

LDH are cationic layered materials with positively charged layers. In this entire dissertation, LDH are abbreviated in the forms of M(II)M(III)-LDH (M(II) denotes divalent cations, M(III) denotes trivalent cations), such as MgAl-LDH. Due to their high charge density, LDH were once considered non-exfoliatable until in 1999, Adachi-Pagano et al.[59] discovered that Zn/Al-LDH pre-intercalated with dodecyl sulfate (DS, $C_{12}H_{25}SO_4$) can be exfoliated in butanol. Delamination of LDH has since been rapidly expanded. Exfoliation driven by strong hydrogen bonding between interlayer moleucues and dispersant such as formamide,[60-64] and driven by mechanical forces including mechanical shaking,[65-67] stirring,[68] and ultrasonicaiton[69] has been developed. The prevalent exfoliation process[13] is schematically shown in Figure 2. The pristine LDH is swelled in a dispersant to lower interlayer interaction initiated by the interactions between the intercalated/ion exchanged molecules with formamide, and then is exfoliated by mechanical force. The discovery of LDH exfoliaiton is profound and has trigered wide applications, including layer by layer assembly of polymer/LDH films,[66, 70] flame retardant coatings,[71-73] supercapacitors,[74-77] catalysts,[78-81] and light emitting materials.[82-84] However, the exfoliation process is time consuming and evolves high temperature treatments. More

importantly, the productivity is low. Thus, developing bottom up methods to prepare LDH nanosheets in a one step process is now a new trend.

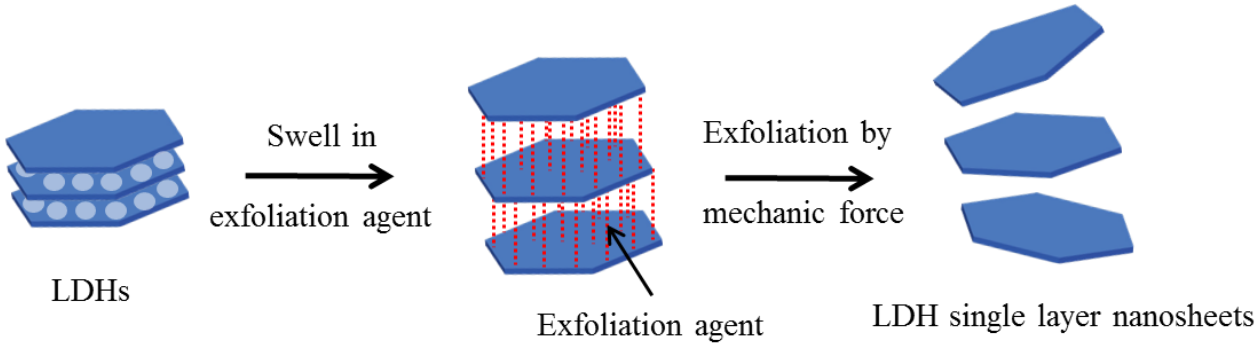

Figure 2. Typical steps to exfoliate LDH.

1.2.3 Review of the existing bottom up methods to prepare LDH nanosheets

In 2005, Hu et al.[85] reported a facile one step method to synthesize LDH monolayers in a reverse micro-emulsion. The traditional method of titrating $Mg(NO_3)_2$ and $Al(NO_3)_3$ solution at a pH $\geq$ 10 was introduced into an oil phase of isooctane with sodium dodecyl sulfate (SDS) as surfactant and 1-butanol as co-surfactant to prepare LDH monolayers. As shown in Figure 3, the aqueous droplets that contained basic components to grow LDH formed in the oil phase were surrounded by SDS. These droplets limited the space and nutrients for the growth of LDH platelets, thus providing a method to control the size of LDH nanosheets both in diameter and thickness. The resulting LDH nanosheets were of ca. 40 nm in diameter and ca. 1.5 nm in thickness, corresponding to single layer nanosheets with the adsorbed dodecyl sulfate ions on their surface. Later, in order to exclude the complex purification process to remove anionic surfactants which usually adsorbed on the surface of LDH nanosheets as counter anions,

Bellezza et al.[86] used cationic surfactants based reverse micro-emulsion to prepare LDH nanosheets without surfactants attached on the surface.

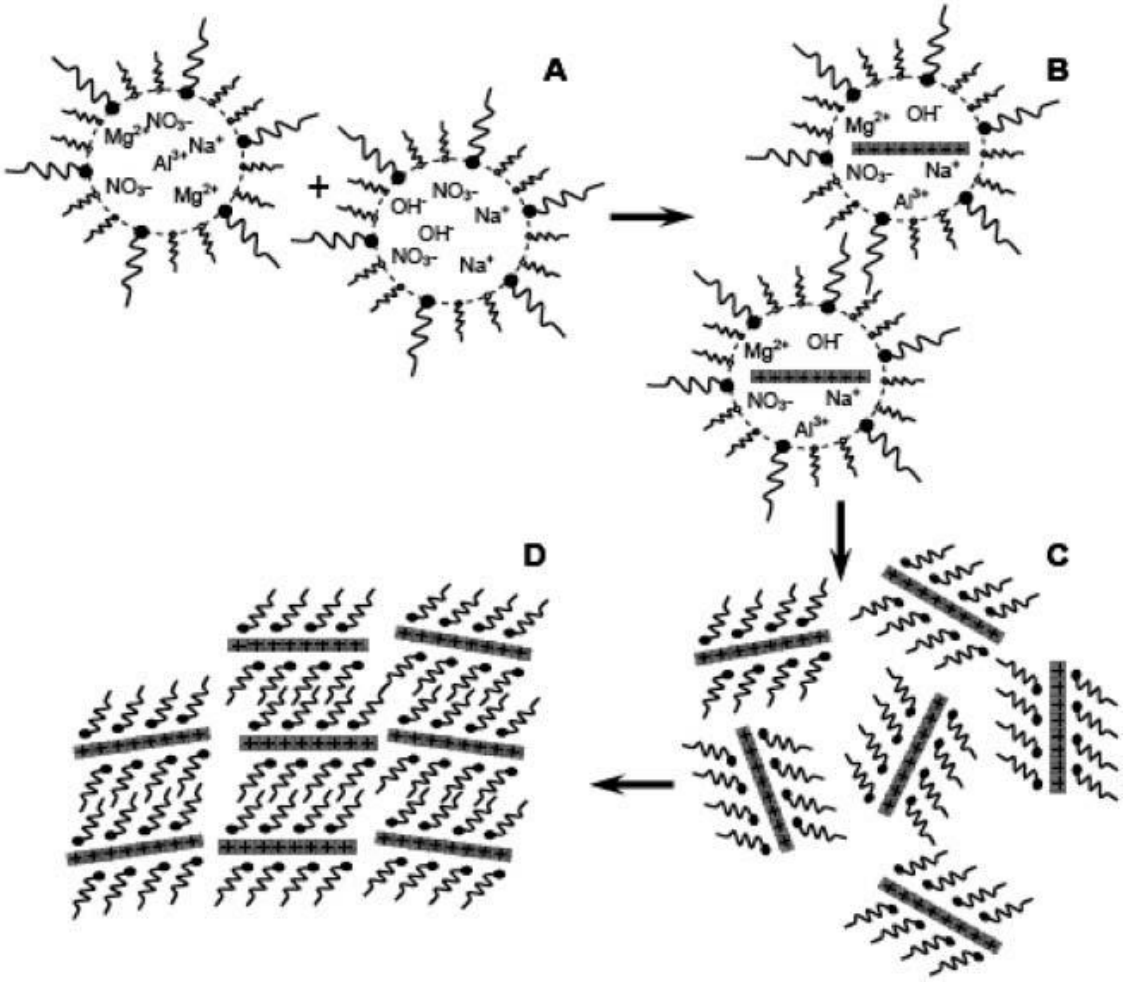

Figure 3. Schematic of the nucleation and growth of LDH nanosheets in isooctane.[85]

Other attempts using mechanical force to prepare LDH nanosheets such as laser ablation method[87] were also reported. The authors claimed that Zn/Al-, Co/Fe-, Co/Al- and Mg/Fe-LDH colloidal solutions containing ultrathin nanosheets can be obtained by directly shining laser beam on the corresponding M^{2+} and M^{3+} metal targets.

1.2.3 Problems and future objectives

Although the existing methods remain as the main source of obtaining single layer nanosheets and have made progress, they suffer from low yield and time consuming process which are difficult to scale up for commercial production. Thus, the development of a facile, efficient and less time demanding method is in urgent need. In this dissertation, Chapter 2 reports a new method to directly grow LDH single layer nanosheets through a chemical bottom up method at a low reaction temperature, requiring a short process time, and with a high yield.

1.3 Summary

In brief, the existing methods to prepare layered intercalation compounds and single layer nanosheets are either of low efficiency, hard to achieve, or having post-treatment issues. A facile method to directly prepare layered intercalation hybrids and single layer nanosheets with a high efficiency and a high yield is needed. Herein we report an effective but very facile method to directly grow layered intercalation compounds and single layer nanosheets through a bottom up route.

Chapter 2 reports the overall methodology for the direct growth of layered intercalation compounds and single layer nanosheets. Chapters 3 and 4 report the detailed mechanism of the direct growth of layered intercalation compounds and single layer nanosheets, respectively.

Chapter 5 studies the direct preparation of α-ZrP based prisms, a NH_4^+ intercalated compound with preferred growth in the Z direction. Chapter 6 utilizes the LDH single layer nanosheets prepared as described in Chapter 3 to prepare LDH/polymer nanocoatings on PET and PLA substrates. Chapter 7 gives an example of a catalytic application utilizing ionic liquid intercalated α-ZrP prepared through the method reported in Chapter 2. Chapter 8 gives a general summery of this dissertation and a brief outlook.

References

1. Alberti, G.; Costantino, U.; Szirtes, L., Effect of ionising radiation on intercalation compounds and organic derivatives of zirconium phosphates I. Effect of irradiation on carboxyethylphosphonic and phenylphosphonic acids and on the corresponding layered zirconium phosphonates. *Radiation Physics and Chemistry* **1997,** *50* (4), 369-376.

2. Nazri, G.-A.; Ohzuku, T.; Thackeray, M., Intercalation Compounds for Battery Materials: Proceedings of the International Symposium. *The Electrochemical Society, Inc* **2000**.

3. Castro Neto, A. H.; Guinea, F.; Peres, N. M. R.; Novoselov, K. S.; Geim, A. K., The electronic properties of graphene. *Reviews of Modern Physics* **2009,** *81* (1), 109-162.

4. Scarpa, F.; Adhikari, S.; Phani, A. S., Effective elastic mechanical properties of single layer graphene sheets. *Nanotechnology* **2009,** *20* (6), 065709.

5. Wang, Q.; O'Hare, D., Recent Advances in the Synthesis and Application of Layered Double Hydroxide (LDH) Nanosheets. *Chemical Reviews* **2012,** *112* (7), 4124-4155.

6. Mellor, J. W., The beginnings of porcelain in China. *Nature (London)* **1917,** *100* (2501), 88-89.

7. Armstrong, A. R.; Bruce, P. G., Synthesis of layered LiMnO2 as an electrode for rechargeable lithium batteries. *Nature* **1996,** *381* (6582), 499-500.

8. Mehnert, C. P., Supported Ionic Liquid Catalysis. *Chemistry – A European Journal* **2005,** *11* (1), 50-56.

9. Müller-Warmuth, W.; Schöllhorn, R., *Progress in Intercalation Research*. Kluwer Academic Publisher: Dordrecht, The Netherlands, 1994.

10. Brousseau, L. C.; Mallouk, T. E., Molecular Design of Intercalation-Based Sensors. 1. Ammonia Sensing with Quartz Crystal Microbalances Modified by Copper Biphenylbis(phosphonate) Thin Films. *Analytical Chemistry* **1997,** *69* (4), 679-687.

11. Al-Othman, A.; Tremblay, A. Y.; Pell, W.; Liu, Y.; Peppley, B. A.; Ternan, M., The effect of glycerol on the conductivity of Nafion-free ZrP/PTFE composite membrane electrolytes for direct hydrocarbon fuel cells. *Journal of Power Sources* **2012,** *199* (0), 14-21.

12. Furman, B. R.; Wellinghoff, S. T.; Thompson, P. M.; Beall, G. W.; Laine, R. M.; Rawls, H. R., Preparation, characterization, and modeling of α-zirconium phosphonates with ether-functional surfaces. *Chemistry of materials : a publication of the American Chemical Society* **2008,** *20* (17), 5491-5499.

13. Fredenhagen, K.; Cadenbach, G., Combination of potassium with carbon. *Zeitschrift fuer Anorganische und Allgemeine Chemie* **1926,** *158*, 249-263.

14. Gordijo, C. R.; Leopoldo Constantino, V. R.; de Oliveira Silva, D., Evidences for decarbonation and exfoliation of layered double hydroxide in N,N-dimethylformamide–ethanol solvent mixture. *Journal of Solid State Chemistry* **2007,** *180* (7), 1967-1976.

15. Marti, A. A.; Colon, J. L., Direct Ion Exchange of Tris(2,2'-bipyridine)ruthenium(II) into an a-Zirconium Phosphate Framework. *Inorganic Chemistry* **2003,** *42* (9), 2830-2832.

16. Bermúdez, R. A.; Colón, Y.; Tejada, G. A.; Colón, J. L., Intercalation and Photophysical Characterization of 1-Pyrenemethylamine in Zirconium Phosphate Layered Materials. *Langmuir* **2004,** *21* (3), 890-895.

17. Wong, M.; Ishige, R.; White, K. L.; Li, P.; Kim, D.; Krishnamoorti, R.; Gunther, R.; Higuchi, T.; Jinnai, H.; Takahara, A.; Nishimura, R.; Sue, H.-J., Large-scale self-assembled zirconium phosphate smectic layers via a simple spray-coating process. *Nat Commun* **2014,** *5*.

18. O'Hare, D., Inorganic intercalation compounds. In *Inorganic Materials*, Bruce, D. W.; O'Hare, D., Eds. John Wiley & Sons: West Sussex, 1992; pp 165-235.

19. Ogawa, M.; Kuroda, K.; Kato, C., Preparation of montmorillonite-organic intercalation compounds by solid-solid reactions. *Chemistry Letters* **1989,** (9), 1659-1662.

20. Hu, H.; Martin, J. C.; Xiao, M.; Southworth, C. S.; Meng, Y.; Sun, L., Immobilization of Ionic Liquids in Layered Compounds via Mechanochemical Intercalation. *The Journal of Physical Chemistry C* **2011,** *115* (13), 5509-5514.

21. Clearfield, A.; Costantino, U., Layered metal phosphates and their intercalation chemistry. In *Comprehensive Supramolecular Chemistry*, Alberti, G.; Bein, T., Eds. Elsevier: Oxford, UK, 1996; Vol. 7, pp 107-149.

22. Keller, S. W.; Kim, H.-N.; Mallouk, T. E., Layer-by-Layer Assembly of Intercalation Compounds and Heterostructures on Surfaces: Toward Molecular "Beaker" Epitaxy. *Journal of the American Chemical Society* **1994,** *116* (19), 8817-8818.

23. Kumar, C. V.; Chaudhari, A., Proteins Immobilized at the Galleries of Layered a-Zirconium Phosphate: Structure and Activity Studies. *Journal of the American Chemical Society* **2000,** *122* (5), 830-837.

24. Leroux, F.; Besse, J.-P., Polymer Interleaved Layered Double Hydroxide:â€‰ A New Emerging Class of Nanocomposites. *Chemistry of Materials* **2001,** *13* (10), 3507-3515.

25. Clearfield, A.; Blessing, R. H.; Stynes, J. A., New crystalline phases of zirconium phosphate possessing ion-exchange properties. *Journal of Inorganic and Nuclear Chemistry* **1968,** *30* (8), 2249-2258.

26. Heinz, H., Clay minerals for nanocomposites and biotechnology: surface modification, dynamics and responses to stimuli. *Clay Minerals* **2012,** *47* (2), 205-230.

27. Kumar, C. V.; Chaudhari, A., Proteins Immobilized at the Galleries of Layered α-Zirconium Phosphate: Structure and Activity Studies. *Journal of the American Chemical Society* **2000,** *122* (5), 830-837.

28. Kumar, C. V.; McLendon, G. L., Nanoencapsulation of Cytochrome c and Horseradish Peroxidase at the Galleries of α-Zirconium Phosphate. *Chemistry of Materials* **1997,** *9* (3), 863-870.

29. Wang, Q.; Cui, X.; Chen, J.; Zheng, X.; Liu, C.; Xue, T.; Wang, H.; Jin, Z.; Qiao, L.; Zheng, W., Well-dispersed palladium nanoparticles on graphene oxide as a non-enzymatic glucose sensor. *RSC Advances* **2012,** *2* (15), 6245-6249.

30. Zhang, S.-L.; Yang, W.-C.; Yu, J.-B.; Lim, J.-O.; Byun, H.-G.; Huh, J.-S., The Size Effect of Exfoliated MoS2 Based Thin Film Humidity Sensor. *Sensor Letters* **2014,** *12* (6-7), 1053-1058.

31. Schmidt, M. E.; Johari, Z.; Ismail, R.; Mizuta, H.; Chong, H. M., Focused ion beam milling of exfoliated graphene for prototyping of electronic devices. *Microelectronic Engineering* **2012,** *98*, 313-316.

32. Popov, V. P. *Extra Thin Silicon Film Structures For Post Silicon Microelectronics*; DTIC Document: 2006.

33. Kovtyukhova, N. I.; Ollivier, P. J.; Martin, B. R.; Mallouk, T. E.; Chizhik, S. A.; Buzaneva, E. V.; Gorchinskiy, A. D., Layer-by-layer assembly of ultrathin composite films from micron-sized graphite oxide sheets and polycations. *Chemistry of Materials* **1999,** *11* (3), 771-778.

34. Lvov, Y. M.; Lu, Z.; Schenkman, J. B.; Zu, X.; Rusling, J. F., Direct electrochemistry of myoglobin and cytochrome P450cam in alternate layer-by-layer films with DNA and other polyions. *Journal of the American Chemical Society* **1998,** *120* (17), 4073-4080.

35. Sasaki, T.; Ebina, Y.; Tanaka, T.; Harada, M.; Watanabe, M.; Decher, G., Layer-by-layer assembly of titania nanosheet/polycation composite films. *Chemistry of Materials* **2001,** *13* (12), 4661-4667.

36. Lv, W.; Tang, D.-M.; He, Y.-B.; You, C.-H.; Shi, Z.-Q.; Chen, X.-C.; Chen, C.-M.; Hou, P.-X.; Liu, C.; Yang, Q.-H., Low-temperature exfoliated graphenes: vacuum-promoted exfoliation and electrochemical energy storage. *ACS Nano* **2009,** *3* (11), 3730-3736.

37. Zhao, X.; Sánchez, B. M.; Dobson, P. J.; Grant, P. S., The role of nanomaterials in redox-based supercapacitors for next generation energy storage devices. *Nanoscale* **2011,** *3* (3), 839-855.

38. Pumera, M., Graphene-based nanomaterials for energy storage. *Energy & Environmental Science* **2011,** *4* (3), 668-674.

39. Sugimoto, W.; Iwata, H.; Yasunaga, Y.; Murakami, Y.; Takasu, Y., Preparation of ruthenic acid nanosheets and utilization of its interlayer surface for electrochemical energy storage. *Angewandte Chemie International Edition* **2003,** *42* (34), 4092-4096.

40. Geim, A. K., Graphene: Status and Prospects. *Science* **2009,** *324* (5934), 1530-1534.

41. Hernandez, Y.; Nicolosi, V.; Lotya, M.; Blighe, F. M.; Sun, Z.; De, S.; McGovern, I. T.; Holland, B.; Byrne, M.; Gun'Ko, Y. K.; Boland, J. J.; Niraj, P.; Duesberg, G.; Krishnamurthy, S.; Goodhue, R.; Hutchison, J.; Scardaci, V.; Ferrari, A. C.; Coleman, J. N., High-yield production of graphene by liquid-phase exfoliation of graphite. *Nat Nano* **2008,** *3* (9), 563-568.

42. Lotya, M.; Hernandez, Y.; King, P. J.; Smith, R. J.; Nicolosi, V.; Karlsson, L. S.; Blighe, F. M.; De, S.; Wang, Z.; McGovern, I. T.; Duesberg, G. S.; Coleman, J. N., Liquid Phase Production of Graphene by Exfoliation of Graphite in Surfactant/Water Solutions. *Journal of the American Chemical Society* **2009,** *131* (10), 3611-3620.

43. Khan, U.; O'Neill, A.; Lotya, M.; De, S.; Coleman, J. N., High-Concentration Solvent Exfoliation of Graphene. *Small* **2010,** *6* (7), 864-871.

44. O'Neill, A.; Khan, U.; Nirmalraj, P. N.; Boland, J.; Coleman, J. N., Graphene Dispersion and Exfoliation in Low Boiling Point Solvents. *The Journal of Physical Chemistry C* **2011,** *115* (13), 5422-5428.

45. Lotya, M.; King, P. J.; Khan, U.; De, S.; Coleman, J. N., High-Concentration, Surfactant-Stabilized Graphene Dispersions. *ACS Nano* **2010,** *4* (6), 3155-3162.

46. Vadukumpully, S.; Paul, J.; Valiyaveettil, S., Cationic surfactant mediated exfoliation of graphite into graphene flakes. *Carbon* **2009,** *47* (14), 3288-3294.

47. Smith, R. J.; King, P. J.; Lotya, M.; Wirtz, C.; Khan, U.; De, S.; O'Neill, A.; Duesberg, G. S.; Grunlan, J. C.; Moriarty, G.; Chen, J.; Wang, J.; Minett, A. I.; Nicolosi, V.; Coleman, J. N., Large-Scale Exfoliation of Inorganic Layered Compounds in Aqueous Surfactant Solutions. *Advanced Materials* **2011,** *23* (34), 3944-3948.

48. Coleman, J. N.; Lotya, M.; O'Neill, A.; Bergin, S. D.; King, P. J.; Khan, U.; Young, K.; Gaucher, A.; De, S.; Smith, R. J.; Shvets, I. V.; Arora, S. K.; Stanton, G.; Kim, H.-Y.; Lee, K.; Kim, G. T.; Duesberg, G. S.; Hallam, T.; Boland, J. J.; Wang, J. J.; Donegan, J. F.; Grunlan, J. C.; Moriarty, G.; Shmeliov, A.; Nicholls, R. J.; Perkins, J. M.; Grieveson, E. M.; Theuwissen, K.; McComb, D. W.; Nellist, P. D.; Nicolosi, V., Two-Dimensional Nanosheets Produced by Liquid Exfoliation of Layered Materials. *Science* **2011,** *331* (6017), 568-571.

49. May, P.; Khan, U.; Hughes, J. M.; Coleman, J. N., Role of Solubility Parameters in Understanding the Steric Stabilization of Exfoliated Two-Dimensional Nanosheets by Adsorbed Polymers. *The Journal of Physical Chemistry C* **2012,** *116* (20), 11393-11400.

50. Lin, Y.; Williams, T. V.; Connell, J. W., Soluble, Exfoliated Hexagonal Boron Nitride Nanosheets. *The Journal of Physical Chemistry Letters* **2010,** *1* (1), 277-283.

51. Cunningham, G.; Lotya, M.; Cucinotta, C. S.; Sanvito, S.; Bergin, S. D.; Menzel, R.; Shaffer, M. S. P.; Coleman, J. N., Solvent Exfoliation of Transition Metal Dichalcogenides: Dispersibility of Exfoliated Nanosheets Varies Only Weakly between Compounds. *ACS Nano* **2012,** *6* (4), 3468-3480.

52. Yao, Y.; Lin, Z.; Li, Z.; Song, X.; Moon, K.-S.; Wong, C.-p., Large-scale production of two-dimensional nanosheets. *Journal of Materials Chemistry* **2012,** *22* (27), 13494-13499.

53. Chen, Y.; Yang, G.; Zhang, Z.; Yang, X.; Hou, W.; Zhu, J.-J., Polyaniline-intercalated layered vanadium oxide nanocomposites-One-pot hydrothermal synthesis and application in lithium battery. *Nanoscale* **2010,** *2* (10), 2131-2138.

54. Murugan, A. V.; Viswanath, A. K.; Gopinath, C. S.; Vijayamohanan, K., Highly efficient organic-inorganic poly(3,4-ethylenedioxythiophene)-molybdenum trioxide nanocomposite electrodes for electrochemical supercapacitor. *Journal of Applied Physics* **2006,** *100* (7), 074319.

55. Mirabal, N.; Lavayen, V.; Benavente, E.; Santa Ana, M. A.; González, G., Synthesis, functionalization, and properties of intercalation compounds. *Microelectronics Journal* **2004,** *35* (1), 37-40.

56. Alberti, G.; Dionigi, C.; Giontella, E.; Murcia-Mascarós, S.; Vivani, R., Formation of Colloidal Dispersions of Layered γ-Zirconium Phosphate in Water/Acetone Mixtures. *Journal of Colloid and Interface Science* **1997,** *188* (1), 27-31.

57. Bhambhani, A.; Kumar, C. V., Enzyme-inorganic nanoporous materials: Stabilization of proteins intercalated in α-zirconium(IV) phosphate by a denaturant. *Microporous and Mesoporous Materials* **2008,** *110* (2–3), 517-527.

58. Luckham, P. F.; Rossi, S., The colloidal and rheological properties of bentonite suspensions. *Advances in Colloid and Interface Science* **1999,** *82* (1–3), 43-92.

59. Adachi-Pagano, M.; Forano, C.; Besse, J.-P., Delamination of layered double hydroxides by use of surfactants. *Chemical Communications* **2000,** *0* (1), 91-92.

60. Hibino, T.; Jones, W., New approach to the delamination of layered double hydroxides. *Journal of Materials Chemistry* **2001,** *11* (5), 1321-1323.

61. Hibino, T., Delamination of Layered Double Hydroxides Containing Amino Acids. *Chemistry of Materials* **2004,** *16* (25), 5482-5488.

62. Wypych, F.; Bubniak, G. A.; Halma, M.; Nakagaki, S., Exfoliation and immobilization of anionic iron porphyrin in layered double hydroxides. *Journal of Colloid and Interface Science* **2003,** *264* (1), 203-207.

63. Bao-guang Li, Y. H., Zu-Yao, Hydrothermal Synthesis of exfoliateive LDH in the presence of Glycine. *Chin. J. Chem. Phys.* **2006,** *19*, 253.

64. Ugur, U., Short-time hydrothermal synthesis and delamination of ion exchangeable Mg/Ga layered double hydroxides. *Journal of Solid State Chemistry* **2007,** *180* (9), 2525-2533.

65. Li, L.; Ma, R.; Ebina, Y.; Iyi, N.; Sasaki, T., Positively Charged Nanosheets Derived via Total Delamination of Layered Double Hydroxides. *Chemistry of Materials* **2005,** *17* (17), 4386-4391.

66. Liu, Z.; Ma, R.; Osada, M.; Iyi, N.; Ebina, Y.; Takada, K.; Sasaki, T., Synthesis, Anion Exchange, and Delamination of Co-Al Layered Double Hydroxide. Assembly of the Exfoliated Nanosheet/Polyanion Composite Films and Magneto-Optical Studies. *Journal of the American Chemical Society* **2006,** *128* (14), 4872-4880.

67. Liu, Z.; Ma, R.; Ebina, Y.; Iyi, N.; Takada, K.; Sasaki, T., General Synthesis and Delamination of Highly Crystalline Transition-Metal-Bearing Layered Double Hydroxides. *Langmuir* **2006,** *23* (2), 861-867.

68. Abellan, G.; Coronado, E.; Marti-Gastaldo, C.; Pinilla-Cienfuegos, E.; Ribera, A., Hexagonal nanosheets from the exfoliation of Ni2+-Fe3+ LDHs: a route towards layered multifunctional materials. *Journal of Materials Chemistry* **2010,** *20* (35), 7451-7455.

69. Wu, Q.; Olafsen, A.; Vistad, O. B.; Roots, J.; Norby, P., Delamination and restacking of a layered double hydroxide with nitrate as counter anion. *Journal of Materials Chemistry* **2005,** *15* (44), 4695-4700.

70. Contributors, M., Comprehensive Supramolecular Chemistry. *Pergamon* **1996**, 189.

71. Wang, D.-Y.; Das, A.; Costa, F. R.; Leuteritz, A.; Wang, Y.-Z.; Wagenknecht, U.; Heinrich, G., Synthesis of Organo Cobalt−Aluminum Layered Double Hydroxide via a Novel Single-Step Self-Assembling Method and Its Use as Flame Retardant Nanofiller in PP. *Langmuir* **2010,** *26* (17), 14162-14169.

72. Liu, S.; Yan, H.; Fang, Z.; Guo, Z.; Wang, H., Effect of graphene nanosheets and layered double hydroxides on the flame retardancy and thermal degradation of epoxy resin. *RSC Advances* **2014,** *4* (36), 18652-18659.

73. Kuila, T.; Srivastava, S. K.; Bhowmick, A. K., Rubber/LDH nanocomposites by solution blending. *Journal of Applied Polymer Science* **2009,** *111* (2), 635-641.

74. Altuntasoglu, O. U., Ugur;Ida, Shintaro;Goto, Motonobu;Matsumoto, Yasumichi, Characterization of self-assembled films of NiGa layered double hydroxide nanosheets and their electrochemical properties. *Journal of Solid State Chemistry* **2008,** *181* (2), Medium: X; Size: page(s) 3257-3263.

75. Ma, R.; Liu, X.; Liang, J.; Bando, Y.; Sasaki, T., Molecular-Scale Heteroassembly of Redoxable Hydroxide Nanosheets and Conductive Graphene into Superlattice Composites for High-Performance Supercapacitors. *Advanced Materials* **2014,** *26* (24), 4173-4178.

76. Zhao, J.; Chen, J.; Xu, S.; Shao, M.; Zhang, Q.; Wei, F.; Ma, J.; Wei, M.; Evans, D. G.; Duan, X., Hierarchical NiMn Layered Double Hydroxide/Carbon Nanotubes Architecture with Superb Energy Density for Flexible Supercapacitors. *Advanced Functional Materials* **2014,** *24* (20), 2938-2946.

77. Yu, L.; Shi, N.; Liu, Q.; Wang, J.; Yang, B.; Wang, B.; Yan, H.; Sun, Y.; Jing, X., Facile synthesis of exfoliated Co-Al LDH-carbon nanotube composites with high performance as supercapacitor electrodes. *Physical Chemistry Chemical Physics* **2014**.

78. Song, F.; Hu, X., Exfoliation of layered double hydroxides for enhanced oxygen evolution catalysis. *Nat Commun* **2014,** *5*.

79. Zhao, Y.; Li, B.; Wang, Q.; Gao, W.; Wang, C. J.; Wei, M.; Evans, D. G.; Duan, X.; O'Hare, D., NiTi-Layered double hydroxides nanosheets as efficient photocatalysts for oxygen evolution from water using visible light. *Chemical Science* **2014,** *5* (3), 951-958.

80. Long, X.; Li, J.; Xiao, S.; Yan, K.; Wang, Z.; Chen, H.; Yang, S., A Strongly Coupled Graphene and FeNi Double Hydroxide Hybrid as an Excellent Electrocatalyst for the Oxygen Evolution Reaction. *Angewandte Chemie International Edition* **2014,** *53* (29), 7584-7588.

81. Liu, S.; Jiang, X.; Zhuo, G., Heck reaction catalyzed by colloids of delaminated Pd-containing layered double hydroxide. *Journal of Molecular Catalysis A: Chemical* **2008,** *290* (1-2), 72-78.

82. Cho, S.; Kwag, J.; Jeong, S.; Baek, Y.; Kim, S., Highly Fluorescent and Stable Quantum Dot-Polymer-Layered Double Hydroxide Composites. *Chemistry of Materials* **2013,** *25* (7), 1071-1077.

83. Tian, R.; Liang, R.; Yan, D.; Shi, W.; Yu, X.; Wei, M.; Li, L. S.; Evans, D. G.; Duan, X., Intelligent display films with tunable color emission based on a supermolecular architecture. *Journal of Materials Chemistry C* **2013,** *1* (36), 5654-5660.

84. Cho, S.; Hong, S. C.; Kim, S., Quantum dot-layered double hydroxide composites for near-infrared emitting codes. *Journal of Materials Chemistry C* **2014,** *2* (3), 450-457.

85. Hu, G.; Wang, N.; O'Hare, D.; Davis, J., One-step synthesis and AFM imaging of hydrophobic LDH monolayers. *Chemical Communications* **2006,** (3), 287-289.

86. Bellezza, F.; Cipiciani, A.; Costantino, U.; Nocchetti, M.; Posati, T., Hydrotalcite-Like Nanocrystals from Water-in-Oil Microemulsions. *European Journal of Inorganic Chemistry* **2009,** *2009* (18), 2603-2611.

87. Hur, T.-B.; Phuoc, T. X.; Chyu, M. K., New approach to the synthesis of layered double hydroxides and associated ultrathin nanosheets in de-ionized water by laser ablation. *Journal of Applied Physics* **2010,** *108* (11), 114312.

CHAPTER 2

TAILORING THE THIRD-DIMENSION IN LAYERED MATERIALS: DIRECT SYNTHESIS OF LAYERED INTERCALATION COMPOUNDS AND SINGLE LAYER NANOSHEETS

2.1 Introduction

Layered structures[1] are ubiquitous in nature, found in clays and other minerals, as well as in biomaterials such as nacre.[2] These materials have found widespread application, predominately in the form of intercalated layered hybrids,[3-4] or as exfoliated nanosheets.[5-7] For both scenarios, layered precursor phases are typically first synthesized as a bulk product, and are then treated by chemical intercalants or exfoliating agents (Figure 4). Since many layered phases may not be intercalated or exfoliated, this two-step process limits the scope of application to a small subset of possible materials. In contrast, biomineralization utilizes organic templating agents to guide growth of the inorganic structure, resulting in strong layered composites, such as nacre, in a single synthetic process.[2] Following this model it should be possible to guide the growth of layered hybrid structures by tuning the interactions between the layer surfaces and templating agents, thereby allowing the direct synthesis of layered intercalation compounds and single layer nanosheets, as already achieved in some inorganic materials.[8]

Crystal growth of layered structures is typically anisotropic, with faster growth along the layer planes, driven by the formation of strong covalent or coordinate bonds. Interlayer growth involves the formation of weaker bonds that vary by structure type, such as Van der Waals

forces,[9] weak electrostatic interactions,[10] or hydrogen bonds.[11] Layered compounds, layered intercalation compounds, and single-layer nanosheets essentially differ only in their ordering in the 3rd ('Z') dimension (Figure 4). If one can tailor the growth of layered materials in the Z-direction, layered intercalation compounds and single-layer nanosheets could potentially be directly synthesized.

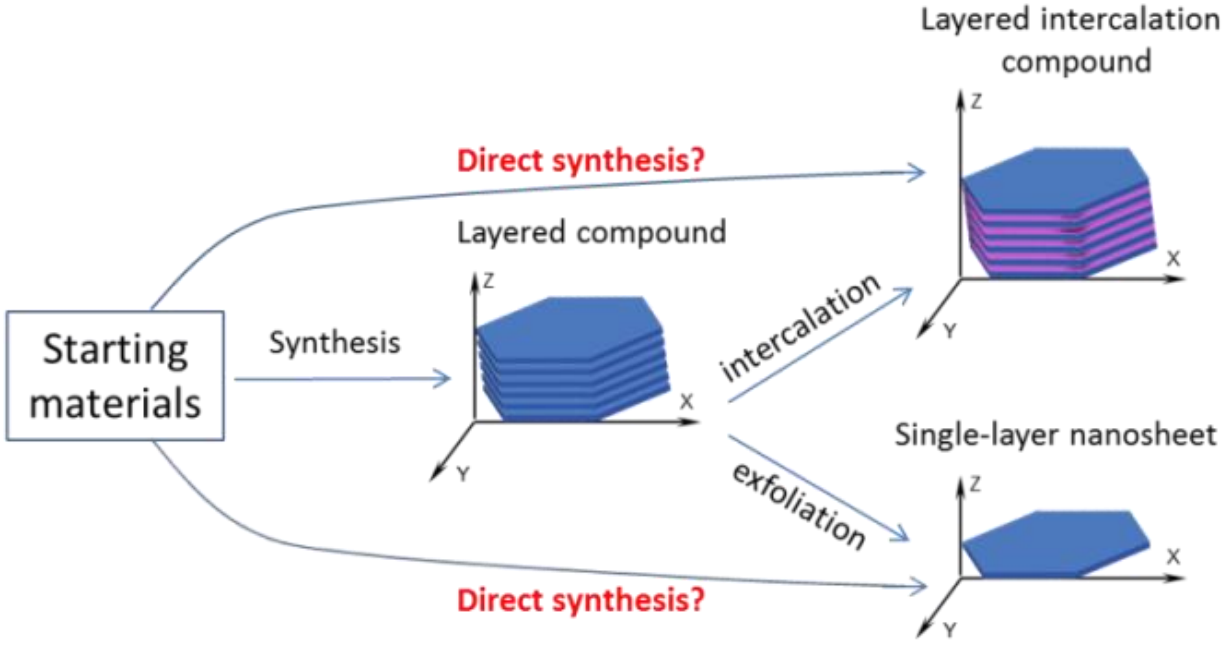

Figure 4. Routes to synthesize intercalated hybrids and single-layer nanosheets. Traditionally, layered precursor phases are first synthesized as a bulk product, and then intercalated or exfoliated to prepare intercalation compounds or single-layer nanosheets, respectively. Herein, we propose to directly synthesize intercalation compounds and single-layer nanosheets by bypassing the synthesis of layered precursors.

Herein, we report our strategies to tailor the growth of selected layered materials in the Z-direction by applying either a layer growth coordinator or inhibitor (Figure 5). Two representative layered compounds (Figure 6), α-zirconium phosphate (α-ZrP, $Zr(HPO_4)_2 \cdot H_2O$)

with a negative layer charge[12] and layered double hydroxide (LDH, $[M^{2+}_{1-x}M^{3+}_{x}(OH)_2]^{x+}[A^{p-}_{x/p}]\cdot mH_2O$) with a positive layer charge,[13] were selected as model systems for the direct synthesis of layered intercalation compounds and single-layer nanosheets, respectively. The intercalation[12, 14] and exfoliation chemistry[15-18] of these two compounds have been well studied, and each can be easily synthesized in the lab.[13, 19] The layer growth coordinators can guide the growth of the layers in the Z-direction, during which the coordinators are embedded within the formed layers to form an intercalation compound (like assembly of building blocks, Figure 5a). The layer growth inhibitors allow the layers to grow in-plane only, but prevent the layers from stacking (Figure 5b). In this way, single-layer nanosheets can potentially be directly synthesized. Such novel methodologies open new routes for achieving intercalated and exfoliated morphologies, and may result in new valuable materials.

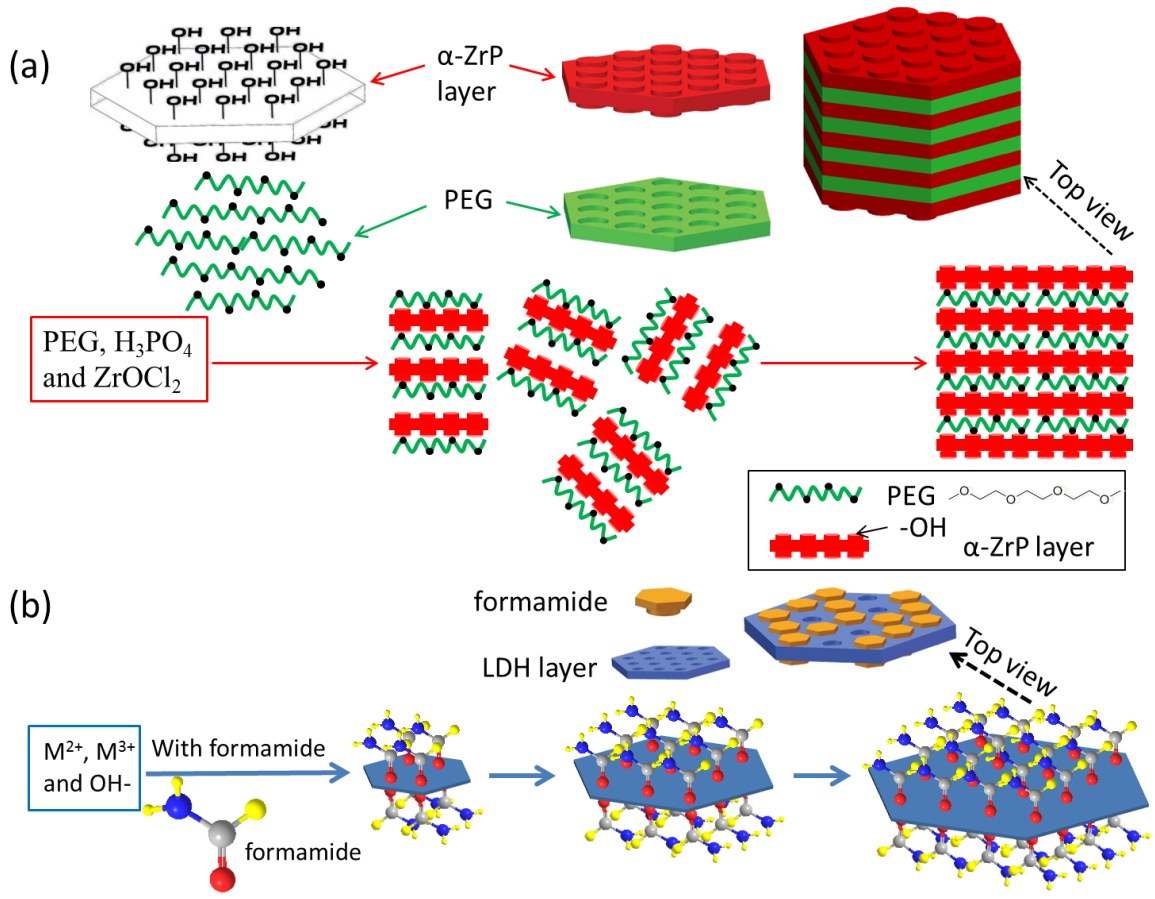

Figure 5. Schematic of direct growth strategies. Direct growth of (a) layered intercalation compounds and (b) single layer nanosheets with the assistance of layer growth coordinators and inhibitors, respectively (not drawn to scale; M^{2+} and M^{3+} represent double and triple charged metal cations).

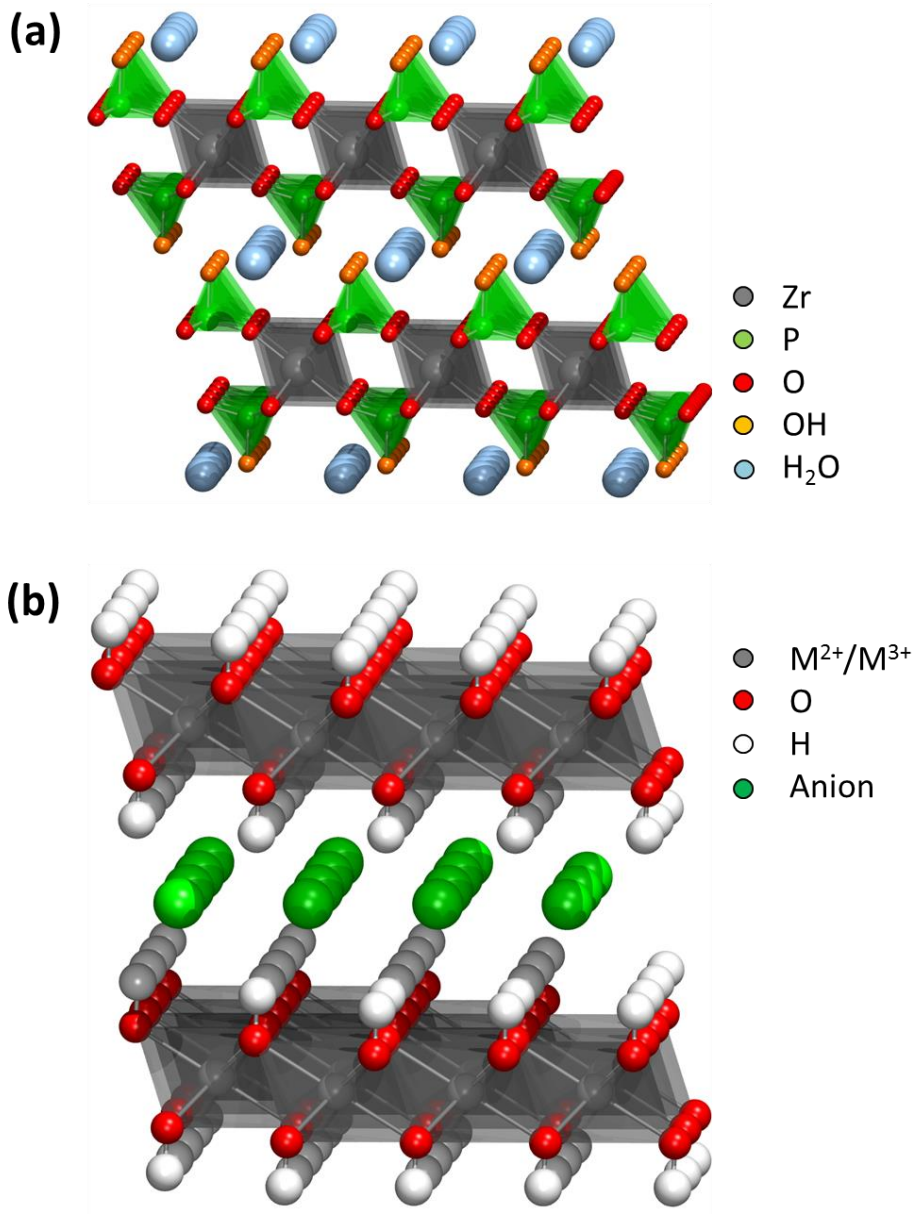

Figure 6. Structure of (a) α-zirconium phosphate and (b) layered double hydroxide.

2.2 Experimental

Materials. A series of linear polyethylene glycols (PEG) with various molecular weights: ca. 400, 600, 1000, 1900, and 8000 (abbreviated as PEG-400, PEG-600, PEG-1000, PEG-1900, PEG-8000) were purchased from Alfa Aesar and used as received. $ZrOCl_2 \cdot 8H_2O$ (98%, Sigma-Aldrich), phosphoric acid (85%, Sigma-Aldrich), poly(sodium 4-styrene-sulfonate) (30 wt.% aqueous solution, Sigma-Aldrich), urea (>99.0%, J.T. Baker), formamide (99%, Alfa Aesar), *N*, *N*-dimethyl formamide (≥99.8%, Sigma-Aldrich), $Mg(NO_3)_2 \cdot 6H_2O$ (98%, Alfa Aesar), $Co(NO_3)_2 \cdot 6H_2O$(>98%, Alfa Aesar), $Al(NO_3)_3 \cdot 9H_2O$ (99%, Acros), sodium hydroxide (98%, Macron), polyethyleneimine (PEI) with an average molecular weight of 600 (Sigma-Aldrich), polyvinyl alcohol (PVA, weight average molecular weight of ~27,000, 98.0-98.8% hydrolysis, Kuraray), acrylamide (98.0%, TCU America), 1-butyl-3-methylimidazolium ($BMIM^+$) chloride (>98.0%, Sigma-Aldrich) were all used as received without further purification.

Characterization. X-ray diffraction (XRD) patterns were recorded on a Bruker D8 diffractometer with Bragg-Brentano θ-2θ geometry (40 kV and 30 mA), using a graphite monochromator with Cu Kα radiation with λ= 1.542 Å. For powder samples, they were gently packed in a sample holder for characterization. For solution samples, they were cast as a thin liquid film on a silicon wafer, which was covered by a Mylar® film during the characterization. In this way, the solution can maintain a flat surface during characterization. In addition, the synthesized LDH nanosheets were cast on a clean silicon wafer and dried at room temperature for XRD characterization.

Scanning electron microscopy (SEM) images were acquired on a field emission-SEM (FE-SEM) from JEOL JSM-6335F. The samples were sputter coated with a thin layer (ca. 3 nm) of Pt/Pd (80/20) prior to the SEM imaging.

Transmission electron microscopy (TEM) imaging was carried out using a FEI Tecnai G2 F20 with field emission gun (FEG) at a working voltage of 200 kV. Observations were made through the holes of the carbon support film, so that no noise from the support film was introduced.

Atomic force microscopy (AFM) characterization was performed on an Asylum Research MFP-3d AFM. AFM images were obtained under the tapping mode using a silicon tip coated with chromium/gold with a force constant of 40 N/m. LDH nanosheets samples were diluted into ca. 0.01 mM and drop-coated on a clean silicon wafer for AFM imaging.

Direct synthesis of α-ZrP based layered intercalation compounds. Polyethylene glycol (PEG)/α-ZrP layered intercalation compounds were synthesized *via* a hydrothermal reaction[20], during which 4.0 g of 20.0 wt% $ZrOCl_2$ aqueous solution was mixed with a pre-determined amount of PEG. After the PEG was dissolved, a pre-determined amount of concentrated H_3PO_4 was added so that the H_3PO_4 and $ZrOCl_2$ mole ratio reached 10:1. Additional deionized water was added to dilute the concentration of H_3PO_4 to reach 4.0 M. The mixture was treated at 100 ℃ for 24 hours in a 20 mL container that was well sealed.

In one series of reactions, PEG-600 was used. The mass ratio of PEG-600 to α-ZrP (assuming all the Zr^{4+} cations were converted to α-ZrP) was varied from 0.25:1 to 2.00:1. In another series of reactions, linear PEGs with various molecular weights (MWs), including PEG-400, PEG-600, PEG-1000, PEG-1900, PEG-8000, were used. The mass ratio of each of these

PEGs to α-ZrP (assuming all the Zr^{4+} cations were converted to α-ZrP) was maintained at 1:00 to 1.

A neat α-ZrP sample was synthesized in the absence of PEG under the same reaction conditions as a control. In addition, this neat α-ZrP was mixed with PEG-600 (mass ratio of PEG-600 to α-ZrP is 2:00 to 1), and the mixture was hydrothermally treated at 100 ℃ for 24 hours in a same container. This reaction was to check whether the pre-synthesized neat α-ZrP can be intercalated by PEG-600 under the same reaction conditions.

The α-ZrP based intercalation compounds containing other guest species, including other polymers (PVA, PEI), small molecules (acrylamide), and ions (1-butyl-3-methylimidazolium $BMIM^+$), were also synthesized *via* the same reaction approach and under the same reaction conditions.

After reaction, the products were washed and collected by centrifugation three times. After that, they were dried at 70 ℃ for 24 hours. The dried samples were ground with an agate mortar and pestle into fine powders for characterizations.

Direct synthesis of MgAl-LDH based layered intercalation compounds. A 30.0 mL solution composed of $Mg(NO_3)_2$ (0.20 M) and $Al(NO_3)_3$ (0.05 M) was mixed with urea at a molar ratio of (urea):(total metal ion)= 4:1 and a pre-determined amount of poly(sodium 4-styrene-sulfonate) (PSS). The mixture was added into a Teflon lined hydrothermal reactor and heated at 100 ℃ for 24 hours. The mass ratio of PSS to LDH (assuming all the metal cations were converted to LDH) was varied from 0.25:1 to 2.00:1. A neat MgAl-LDH sample was synthesized in the absence of PSS under the same reaction conditions as a control. After reaction, the products were washed and collected by centrifugation three times. After that, they were dried

at 100 ℃ for 24 hours. The dried samples were ground with an agate mortar and pestle into fine powders for characterizations.

Direct synthesis of colloidal single-layer nanosheets. The traditional titration method[21] was modified slightly to directly synthesize single-layer MgAl-LDH by adding 23 vol% formamide as inhibitors. A 10.0 mL solution composed of $Mg(NO_3)_2$ (0.040 M) and $Al(NO_3)_3$ (0.010 M) was added drop by drop to a solution of 10.0 mL NaCl (0.010 M) containing 23 vol% formamide. Simultaneously, a solution of 0.25 M NaOH was added dropwise with magnetic stirring at 80 ℃ to maintain the system at a pH value of ca. 10. The reaction was completed within 10 min. After that, the prepared sample was centrifuged and washed with water. By repeating the process three times, single-layer LDH nanosheets dispersed in water were obtained. A control sample of conventional layered MgAl-LDH was prepared using the same formulation and under the same conditions but in the absence of formamide.

MgAl-LDH nanosheets were also synthesized using 23 vol% N, N-dimethyl formamide as inhibitor through the same procedures.

Similarly, Co^{2+}/Al^{3+} layered double hydroxide (CoAl-LDH) was also prepared [using $Co(NO_3)_2$ to replace $Mg(NO_3)_2$] following the same method in the presence of formamide. In the synthesis of CoAl-LDH nanosheets, 20.0 mL solution of $Co(NO_3)_2$ (0.032 M) and $Al(NO_3)_3$ (0.018 M) was added drop by drop into a solution of 20.0 mL NaCl (0.018 M) containing 23 vol% formamide. Reaction was carried out at 80 ℃ with magnetic stirring, during which a solution of 0.25 M NaOH was added dropwise to maintain the system at a pH value of ca. 10.

2.3 Results and discussion

We hypothesize that the direct synthesis of an intercalated layered hybrid requires the formation of a network of interactions between the intercalant and the inorganic structure. The

model compound α-ZrP crystallizes with hydroxyl groups projecting from the platelet surface.[12] This surface is ideally suited to form hydrogen bonded networks with a hydrogen bond acceptor such as polyethylene glycol (PEG, Figure 5a).

Preliminary studies showed that it is not possible to intercalate PEG into pre-synthesized α-ZrP using conventional methods (See Figure 7). However, when PEG is added to the hydrothermal reaction mixture used to synthesize α-ZrP, the interlayer distance of the formed compounds increases from the native 7.6 to 10.4 Å, indicating the formation of an intercalated phase. Different mass ratios of PEG with a molecular weight (MW) of ca. 600 g/mol (PEG-600) were added to reaction mixtures to evaluate the effect on intercalation efficiency (Figure 8a). At low mass ratios (less than 0.50:1 PEG-600:α-ZrP) a mixture of un-intercalated α-ZrP and intercalated PEG/α-ZrP hybrid was observed. At higher mass ratios (≥ 0.5:1 PEG-600:α-ZrP), only a very small amount of un-intercalated α-ZrP was found. Further increasing the mole ratio did not alter the distribution of the products much, indicating that the mixture has reached an equilibrium distribution. It is possible that the two phases are present within a single crystal, with alternating intercalated/un-intercalated layers.

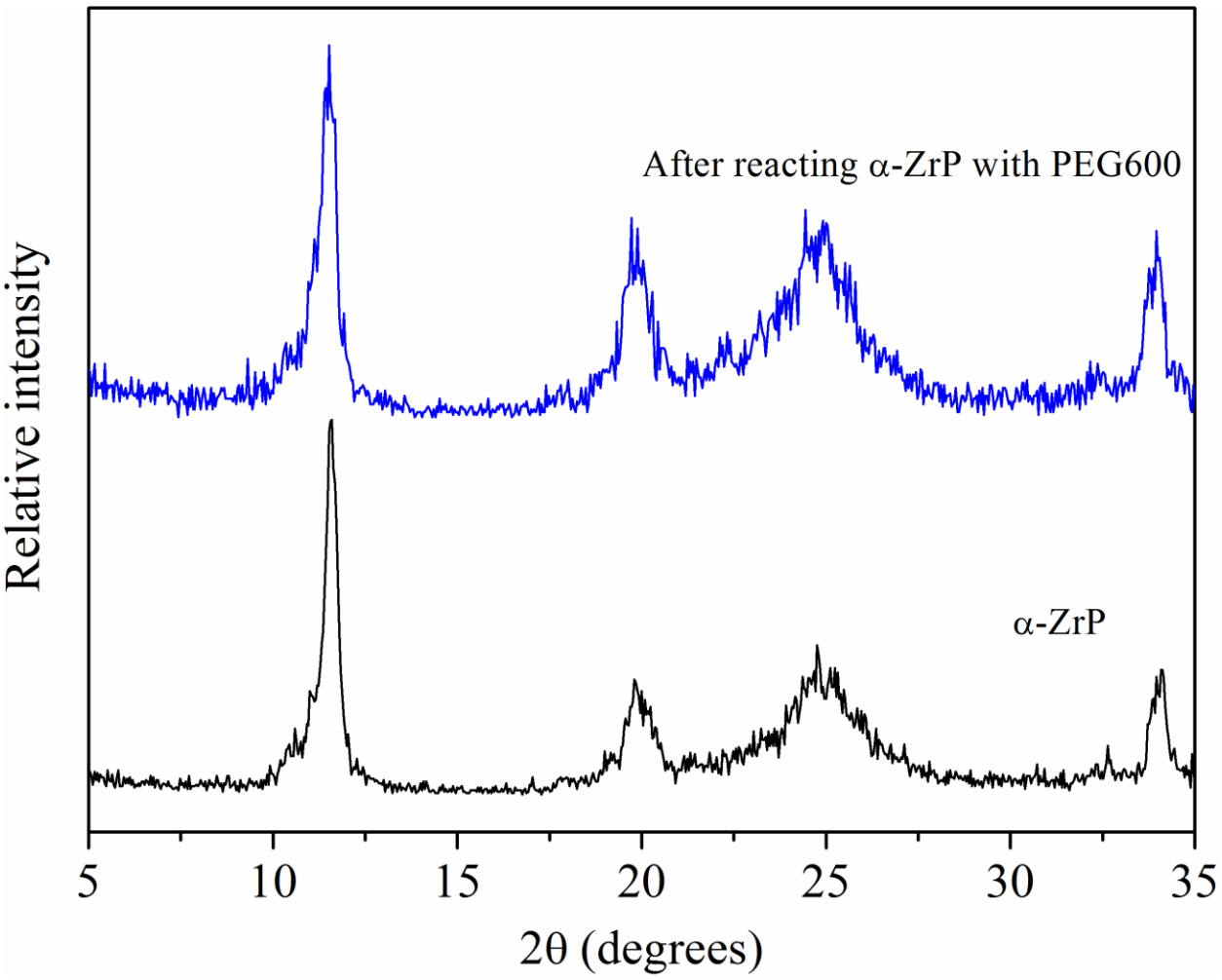

Figure 7. XRD patterns of pristine α-ZrP and the mixture of α-ZrP and PEG-600 (2.00:1 mass ratio) after mixing under the hydrothermal reaction conditions (100 ℃ for 24 hours).

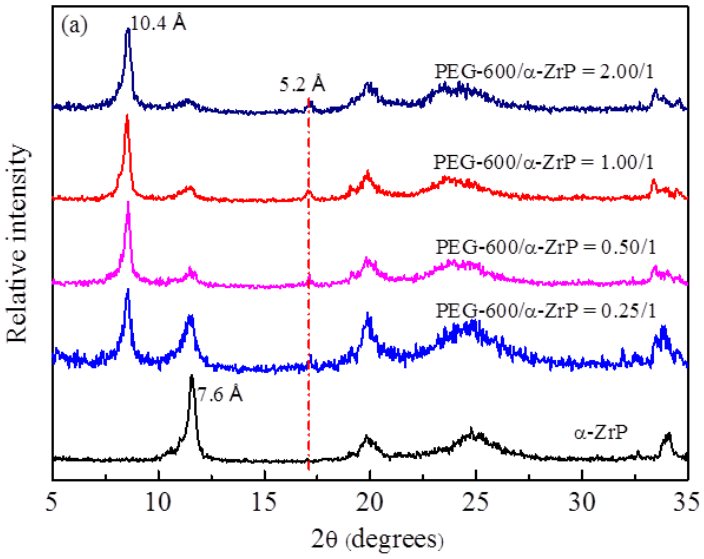
(a)
10.4 Å
5.2 Å
PEG-600/α-ZrP = 2.00/1
PEG-600/α-ZrP = 1.00/1
PEG-600/α-ZrP = 0.50/1
PEG-600/α-ZrP = 0.25/1
7.6 Å
α-ZrP
Relative intensity
5
10
15
20
25
30
35
2θ (degrees)

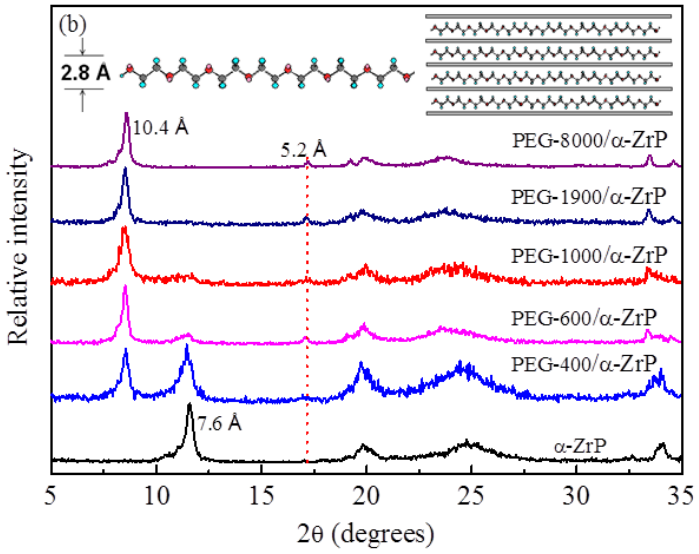
(b)
2.8 Å
10.4 Å
5.2 Å
PEG-8000/α-ZrP
PEG-1900/α-ZrP
PEG-1000/α-ZrP
PEG-600/α-ZrP
PEG-400/α-ZrP
7.6 Å
α-ZrP
Relative intensity
5
10
15
20
25
30
35
2θ (degrees)

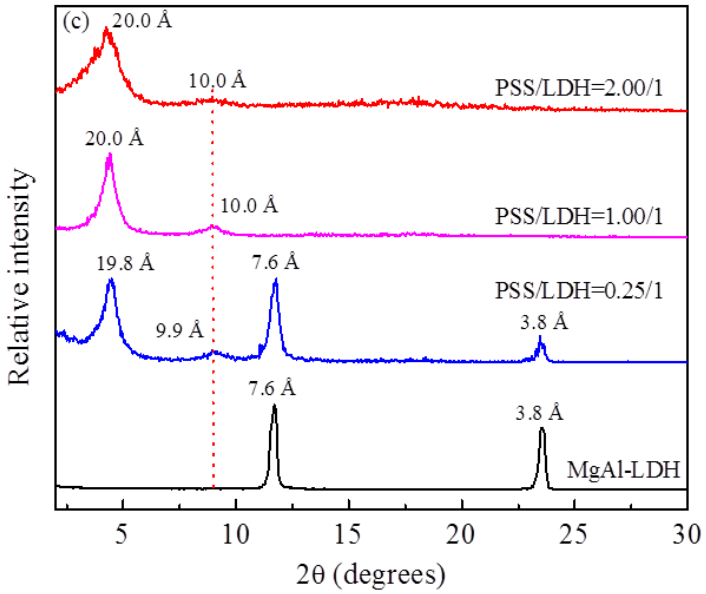
(c)
20.0 Å
10.0 Å
PSS/LDH=2.00/1
20.0 Å
10.0 Å
PSS/LDH=1.00/1
19.8 Å
7.6 Å
PSS/LDH=0.25/1
9.9 Å
3.8 Å
7.6 Å
3.8 Å
MgAl-LDH
Relative intensity
5
10
15
20
25
30
2θ (degrees)

Figure 8. XRD patterns of directly synthesized intercalation compounds. (a) Intercalation compounds synthesized with various PEG-600/α-ZrP mass ratios (100 ℃ for 24 hours); (b) intercalation compounds synthesized with PEGs with different MWs (100 ℃ for 24 hours, PEG/α-ZrP=1.00:1 in mass ratio); (c) intercalation compounds synthesized with various PSS/LDH mass ratios (100 ℃ for 24 hours).

The degree of intercalation efficiency was found to scale with the chain length of the polymer coordinators (Figure 8b). When α-ZrP is synthesized in the presence of PEG with a MW exceeding 1000 g/mol, only the intercalated product is observed. This result can be attributed to the cooperative action of ether subunits that allow PEG to be tethered to the growing α-ZrP framework. In order for PEG chains to be included within the growing crystal they must be sufficiently anchored onto the surface to prevent them from being displaced as the subsequent layer is nucleated. A long chain would statistically favor the anchoring of PEG chains, thus facilitating the formation of an intercalation compound.

It should be noted that the synthesized PEG/α-ZrP intercalation compounds exhibit the same interlayer distance, regardless of the PEG chain length or the PEG/α-ZrP mass ratio. This suggests that the intercalated PEG chains are parallel to the layers. Moreover, the thickness of linear PEG of ca. 2.8 Å (based on ChemDraw Ultra 7.0) is in an excellent agreement with the interlayer distance difference between the PEG/α-ZrP intercalation compounds (10.4 Å) and α-ZrP (7.6 Å), which further suggests PEG chains are parallel to the layer surface.

While the parallel conformation of PEG chains are expected based on the aforementioned formation hypothesis of the intercalated hybrids (Figure 5a), it should be noted that it is highly in contrast to the dominant trend in which intercalants tilt away from the layer surface to a certain angle, resulting in an interlayer distance proportional to chain length.[22] While many conventional

intercalants feature an interacting head group and an organic tail group, PEG forms hydrogen bonds to α-ZrP through its backbone oxygen atoms, favoring an extended conformation.

Figure 9 shows the SEM images of pristine α-ZrP and the intercalated PEG/α-ZrP compounds. Overall, all the intercalation compounds are similar in morphology. They are slightly smaller than the α-ZrP grown in the absence of PEG, which indicates that the presence of PEG only has marginal impact on the crystal growth in the lateral direction. This is consistent with our hypothesis that PEG predominately affects interlayer growth.

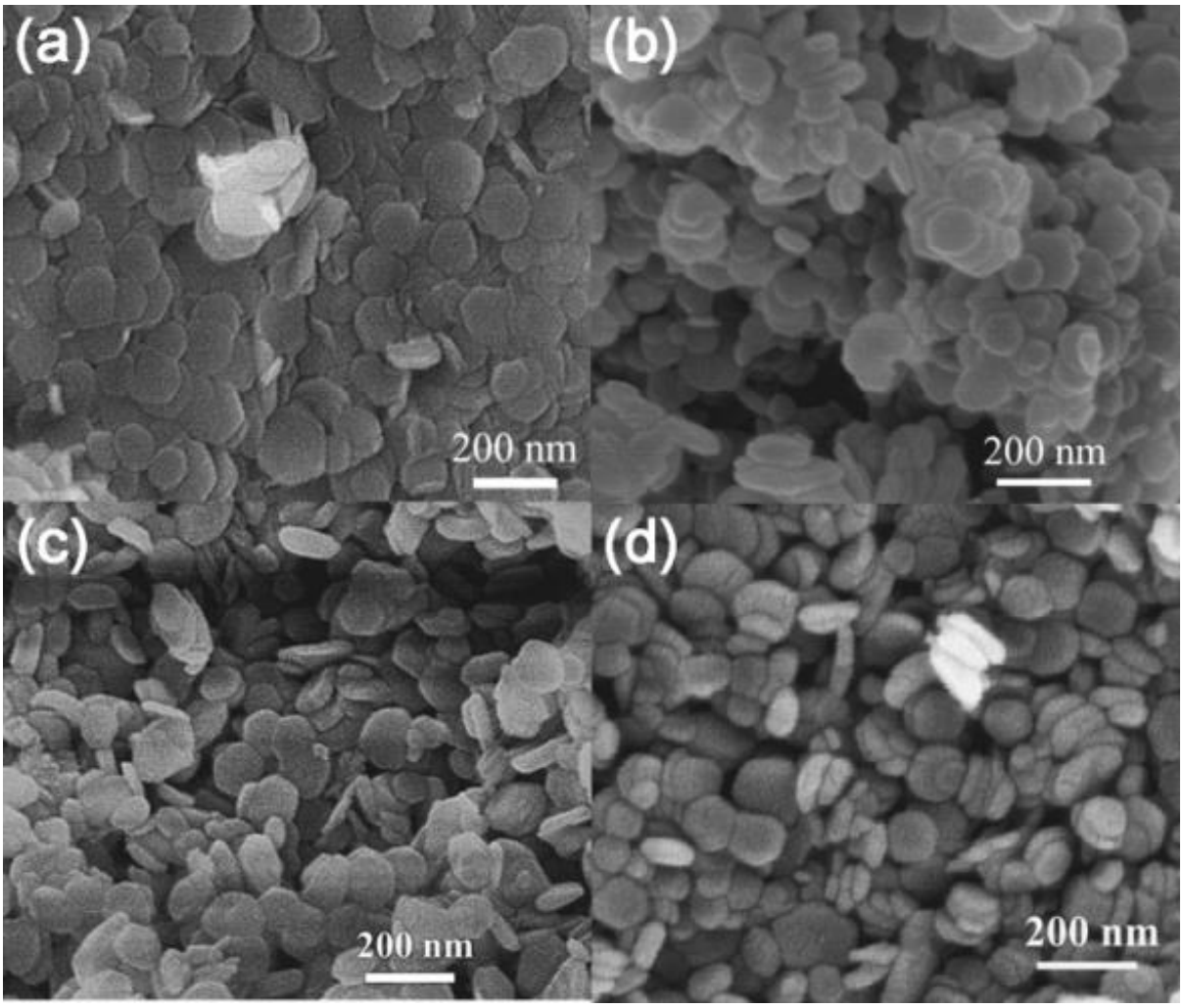

Figure 9. SEM images of α-ZrP based intercalation compounds. (a) α-ZrP, (b) PEG-600/α-ZrP (1.00:1), (c) PEG-1900/α-ZrP (1.00:1), and (d) PEG-8000/α-ZrP (1.00:1).

Various other coordinators, including other polymers (*e.g.*, polyethyleneimine (PEI), polyvinyl alcohol (PVA)), small molecules (*e.g.*, acrylamide), and ions (*e.g.*, 1-butyl-3-methylimidazolium ($BMIM^+$)) were also evaluated for the direct synthesis of α-ZrP based intercalation compounds because they can either form hydrogen bonds (*e.g.*, PEI, PVA, acrylamide) or electrostatic force (*e.g.*, $BMIM^+$) with α-ZrP layers. The characterization results proved that they can similarly form intercalation compounds with α-ZrP *via* a single step synthesis (see Figure 10), suggesting that the proposed methodology is general.

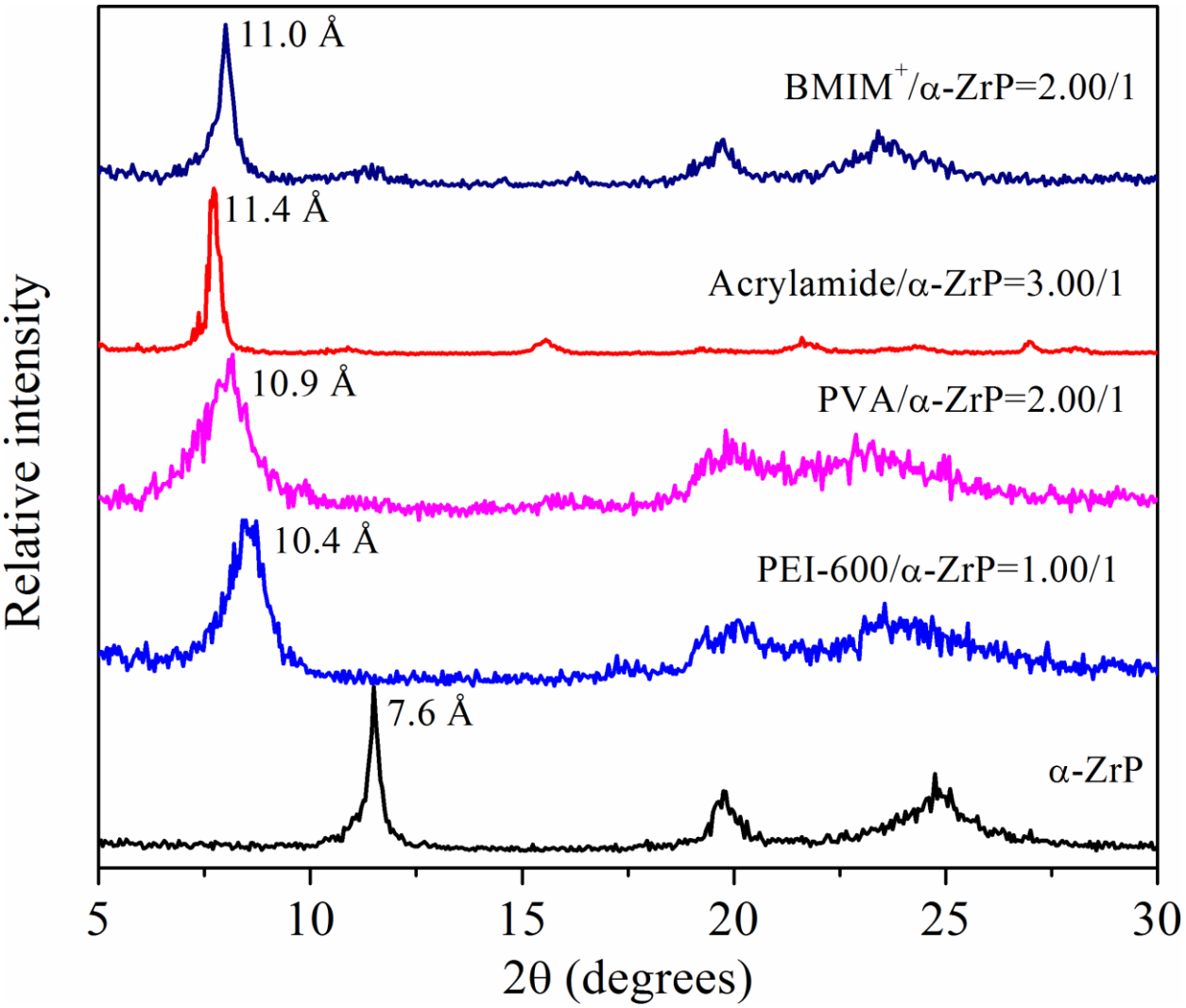

Figure 10. XRD patterns of α-ZrP based intercalation compounds. Those intercalation compounds were synthesized with various coordinators at 100 ℃ for 24 hours. The labeled ratio represents mass ratio.

Moreover, the direct synthesis of intercalation compounds based on another typical layered compound, Mg^{2+}/Al^{3+} LDH (hereafter MgAl-LDH), was also explored. Since the layers of MgAl-LDH is positively charged, a negatively charged polyelectrolyte, poly(sodium 4-styrenesulfonate) (PSS), was chosen as the coordinator, with an expectation that LDH layers and PSS can form a weak electrostatic force. The XRD characterization results are shown in Figure 8c, which shows a very similar trend as the direct synthesis of PEG/α-ZrP intercalation compounds as shown in Figure 8a). During the synthesis, a higher concentration of PSS favored the growth of the PSS/MgAl-LDH layered intercalation compounds. Meanwhile, the interlayer distance of the PSS/MgAl-LDH layered intercalation compounds remained virtually the same (20.0 Å), because PSS stayed parallel to the layer planes.

Overall, the above results on the direct growth of layered intercalation compounds based on two different layered materials using various coordinators, support that this one-step direct synthesis approach reported here is a general method applicable to various systems, thus promising to be adopted for widespread application.

The exfoliation of a layered phase typically requires the use of a large intercalant to weaken the interlayer interaction. Extensive processing may be required in order to complete the delamination process. For example, LDH may be exfoliated by first intercalating to increase the interlayer distance and then violently agitating the product for extended periods of time (usually 24 hours or longer) in a number of solvents, including butanol, acrylates, toluene, and formamide.[17] Li *et al*. reported the exfoliation of LDH in formamide without the intercalation

step, but it required ca. 2.5 days and large excess of formamide (ca. 0.05 g LDH in 100 mL formamide).[23] While the exact exfoliation mechanism of LDH has not yet been fully clarified, it was proposed that this occurs because the carbonyl group of formamide can solvate the LDH sheet surface, displacing the inherent interlayer water molecules.[24] The amine terminus of formamide forms relatively weak interactions with the interlayer anions, thereby weakening the overall interlayer attraction.[24] Other attempts to prepare thin LDH nanosheets focused on the control of reaction media (micelles) size. This allowed for the synthesis of LDH with controllable overall dimension and obtained LDH with only a few layers.[25-26] In contrast, our method focuses on tailoring the reaction conditions to inhibit Z-direction growth.

We conducted a quick synthesis (10 min) of Mg^{2+}/Al^{3+}-LDH (MgAl-LDH) directly in the presence of formamide (23 vol%) (See supporting information for details) with an expectation that formamide molecules can adhere to the LDH sheet surface, thus allowing the sheets to grow laterally while inhibiting interlayer growth (Figure 5b)). MgAl-LDH control sample synthesized in water using the titration method has an interlayer spacing of 7.9 Å, which is observable by X-ray diffraction when the particles are both in power form (See Figure 11 insert) and suspended in water (along with a broad peak at ca. 25.8 ° from Mylar® film[20] used to cover the liquid sample during analysis), as shown in Figure 12a-I. When MgAl-LDH was synthesized in the presence of formamide and characterized in a dispersion under the same conditions, no diffraction peaks were visible (Figure 12a-II), indicating the lack of long range ordering. When this dispersion sample was cast and dried onto a silicon wafer, a broad and intense diffraction peak at 11.02 ° (8.0 Å) was observed (Figure 12a-III). The diffraction peak is assigned to the interlayer spacing of the re-stacked colloidal MgAl-LDH nanosheets. The slightly increased interlayer distance is attributed to turbostratic disordering and residual water within the interlayer galleries.[27] The

virtually transparent MgAl-LDH aqueous dispersion clearly exhibited the Tyndall effect (Figure 12a inset), which supports the existence of colloidal LDH nanosheets in the dispersion. After centrifuge, a gel like sample was collected, which were loosely and randomly stacked LDH nanosheets. This gel like sample did not show any peak in low-angle regions, but a (*110*) peak at ca. 60 ° corresponding to LDH in-plane diffraction[28] was observed, indicating the presence of sheet structure in the sample (Figure 13). This further supports the formation of LDH nanosheets with virtually no stacking. Analysis of the synthesized MgAl-LDH by transmission electron microscopy (TEM, Figure 12b) revealed pseudohexagonal nanosheets with a size distribution of ca. 25-50 nm in diameter.

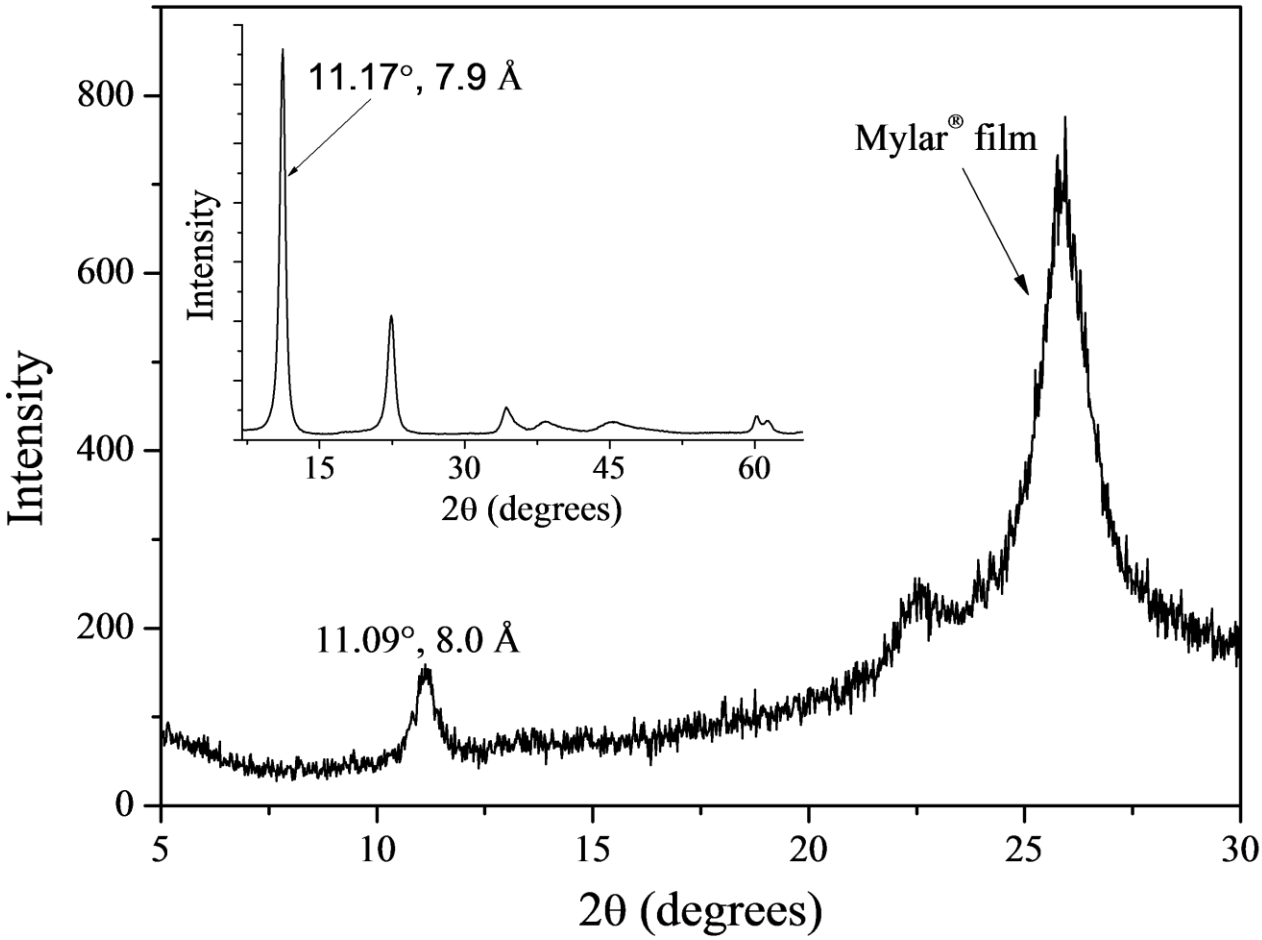

Figure 11. XRD patterns of the pre-synthesized MgAl-LDH before (insert, dry solid) and after being stirred in an aqueous dispersion containing 23 vol% formamide at 80 ℃ for 10 min.

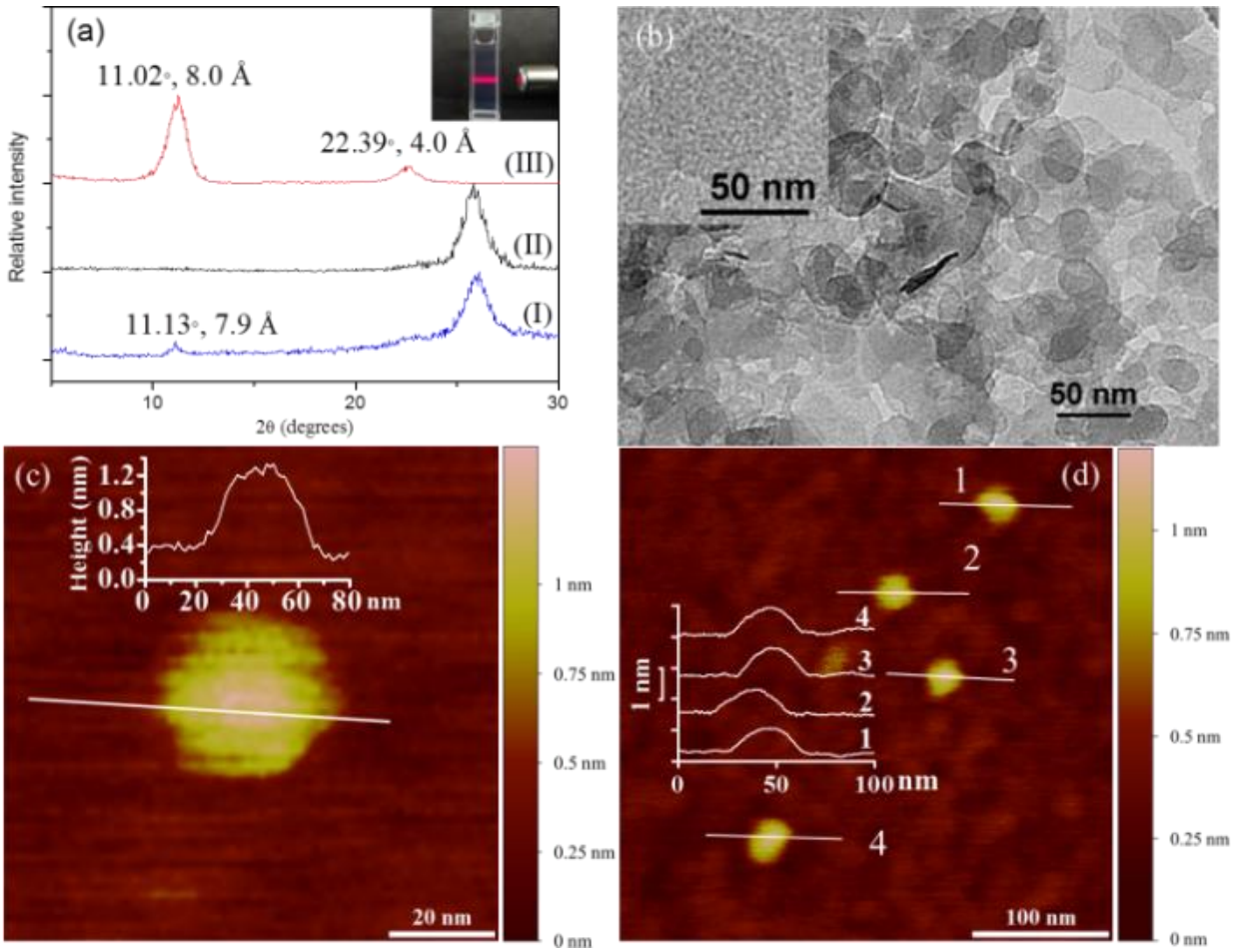

Figure 12. (a) XRD patterns of: (I) aqueous dispersion of MgAl-LDH control sample; (II) aqueous dispersion of directly synthesized MgAl-LDH single-layer nanosheets in the presence of formamide; and (III) re-stacked MgAl-LDH nanosheets on a silicon wafer after drying. Inset: sample (II) exhibiting Tyndall effect. (b) TEM image of MgAl-LDH single-layer nanosheets. Inset: an individual hexagon shaped LDH nanosheet. (c) AFM image of a pseudohexagonal MgAl-LDH nanosheet; (d) AFM image of multiple neighboring single-layer nanosheets.

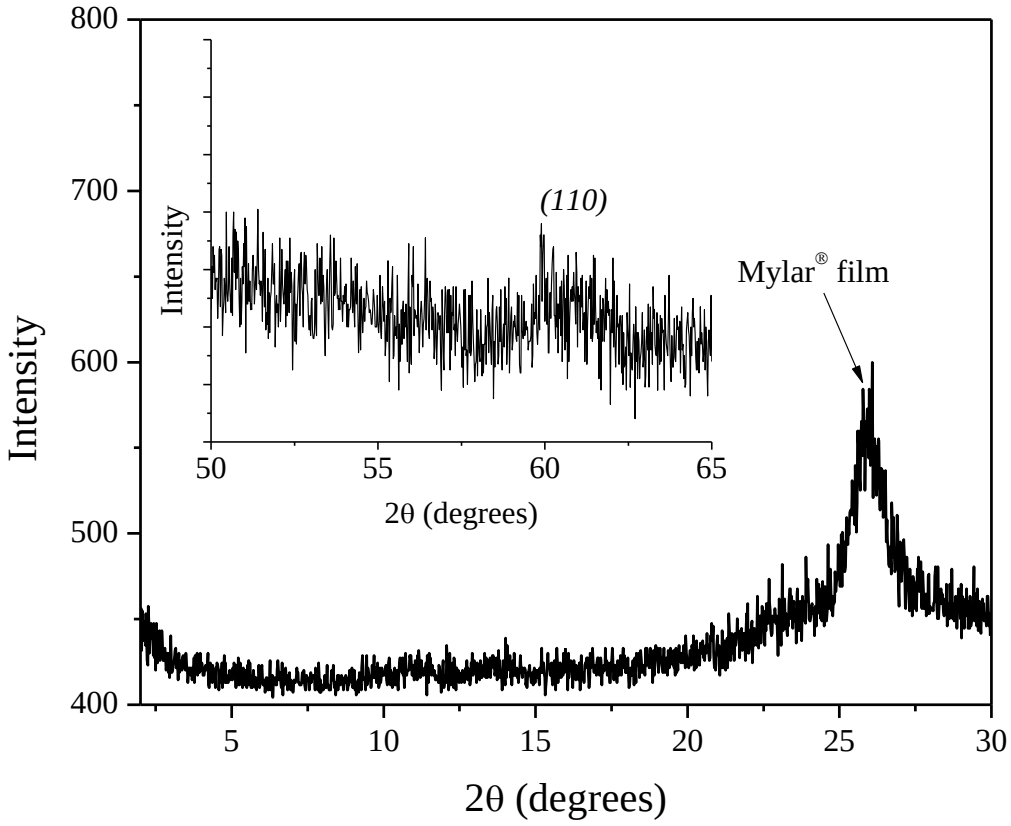

Figure 13. XRD patterns of the gel like MgAl-LDH nanosheets collected after centrifuge.

To further confirm the formation of single-layer MgAl-LDH nanosheets, the synthesized sample was cast on a silicon wafer and characterized by AFM. Figure 12c and d show representative AFM images of the MgAl-LDH nanosheets. The height of the nanosheets is ca. 0.8 nm. The theoretical thickness of a single layer of metal hydroxide is ca. 0.48 nm.[13, 29-30] The adsorption of formamide and counter-anions (NO_3^-) layer on the sheet surface is expected to be about 0.3 nm.[23, 31] Thus, the thickness from AFM imaging agrees well with the thickness of a single-layer MgAl-LDH nanosheet sandwiched by a layer of formamide and NO_3^- counter-anions, thus supporting that we indeed synthesized MgAl-LDH single-layer nanosheets.

In order to verify that the MgAl-LDH single-layer nanosheets were not generated through the exfoliation of the conventional multi-layered LDH, the MgAl-LDH control sample (as characterized in Figure 12a-I and Figure 14) was mixed in 23 vol% formamide aqueous solution and stirred vigorously for 10 min (the same duration used for the synthesis of MgAl-LDH in the presence of formamide). XRD analysis of this post-treated sample (Figure 11) revealed the presence of the characteristic (003) diffraction, demonstrating that it is not possible to delaminate pre-formed LDH by this brief treatment (the slightly increased interlayer distance from 7.9 to 8.0 Å is owing to the marginal swelling). To be noted, Figure 14 shows that the control LDH sample was barely crystalized, which is expected because of the very short reaction time. But their lateral dimension is close to the LDH single layer nanosheets as shown in Figure 12b.

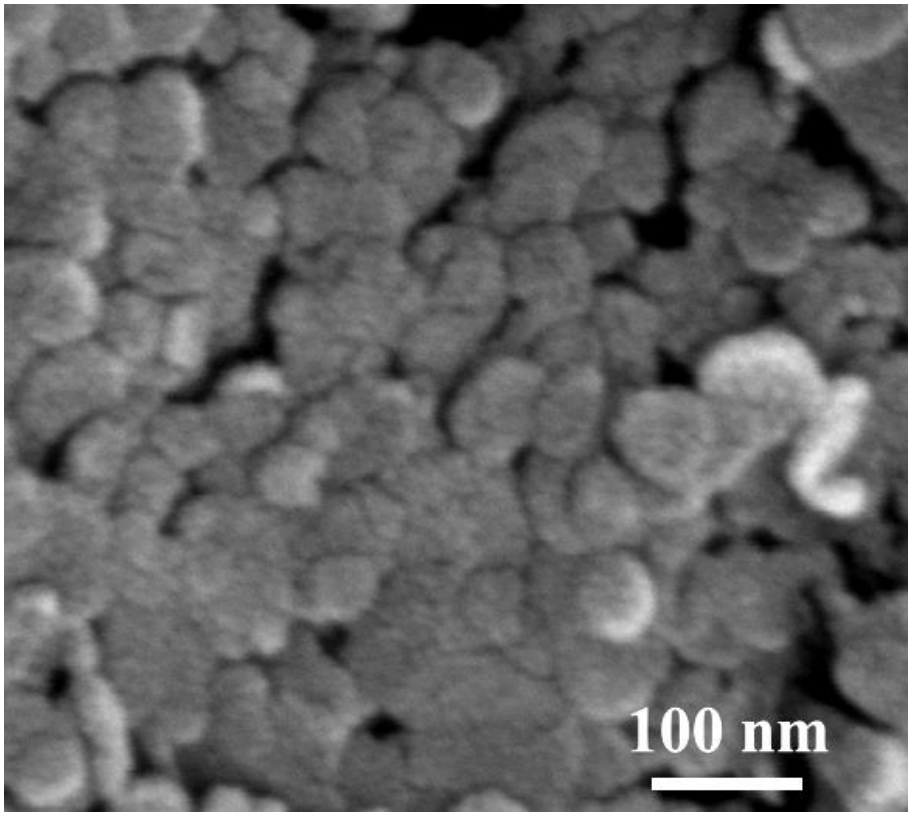

Figure 14. SEM image of the control MgAl-LDH sample synthesized at the absence of formamide.

It is possible that formamide serves multiple functions during the synthesis of single-layer nanosheets. In addition to the previously proposed interactions between the carbonyl groups of formamide with the hydroxide groups on the LDH sheet surfaces,[24] it is worth considering the unusually high dielectric constant of formamide ($\varepsilon = 111$ at 20 °C).[32] Formamide is used to prevent the precipitation of polyions, such as DNA.[33] The presence of formamide weakens the electrostatic interactions between the positively charged sheets and the negatively charged counterions,[34] which in turn lowers layer-layer interactions. Such an ion-ion interaction weakening effect by high dielectric constant solvents have been simulated and modeled.[35]

Likewise, Co^{2+}/Al^{3+} LDH (CoAl-LDH) single-layer nanosheets have been prepared *via* the one-step synthesis using formamide as a layer growth inhibitor (See Figure 15), and MgAl-LDH single-layer nanosheets have also been synthesized using another inhibitor, *N*, *N*-dimethyl formamide (See Figure 16). Based on the general principle of inhibiting as illustrated in Figure 5b, it is believed that these processes can be extended to other layered structures once a suitable inhibitor is identified.

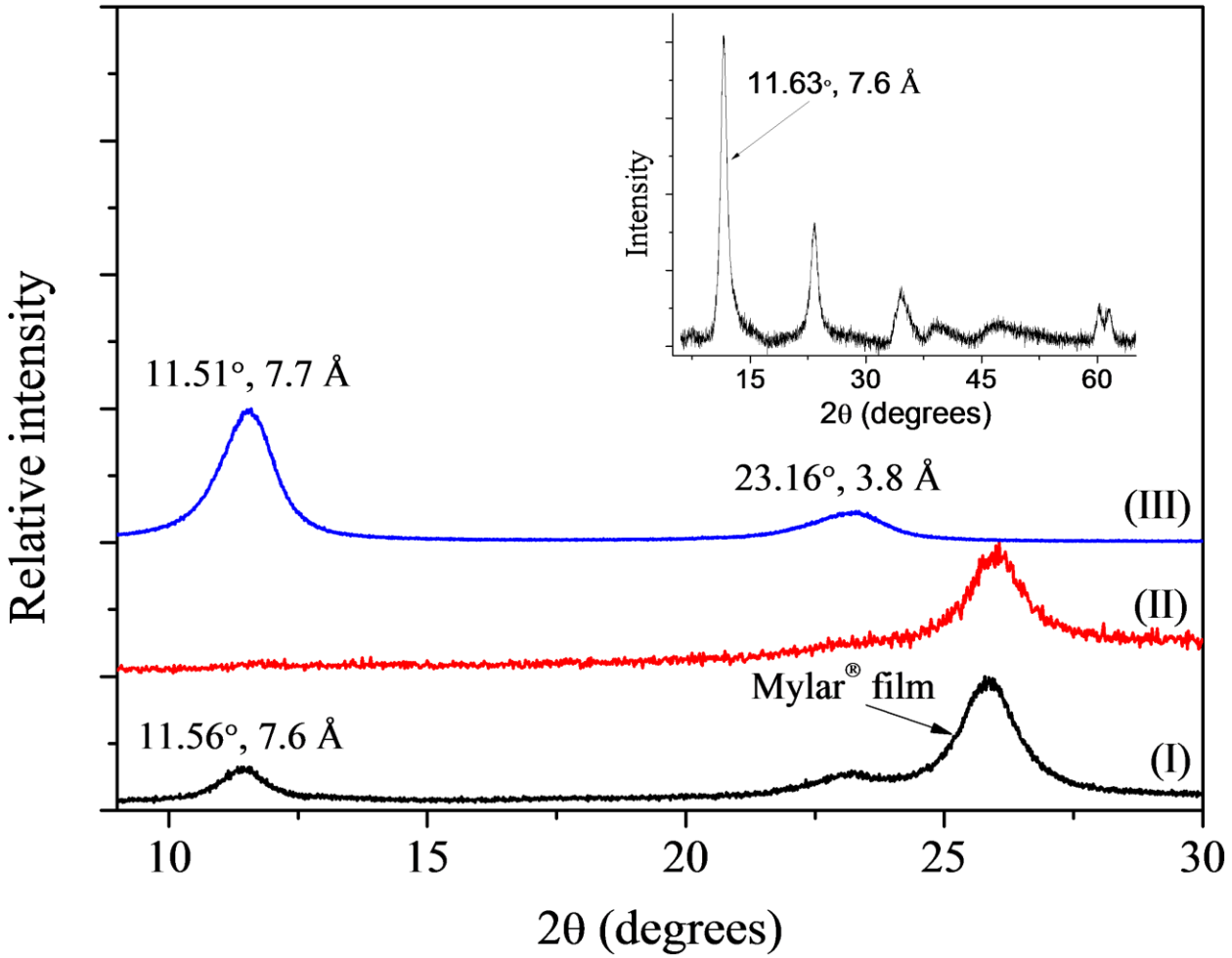

Figure 15. XRD patterns of CoAl-LDH single-layer nanosheets synthesized in the presence of formamide. (I) Aqueous dispersion of CoAl-LDH control sample, (II) aqueous dispersion of directly synthesized CoAl-LDH single-layer nanosheets in the presence of formamide; and (III) re-stacked CoAl-LDH nanosheets on a silicon wafer after drying. Inset: XRD pattern of CoAl-LDH control sample in powder form.

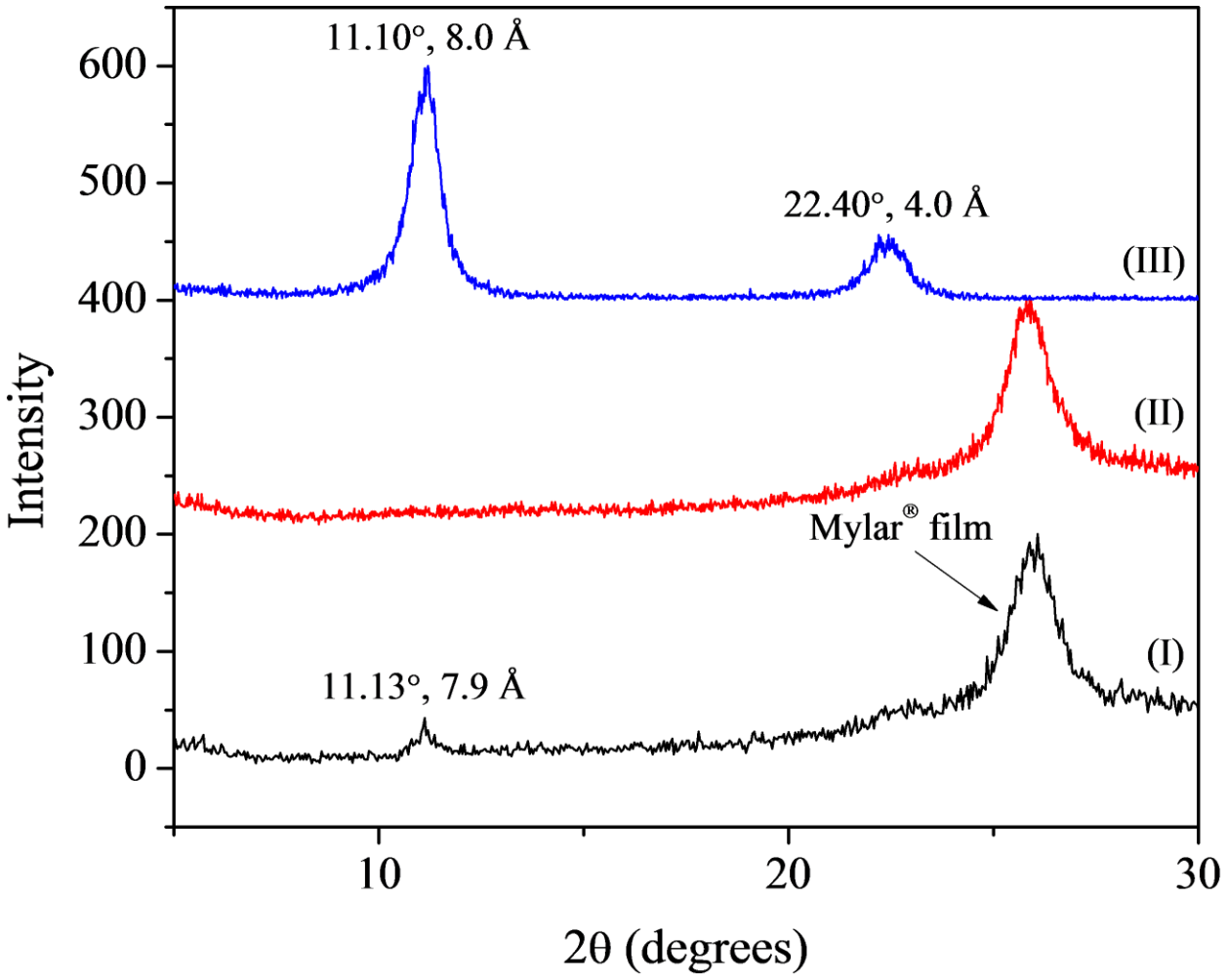

Figure 16. XRD patterns of MgAl-LDH single-layer nanosheets synthesized at the presence of another inhibitor, *N, N*-dimethyl formamide. (I) aqueous dispersion of MgAl-LDH control sample, (II) aqueous dispersion of directly synthesized MgAl-LDH single-layer nanosheets at the presence of *N, N*-dimethyl formamide; and (III) re-stacked MgAl-LDH nanosheets on a silicon wafer after drying.

2.4 Conclusions

We have shown that by introducing either a layer growth coordinator or inhibitor during synthesis, one can control morphology of the as-synthesized product. Such tunability is highly desirable for the design of layered intercalation compounds or single-layer nanosheets for various applications. The multiple examples have clearly demonstrated that the new methodology for direct synthesis of layered intercalation compounds and single layer nanosheets is very general. In fact, the underlying fundamental mechanism of the methodology is the control of the weak interactions between layers. Since weak interactions, including electrostatic forces and hydrogen bonds, widely exist, it is not surprising that this methodology can be applied to a wide range of layered materials and can serve as a valuable tool to create new materials.

The observation of single polymer layers between inorganic sheets in the PEG/α-ZrP intercalated hybrids also presents a unique nano-confinement environment for various molecules, which will be investigated later as a separate topic. This methodology not only allows access to materials that may not otherwise be synthesized, but the one step process also offers significant savings in both cost and time. For example, the 10-minute procedure outlined here to synthesize LDH single-layer nanosheets should be contrasted with the classical synthesis of LDH layered

structures typically requiring multiple hours, followed by an exfoliation process that can take multiple days.

References

1. Auerbach, S. M.; Carrado, K. A.; Dutta, P. K., *Handbook of Layered Materials*. Marcel Dekker, Inc.: New York, USA, 2004.

2. Addadi, L.; Weiner, S., Biomineralization: A pavement of pearl. *Nature* **1997,** *389*, 912-915.

3. O'Hare, D., Inorganic intercalation compounds. In *Inorganic Materials*, Bruce, D. W.; O'Hare, D., Eds. John Wiley & Sons: West Sussex, 1992; pp 165-235.

4. Müller-Warmuth, W.; Schöllhorn, R., *Progress in Intercalation Research*. Kluwer Academic Publisher: Dordrecht, The Netherlands, 1994.

5. Mallouk, T. E.; Kim, H.-N.; Ollivier, P. J.; Keller, S. W., Ultrathin Films Based on Layered Materials. In *Comprehensive Supramolecular Chemistry*, Alberti, G.; Bein, T., Eds. Elsevier: Oxford, UK, 1996; Vol. 7, pp 189-217.

6. Ma, R.; Sasaki, T., Nanosheets of Oxides and Hydroxides: Ultimate 2D Charge-Bearing Functional Crystallites. *Advanced Materials* **2010,** *22* (45), 5082-5104.

7. Coleman, J. N.; Lotya, M.; O'Neill, A.; Bergin, S. D.; King, P. J.; Khan, U.; Young, K.; Gaucher, A.; De, S.; Smith, R. J.; Shvets, I. V.; Arora, S. K.; Stanton, G.; Kim, H.-Y.; Lee, K.; Kim, G. T.; Duesberg, G. S.; Hallam, T.; Boland, J. J.; Wang, J. J.; Donegan, J. F.; Grunlan, J. C.; Moriarty, G.; Shmeliov, A.; Nicholls, R. J.; Perkins, J. M.; Grieveson, E. M.; Theuwissen, K.; McComb, D. W.; Nellist, P. D.; Nicolosi, V., Two-Dimensional Nanosheets Produced by Liquid Exfoliation of Layered Materials. *Science* **2011,** *331*, 568-571.

8. Heywood, B. R.; Mann, S., Template-directed nucleation and growth of inorganic materials. *Advanced Materials* **1994,** *6* (1), 9-20.

9. Gabriella, G.; Jiří, K.; Felix, F.-A.; Angelos, M., Improved description of soft layered materials with van der Waals density functional theory. *Journal of Physics: Condensed Matter* **2012,** *24* (42), 424216.

10. Grégoire, B.; Ruby, C.; Carteret, C., Structural Cohesion of MII-MIII Layered Double Hydroxides Crystals: Electrostatic Forces and Cationic Polarizing Power. *Crystal Growth & Design* **2012,** *12* (9), 4324-4333.

11. Tosoni, S.; Doll, K.; Ugliengo, P., Hydrogen Bond in Layered Materials: Structural and Vibrational Properties of Kaolinite by a Periodic B3LYP Approach. *Chemistry of Materials* **2006,** *18* (8), 2135-2143.

12. Clearfield, A.; Costantino, U., Layered metal phosphates and their intercalation chemistry. In *Comprehensive Supramolecular Chemistry*, Alberti, G.; Bein, T., Eds. Elsevier: Oxford, UK, 1996; Vol. 7, pp 107-149.

13. Cavani, F.; Trifiro, F.; Vaccari, A., Hydrotalcite-type anionic clays: Preparation, properties and applications. *Catalysis Today* **1991,** *11* (2), 173-301.

14. Khan, A. I.; O'Hare, D., Intercalation chemistry of layered double hydroxides: recent developments and applications. *Journal of Materials Chemistry* **2002,** *12* (11), 3191-3198.

15. Kim, H. N.; Keller, S. W.; Mallouk, T. E.; Schmitt, J.; Decher, G., Characterization of zirconium phosphate polycation thin films grown by sequential adsorption reactions. *Chemistry of Materials* **1997,** *9* (6), 1414-1421.

16. Alberti, G.; Casciola, M.; Costantino, U., Inorganic ion-exchange pellicles obtained by delamination of α-zirconium phosphate crystals. *Journal of Colloid and Interface Science* **1985,** *107* (1), 256-263.

17. Wang, Q.; O'Hare, D., Recent Advances in the Synthesis and Application of Layered Double Hydroxide (LDH) Nanosheets. *Chemical Reviews* **2012,** *112* (7), 4124-4155.

18. Wang, J.; Huang, L.; Gao, Y.; Yang, R.; Zhang, Z.; Guo, Z.; Wang, Q., A simple and reliable method for determining the delamination degree of nitrate and glycine intercalated LDHs in formamide. *Chemical Communications* **2014,** *50* (70), 10130-10132.

19. Sun, L.; Boo, W. J.; Sue, H.-J.; Clearfield, A., Preparation of [small alpha]-zirconium phosphate nanoplatelets with wide variations in aspect ratios. *New Journal of Chemistry* **2007,** *31* (1), 39-43.

20. Sun, L.; Boo, W. J.; Sun, D.; Clearfield, A.; Sue, H.-J., Preparation of Exfoliated Epoxy/α-Zirconium Phosphate Nanocomposites Containing High Aspect Ratio Nanoplatelets. *Chemistry of Materials* **2007,** *19* (7), 1749-1754.

21. Hibino, T.; Yamshita, Y.; Kosuge, K.; Tsunashima, A., Decarbonation Behavior of Mg-Al-CO_3 Hydrotalcite-like Compounds During Heat-treatment. *Clays and Clay Minerals* **1995,** *43* (4), 427-432.

22. Clearfield, A.; Tindwa, R. M., On the mechanism of ion exchange in zirconium phosphates—XXI Intercalation of amines by α-zirconium phosphate. *Journal of Inorganic and Nuclear Chemistry* **1979,** *41* (6), 871-878.

23. Li, L.; Ma, R.; Ebina, Y.; Iyi, N.; Sasaki, T., Positively Charged Nanosheets Derived via Total Delamination of Layered Double Hydroxides. *Chemistry of Materials* **2005,** *17* (17), 4386-4391.

24. Ma, R.; Liu, Z.; Li, L.; Iyi, N.; Sasaki, T., Exfoliating layered double hydroxides in formamide: a method to obtain positively charged nanosheets. *Journal of Materials Chemistry* **2006,** *16* (39), 3809-3813.

25. Wang, C. J.; Wu, Y. A.; Jacobs, R. M. J.; Warner, J. H.; Williams, G. R.; O'Hare, D., Reverse Micelle Synthesis of Co−Al LDHs: Control of Particle Size and Magnetic Properties. *Chemistry of Materials* **2010,** *23* (2), 171-180.

26. Wongariyakawee, A.; Schaeffel, F.; Warner, J. H.; O'Hare, D., Surfactant directed synthesis of calcium aluminum layered double hydroxides nanoplatelets. *Journal of Materials Chemistry* **2012,** *22* (16), 7751-7756.

27. Hou, X.; Bish, D. L.; Wang, S.-L.; Johnston, C. T.; Kirkpatrick, R. J., Hydration, expansion, structure, and dynamics of layered double hydroxides. *American Mineralogist* **2003,** *88* (1), 167-179.

28. Liu, Z.; Ma, R.; Osada, M.; Iyi, N.; Ebina, Y.; Takada, K.; Sasaki, T., Synthesis, Anion Exchange, and Delamination of Co-Al Layered Double Hydroxide. Assembly of the Exfoliated Nanosheet/Polyanion Composite Films and Magneto-Optical Studies. *Journal of the American Chemical Society* **2006,** *128* (14), 4872-4880.

29. Hibino, T., Delamination of Layered Double Hydroxides Containing Amino Acids. *Chemistry of Materials* **2004,** *16* (25), 5482-5488.

30. Miyata, S., The Syntheses of Hydrotalcite-Like Compounds and Their Structures and Physico-Chemical Properties I: The Systems Mg^{2+}-Al^{3+}-NO_3^-, Mg^{2+}-Al^{3+}-Cl^-, Mg^{2+}-Al^{3+}-ClO_4^-, Mg^{2+}-Al^{3+}-Cl^- and Zn^{2+}-Al^{3+}-Cl^-. *Clays and Clay Minerals* **1975,** *23*, 369-375.

31. Liu, Z.; Ma, R.; Ebina, Y.; Iyi, N.; Takada, K.; Sasaki, T., General Synthesis and Delamination of Highly Crystalline Transition-Metal-Bearing Layered Double Hydroxides. *Langmuir* **2006,** *23* (2), 861-867.

32. Wohlfarth, C., Permittivity (dielectric constant) of liquids. In *Handbook of Chemistry and Physics (77th)*, Lide, D. R., Ed. CRC Press, Inc.: Boca Raton, Florida, 1996; pp 6-151.

33. Flock, S.; Labarbe, R.; Houssier, C., Dielectric constant and ionic strength effects on DNA precipitation. *Biophysical Journal* **1996,** *70* (3), 1456-1465.

34. Essex, J. W.; Jorgensen, W. L., Dielectric constants of formamide and dimethylformamide via computer simulation. *Journal of Physical Chemistry* **1995,** *99* (51), 17956-17962.

35. Hwang, K.-J.; Nam, K.-Y.; Kim, J. S.; Cho, K.-H.; Kong, S.-G.; No, K. T., The influence of dielectric constant on ionic and non-polar interactions. *Bulletin of the Korean Chemical Society* **2003,** *24*, 55-59.

CHAPTER 3

IN SITU SYNTHESIS OF LAYERED DOUBLE HYDROXIDE/POLYELECTROLYTE INTERCALATION COMPOUNDS

3.1 Introduction

Layered double hydroxide (LDH) with positively charged layers as the host layered material and poly(sodium 4-styrene-sulfonate) (PSSNa) as the layer growth coordinator were selected to study the one-step direct synthesis of layered intercalation compounds. PSSNa is a strong polyelectrolyte that fully dissociates in water and forms PSS^-. Thus, the negatively charged PSS^- can coordinate the growth of LDH layers due to electrostatic interactions, as reported in Chapter 2.

However, only one type of PSSNa with a weight average molecular weight (M_w) of 70,000), and only one PSSNa/LDH weight ratio (2.2:1, where PSSNa was in excess) was investigated.[1] The detailed intercalation mechanism is to be further investigated to achieve a deeper understanding. It is important to understand how the chain length and the concentration of the polyelectrolytes will affect the growth of the intercalation compounds. It was revealed in our previous work that at relatively low molecular weights, the intercalation efficiency increases when the molecular weight is relatively higher during the direct growth of α-zirconium phosphate/poly(ethylene glycol) (α-ZrP/PEG) layered intercalation compounds (Chapter 2). In this chapter, we will focus to investigate the effect of high molecular weight polyelectrolytes.

Magnesium and aluminum layered double hydroxide (MgAl-LDH, with a formula Mg/Al molar ratio of 4) was chosen as the layer host. A series of PSSNa electrolytes with three different M_w of 70,000, 200,000, and 500,000 were chosen as the targeted polyelectrolytes in high molecular weights range. The growth of MgAl-LDH was achieved through a urea hydrolysis method.[2] Well crystalized LDH can be obtained because urea hydrolyzes at elevated temperatures and allows for a slow release of OH^-, which ensures a homogeneous pH distribution throughout the reaction, leading to the formation LDH with an overall high crystallinity.

3.2 Experimental

Materials

Poly(sodium 4-styrene-sulfonate) (M_w 70,000, 35 wt.% aqueous solution; M_w 200,000, 30 wt.% aqueous solution; M_w 500,000, powder; all from Sigma-Aldrich), urea (>99.0%, J.T. Baker), $Mg(NO_3)_2$ $6H_2O$ (98%, Alfa Aesar), and $Al(NO_3)_3$ $9H_2O$ (99%, Acros Organics) were all used as received without further purification.

Direct growth of layered intercalation compounds

In a typical experiment, PSSNa/LDH intercalation compound was synthesized by mixing a pre-determined amount of PSSNa with metal salts ($Mg(NO_3)_2$, $Al(NO_3)_3$) in 30 mL of D.I. water. The molar ratio of Mg^{2+}:Al^{3+} was set at 4:1. The total metal ion concentration was 0.25 M. Urea was added to the metal salts solution at a molar ratio of urea:total metal ion at 4:1. The reaction mixture was well mixed, and then added to a Teflon lined hydrothermal reactor and heated at 100 ℃ for 24 hours. After reaction, the samples were washed and centrifuged with D.I. water for three times. The products recovered from centrifugation were dried in an oven at 80 ℃

for 24 hours. All samples were ground into powders with a mortar and pestle for characterization.

PSSNa /LDH intercalation compounds were prepared using three PSSNa with an M_w of 500,000, 200,000, and 70,000. The mass ratio of PSSNa to LDH was varied from 0.125:1 to 1.000:1 (assume all metal salts were converted to LDH) to study the intercalation behaviors.

Characterization

Fourier transform infrared (FT-IR) spectra were recorded on a Nicolet Magna 560 FT-IR spectrophotometer. The samples were mixed with KBr and compressed into pellets for characterization. Thermal properties of the samples were characterized by a thermogravimetric analyzer (TGA, TA Instruments model Q500) in an air atmosphere (40 mL/min) at a heating rate of 10 ℃/min. X-ray diffraction (XRD) patterns were recorded on a Bruker D5 diffractometer with Cu Kα radiation (λ = 1.5406 Å, 40 kV, 40 mA). Helios NanoLab 400 Dual Beam field emission scanning electron microscope (FE-SEM) from FEI was employed for SEM imaging.

3.3 Results and discussion

After reaction, three sets of PSSNa/LDH intercalation compounds with various PSSNa/LDH mass ratios were obtained. XRD and FT-IR were performed to characterize the products and study the intercalation efficiency. TGA was performed to study the thermal behavior of the products and estimate the content of organic components in the intercalation compounds. SEM images revealed the morphology of the synthesized intercalation compounds.

XRD analysis

XRD patterns of PSSNa/LDH intercalation compounds are shown in Figure 17 ((a)-(c)), where the position of the first diffraction peak (corresponding to the interlayer distance) of all intercalation compounds was shifted to lower angles compared to the LDH control sample.

All intercalation compounds exhibited an interlayer distance close to ca. 20.0 Å,[1, 3-4] regardless of PSSNa/LDH weight ratio. This interlayer distance was the result of the strong electrostatic interactions between the positively charged LDH layers and the negatively charged PSS^-, where the interlayer expansion of ca. 12.4 Å (from ca. 7.6 to 20.0 Å) was ascribed to the incorporation of one layer of PSS^-.

A one-layer PSS^- packing structure was proposed (Figure 17(d)) where the negatively charged sulfonic groups facing the positively charged LDH layers, maximizing the electrostatic interactions. Commercially available polystyrenes are atactic, thus, the phenyl groups are randomly distributed on both sides of the linear polymer chain. The largest distance from an oxygen atom on one sulfonic group to another oxygen atom at the opposite side of the polymer backbone is ca. 13.6 Å (based on ChemBioDraw Ultra 12.0). Because of the bond angles and geometry, the thickness of PSS^- should be slightly less than 13.6 Å, which explains the interlayer expansion (12.4 Å) of the PSSNa/LDH intercalation compounds.

This proposed one-layer arrangement of PSS^- in between LDH layers is supported by the XRD results that when the mass ratio of PSSNa/LDH was increased from 0.125/1 to 0.500/1, two phases (pristine LDH and PSSNa intercalated LDH) co-existed and the d value barely changed (ca. 19.0 Å). For PSSNa with a M_w of 70,000 (Figure 17 (a)), further increasing the PSSNa/LDH mass ratio to 0.750/1 and 1.000/1, the interlayer distance was increased to ca. 20.0 Å and only the intercalated LDH phase was observed, which indicates that the proposed structure is stable. Results of PSSNa/LDH mass ratio of 2.000/1 was also obtained (shown in Chapter 2,

Figure 8c), the interlayer distance remained at ca. 20.0 Å, which further supports the stability of the single layer arrangement of PSS^- in between LDH layers originated from the strong electrostatic interactions.

For PSSNa with an M_w of 200,000 (Figure 17 (b)), the same trend was observed. However, for PSSNa with an M_w of 500,000 (Figure 17 (c)), at PSSNa/LDH mass ratios as high as 0.750/1, there was still an observable amount of un-intercalated LDH phase present, which suggests the poor intercalation efficiency at high PSSNa M_w.

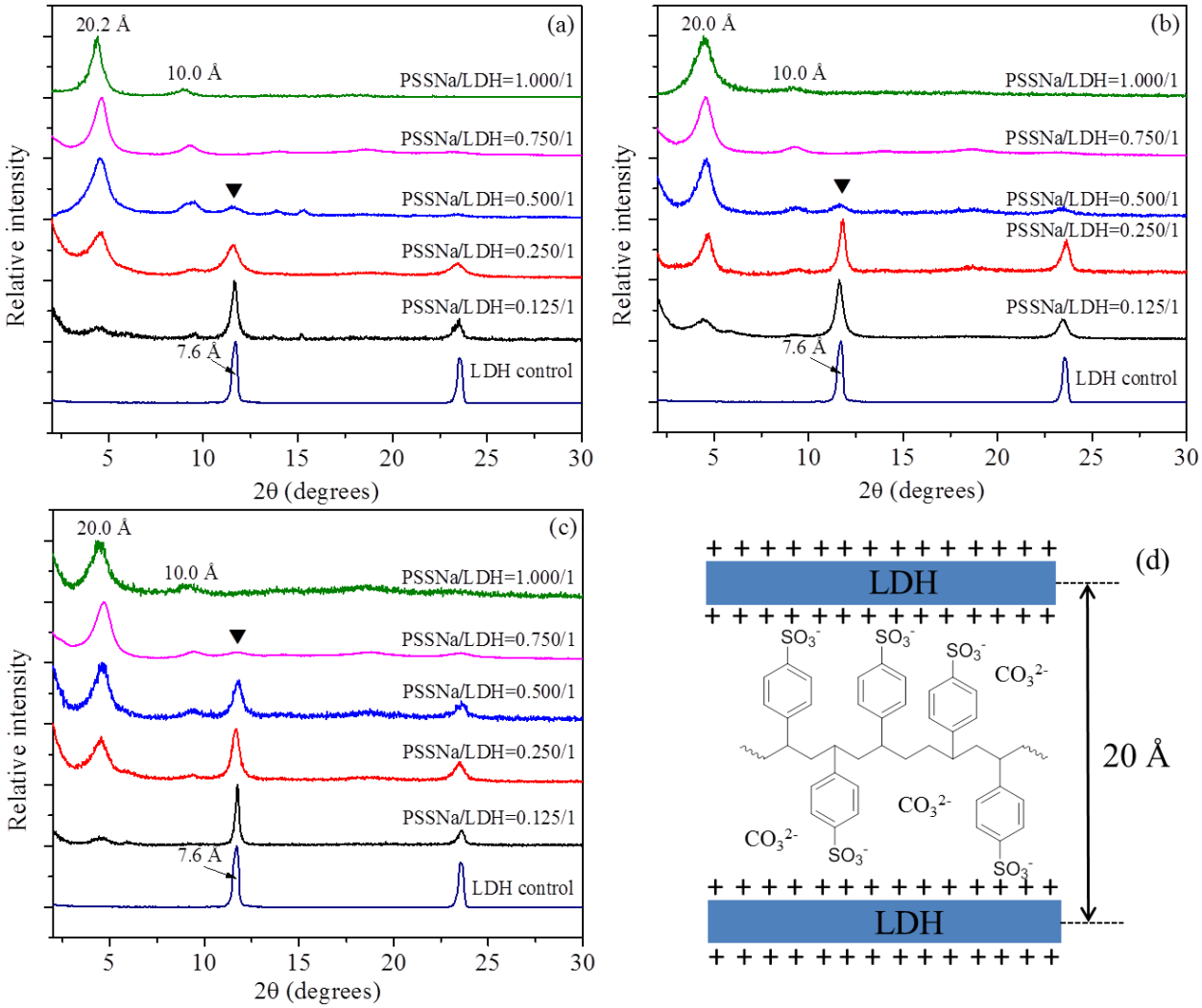

Figure 17. XRD patterns of PSSNa/LDH intercalation compounds with various PSSNa/LDH weight ratios: (a) PSSNa M_w 70,000, (b) PSSNa M_w 200,000, (c) PSSNa M_w 500,000 (▼

indicate the pristine LDH characteristic peak) and (d) proposed one-layer packing of PSS^- in the intercalation compounds.

XRD patterns of the intercalation compounds with the same M_w but various PSSNa/LDH mass ratios are compared in Figure 18. At a low PSSNa loading (Figure 18(a)), three M_w of PSSNa had virtually the same intercalation efficiency, where two phases co-existed in the product and LDH phase was the dominant phase over the PSSNa/LDH intercalation compound phase. This is probably because the amount of PSSNa used was so small, where only partial LDH can be intercalated by PSSNa. And because of the small amount, PSSNa could be fully incorporated into LDH interlayer regions regardless of the M_w. When the PSSNa/LDH mass ratio was increased to 0.250/1, the amount of the intercalation phase increased evidently for all three M_w (Figure 18(b)). When PSSNa/LDH mass ratio was at 0.500/1 (Figure 18(c)), the intercalation phase became the dominant phase and the intercalation efficiency of three M_w of PSSNa varied. The lowest M_w of 70,000 led to the highest intercalation efficiency and the efficiency decreased with an increasing M_w. Further increasing the PSSNa/LDH mass ratio to 0.750/1 (Figure 18(d)), only the intercalation phase existed for PSSNa M_w of 70,000 and 200,000. For PSSNa M_w of 500,000, LDH and the intercalation phase co-existed, which was consistent with the result from PSSNa/LDH =0.500/1, where the intercalation efficiency declined with an increasing M_w.

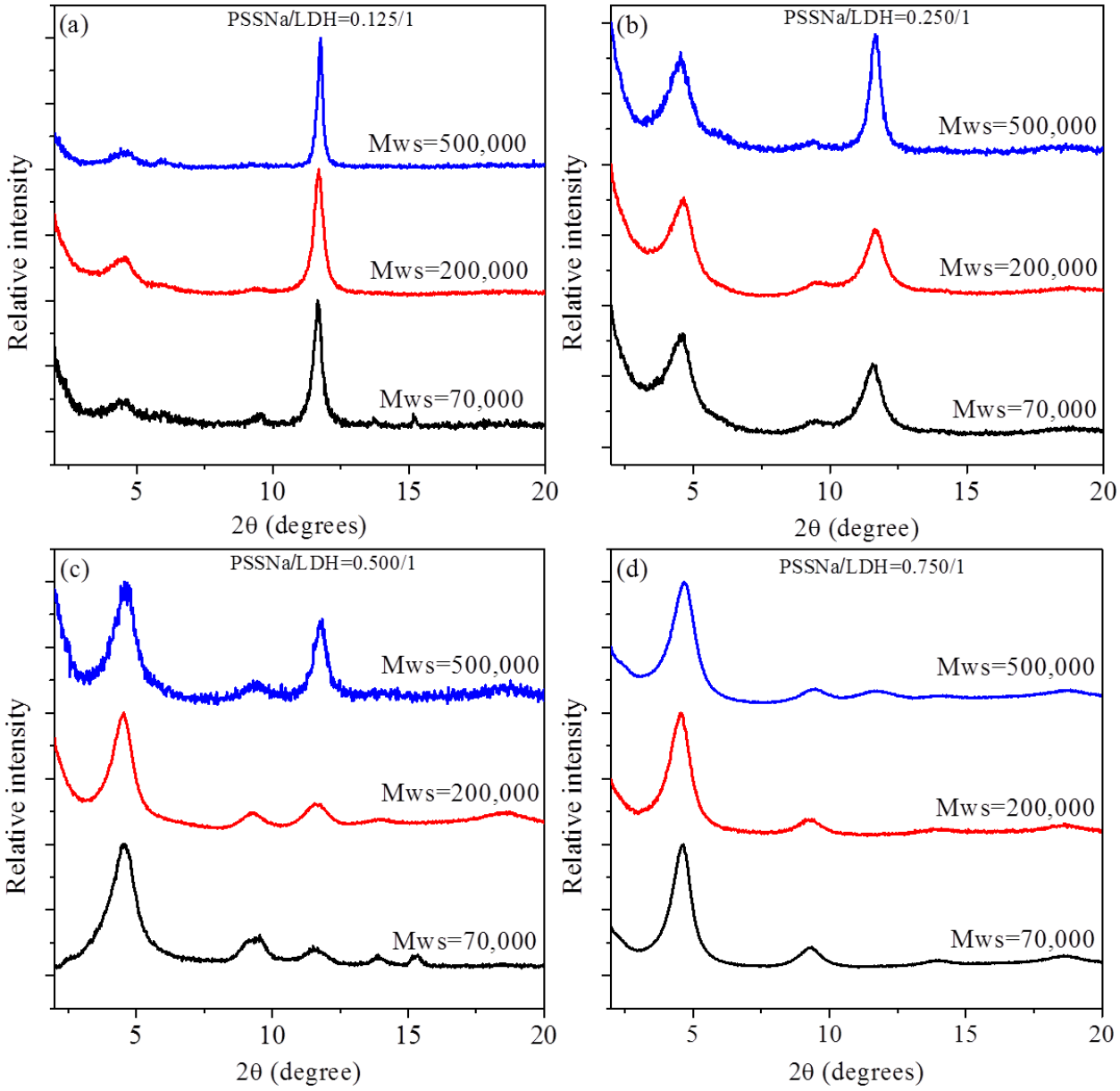

Figure 18. XRD patterns of the intercalation compounds formed with PSSNa with different M_w: **(**a) PSSNa/LDH =0.125/1; **(**b) PSSNa/LDH=0.250/1; **(**c) PSSNa/LDH=0.500/1; **(**d) PSSNa/LDH =0.750/1.

The intercalation efficiency of the three M_w of PSSNa was compared at PSSNa/LDH mass ratio from 0.125/1 to 0.750/1. The intercalation peak area and the LDH peak area of all the

samples were calculated, and are presented in Figure 19 and summarized in Table 1. The intercalation efficiency was similar when PSSNa was not sufficient (0.125/1and 0.250/1) regardless of M_w. When the PSSNa/LDH mass ratio was increased to 0.500/1, we found that the intercalation efficiency decreased with an increasing M_w.

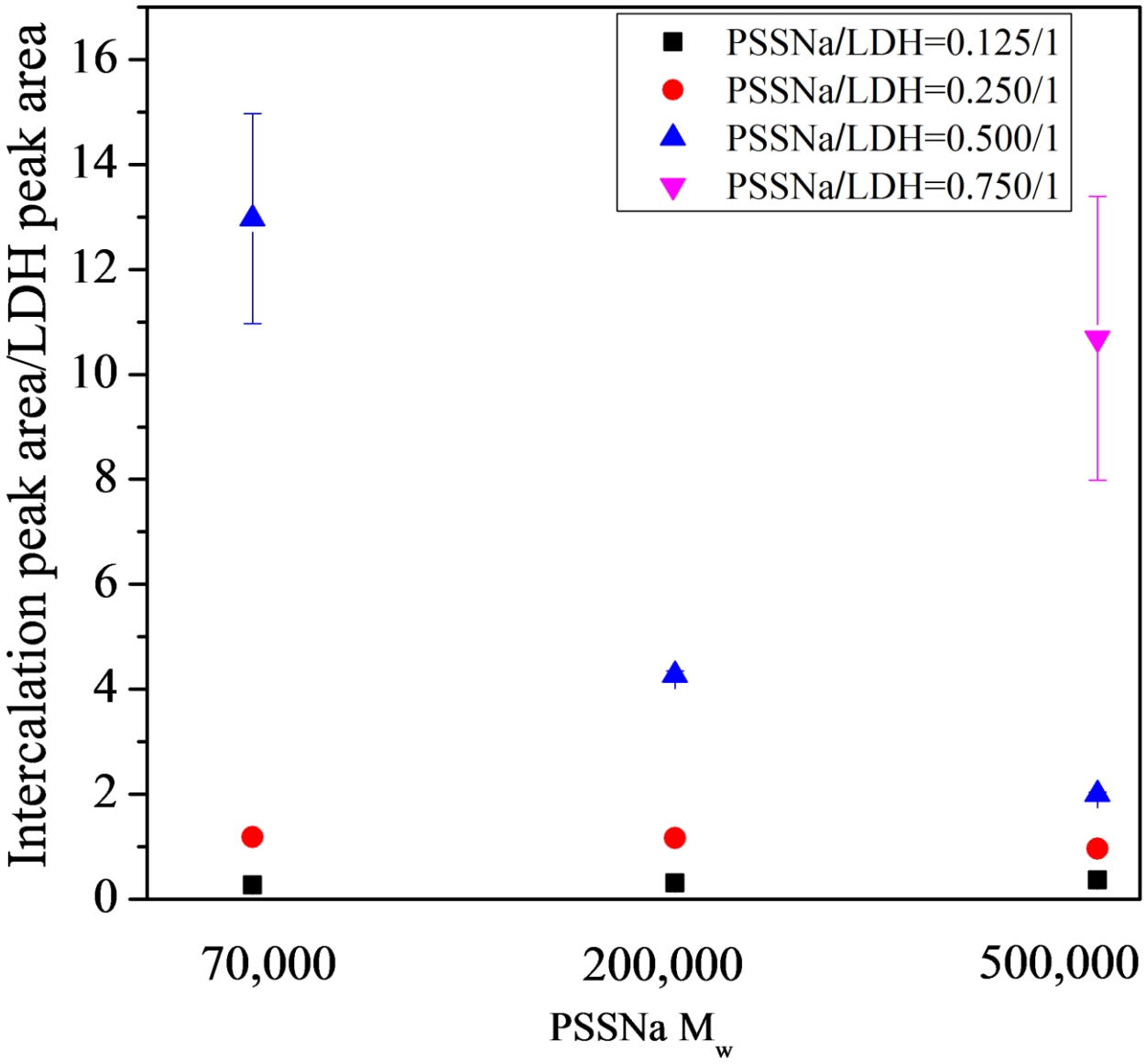

Figure 19. Intercalation trend of different M_w of PSSNa.

For PSSNa with relatively low $M_{w,}$ a larger amount of PSSNa can be incorporated into LDH interlayer region at same mass ratio of PSSNa/LDH (0.250/1) (Figure 18(c)) compared with the intercalation compounds of higher M_w PSSNa. The same trend was also observed at PSSNa/LDH mass ratio of 0.500/1, the peak area ratio of intercalation phase (d=20.0 Å) to LDH phase is decreased when PSSNa M_w is increased from 70,000 to 500,000. At PSSNa/LDH mass ratio of 0.750/1, this trend is more prominent where the peak area ratio is infinite for PSSNa M_w of 70,000 and 200,000 while the ratio is ca. 11 for PSSNa M_w of 500,000. This phenomenon indicates that at same PSSNa/LDH weight ratio, PSSNa with low M_w has higher intercalation efficiency.

Table 1. Summary of intercalation peak area to LDH peak area ratios.

M_w / PSSNa/LDH Ratio	70,000	200,000	500,000
0.125/1	0.27±0.020	0.31±0.010	0.37±0.025
0.250/1	1.18±0.075	1.16±0.030	0.96±0.015
0.500/1	12.97±2.000	4.27±0.080	2.00±0.035
0.750/1	∞	∞	10.96±2.700

In salt solution, PSSNa tends to shrink as the salt concentration is increased. Previous study[5] showed that the radius of gyration (R_g) of PSSNa decreased as the salt concentration was increased. When PSSNa M_n was ca. 55,000, its R_g decreased from 80±2 Å to 54±2 Å when salt concentration was increased from 0.0078 M to 0.3375 M. When salt concentration was 0.25 M, PSSNa had an R_g of 59.8±1.5 Å. It is known that the radius of gyration of a linear polyelectrolyte obeys the classical scaling law[6-7] in monovalent electrolyte solutions:

$$R_g \propto M^{\alpha}$$

where M is the molecular weight and α is the Flory exponent in the range of 0.5-0.6. Thus, R_g of PSSNa with various M_w under the same condition can be estimated. At PSSNa M_w of 55,000, its R_g reached a value of ca. 60 Å at salt concentration of 0.25 M,[5] which is much larger than the interlayer expansion of ca. 12.4 Å caused by one layer of PSS^- in between LDH layers as we observed in Figure 17. Under the same salt concentration, the R_g of each PSSNa with an increased M_w (70,000, 200,000, and 500,000) will increase exponentially. Thus, one can imagine that it will be much more difficult to align a layer of PSS^- in between LDH layers when the R_g of PSSNa is much larger than the interlayer expansion of ca. 12.4 Å. Difficulties to disentangle polymer chains, to unfold polymer chains, and to realign polymer chains may be the causes of the decreased intercalation efficiency when PSSNa M_w was increased.

FTIR analysis

FTIR was performed to further characterize the PSSNa/LDH intercalation compounds. Intercalation compounds with PSSNa M_w of 70,000, 200,000, and 500,000 were compared with LDH and PSSNa control samples (Figure 20, 21, and 22, respectively). LDH control sample showed one strong peak at 1370 cm^{-1}, which is ascribed to the stretching of C=O from CO_3^{2-} as shown in the spectra.[8] In the FTIR spectra, when PSSNa/LDH mass ratio was increased from 0.125/1 to 1.000/1, the intensity of the peak at 1370 cm^{-1} decreased. This result corresponded well with the XRD results that the intercalation phase increased when PSSNa/LDH mass ratio was increased. This indicates that the carbonate anions in LDH were gradually replaced by PSS^-. At 1040 and 1196 cm^{-1}, two strong peaks were caused by the symmetric stretch and asymmetric stretch of the vibrations of sulfonate $-SO_3^-$ in PSSNa.[9] These two characteristic absorption peaks were observed in all PSSNa/LDH intercalation compounds, which confirmed the presence of

PSSNa in these compounds. And an opposite trend compared to the peak at 1370 cm^{-1} was observed that when the PSSNa/LDH mass ratio was increased from 0.125/1 to 1.000/1, the intensity of the two peaks increased regardless of the M_w of PSSNa. This result is consistent with the result from the XRD patterns as well as the trend of the peak at 1370 cm^{-1} that PSS^- gradually replaced the carbonate anions in between LDH interlayer region.

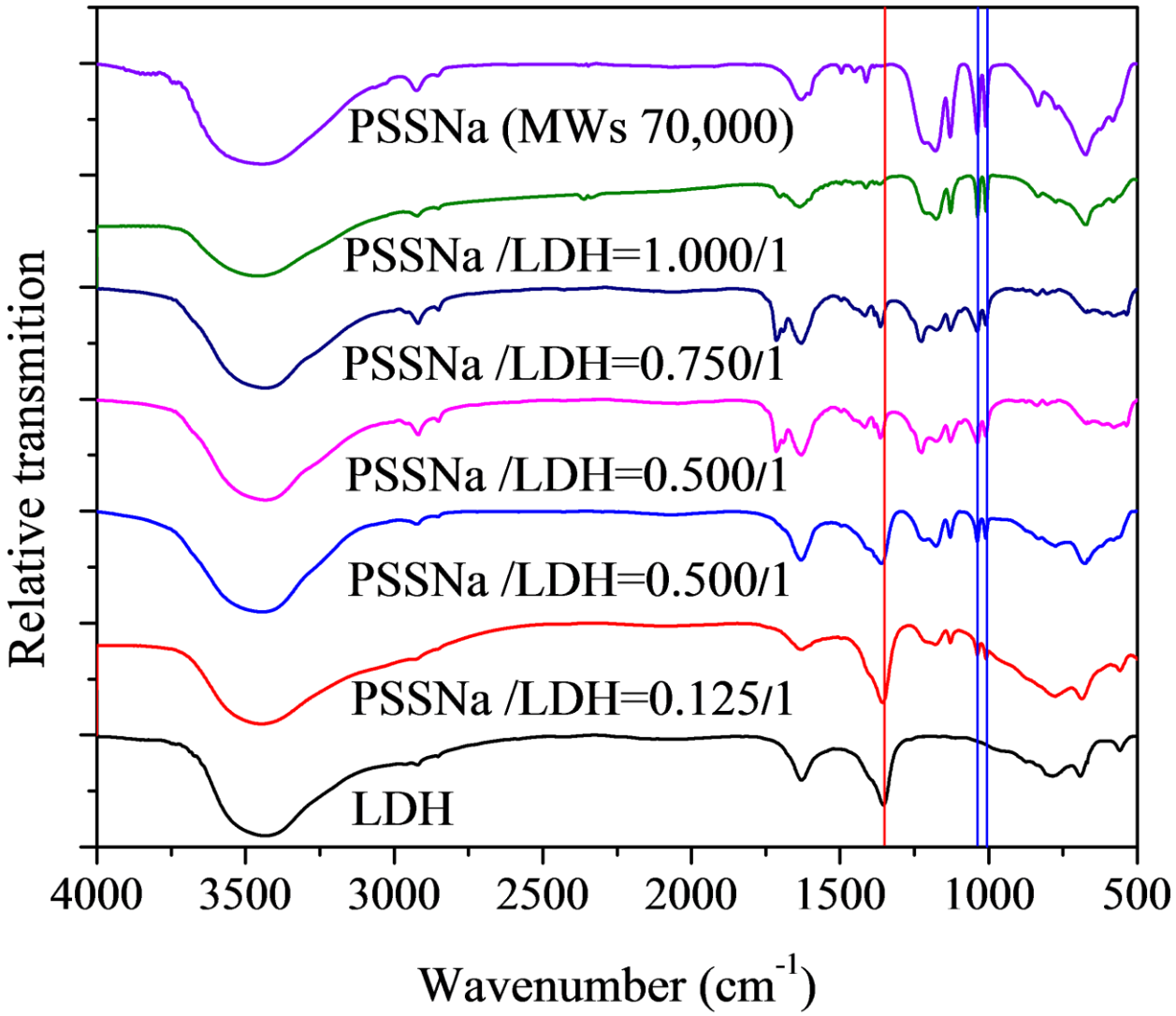

Figure 20. FTIR spectra of PSSNa/LDH intercalation compounds synthesized using PSSNa with a M_w of 70,000.

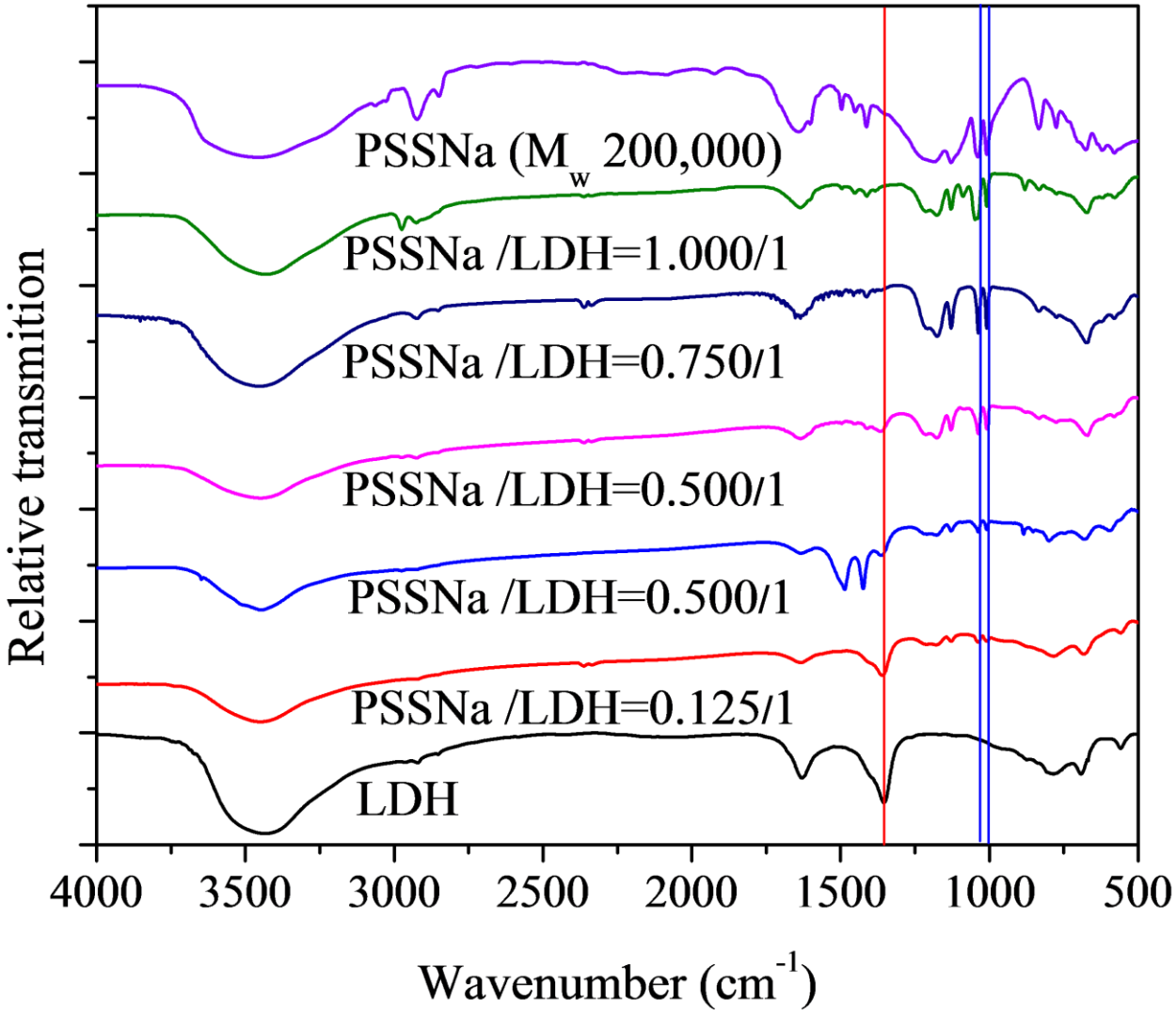

Figure 21. FTIR spectra of PSSNa/LDH intercalation compounds synthesized using PSSNa with a M_w of 200,000.

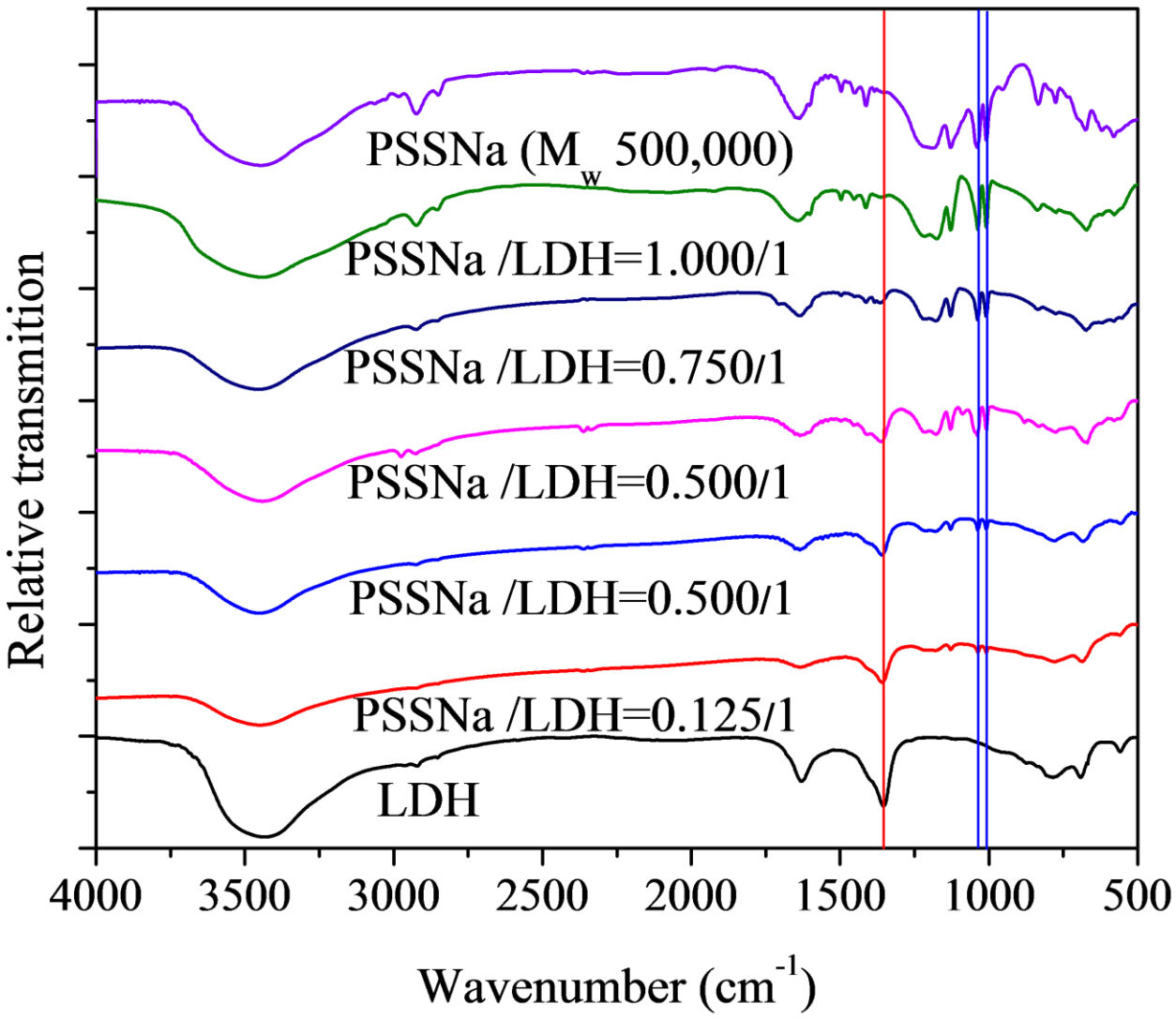

Figure 22. FTIR spectra of PSSNa/LDH intercalation compounds synthesized using PSSNa with a M_w of 500,000.

TGA analysis

For thermal analysis, all samples were tested in the solid phase (Figures 27, 28 and 29). PSSNa with an M_w of 70,000 and 200,000 were purchased in solution, thus they were dried in oven at 70 ℃ for 24 hours before testing.

Pristine LDH control sample has three stages of weight loss as observed from its TGA thermogram. The first weight loss at ca. 70-190 ℃ was ascribed to the loss of physically absorbed water. The second weight loss at ca. 190-320 ℃ was the loss of the water residing in the LDH interlayer regions.[10] The third weight loss at ca. 320-540 ℃ was from the decomposition of carbonate in between LDH layers and deconstruction of the hydroxyl layers.[10] The TGA thermograms of PSSNa with various M_w showed that they all started to decompose at ca. 420 ℃. Figure 23 showed the TGA thermograms of the PSSNa/LDH intercalation compounds (PSSNa M_w 70,000) in comparison to LDH and PSSNa (M_w 70,000) control samples. At PSSNa/LDH mass ratio of 1.000:1, two stages of weight loss were observed. The first weight loss stage at ca. 30-430 ℃ was due to the evaporation of physically absorbed water and loss of interlayer water. The second stage was between ca. 430-650 ℃, owing to the de-hydroxylation of LDH layers, de-carbonation, and partial decomposition of PSSNa.[11]

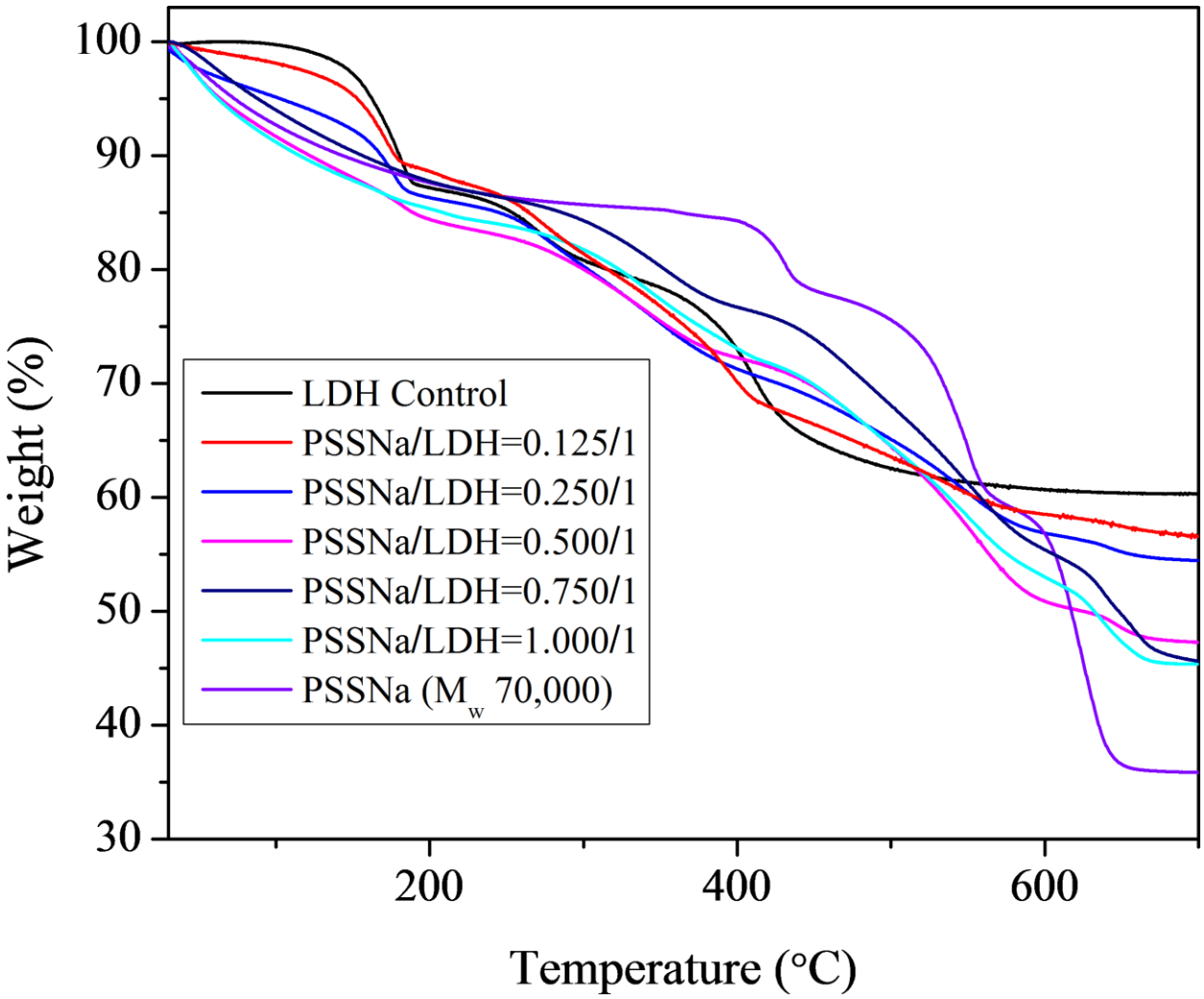

Figure 23. TGA profile of PSSNa/LDH intercalation compounds with different mass ratios of PSSNa (M_w 70, 000).

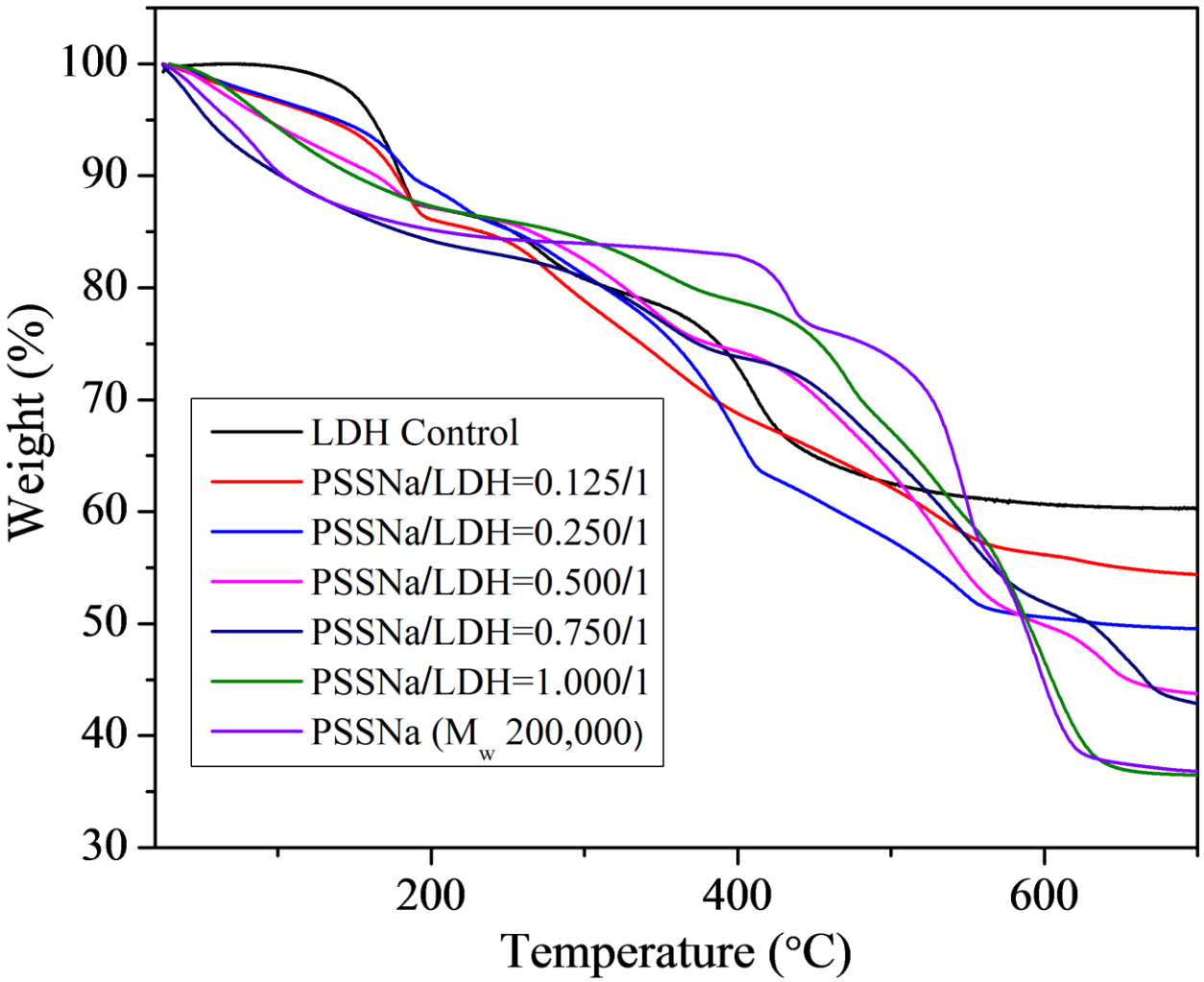

Figure 24. TGA profile of PSSNa/LDH intercalation compounds with different mass ratios of PSSNa (M_w 200, 000).

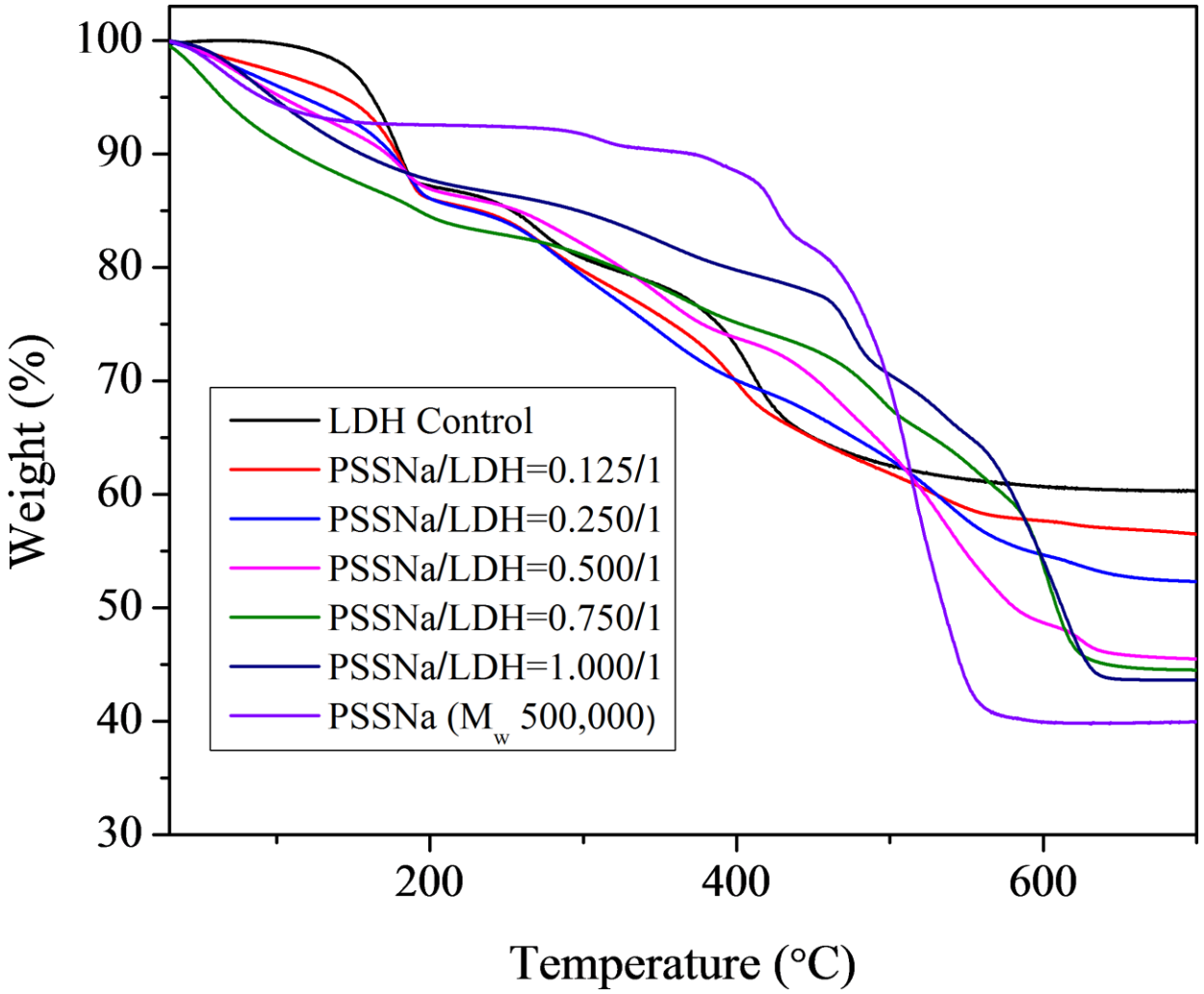

Figure 25. TGA profile of PSSNa/LDH intercalation compounds with different mass ratios of PSSNa (M_w 500, 000).

The total weight loss of PSSNa/LDH intercalation compounds increased when the PSSNa/LDH mass ratio was increased. At PSSNa M_w of 70,000 (Figure 23), the weight loss of the intercalation compounds with the PSSNa/LDH mass ratio ranging from 0.125/1 to 1.000/1 was ca. 43.4%, 46.5%, 53.7%, 55.3%, and 55.4%, respectively. When PSSNa M_w was increased to 200,000 (Figure 24), the weight loss of the intercalation compounds with the PSSNa/LDH mass ratio ranging from 0.125/1 to 1.000/1 was ca. 45.6% , 50.5%, 56.2%, 57.1%, and 63.2%

accordingly. Further increasing PSSNa M_w to 500,00 (Figure 25), the weight loss of the intercalation compounds with PSSNa/LDH mass ratio ranging from 0.125/1 to 1.000/1 was ca. 43.5% , 47.7%, 54.5%, 55.5%, and 56.4% respectively. The TGA data of the three sets of intercalation compounds showed that the decomposition temperature increased as the LDH content was increased. All of the intercalation compounds exhibited a higher polymer onset decomposition temperature owing to the protection effect from LDH layers, which further supports the successful intercalation of the polyelectrolyte into the LDH layers.[12-13]

SEM analysis

The morphology of the control LDH and selected PSSNa/LDH intercalation compounds were characterized by scanning electron microscope. Figure 26 showed the SEM images of the LDH control sample which is pseudo-hexagonal with a diameter of ca. 3-6 μm.

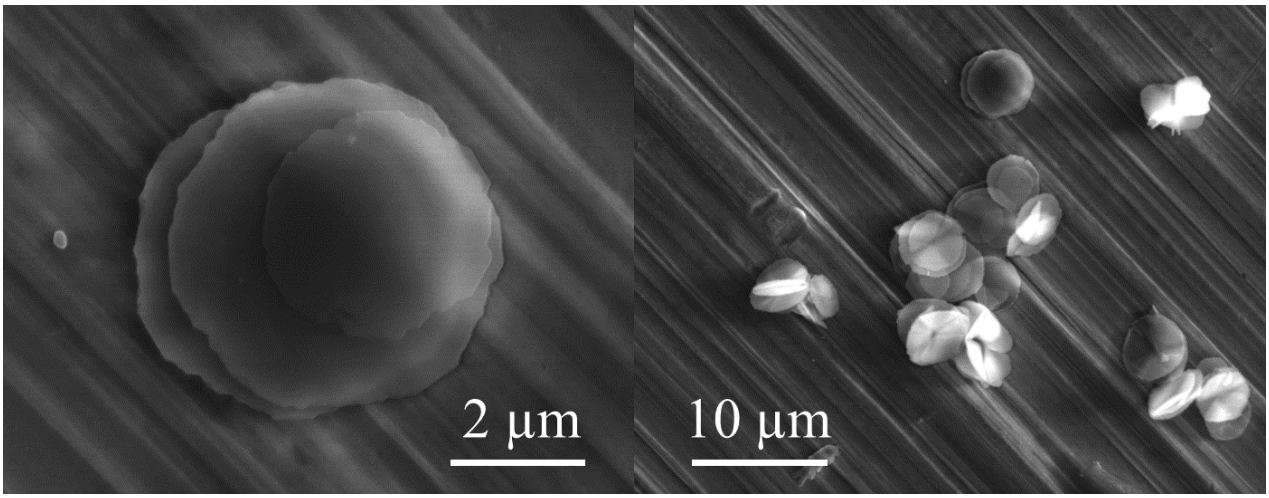

Figure 26. SEM images of the hydrothermally synthesized pristine LDH.

The SEM images of the selected intercalation compounds are shown in Figure 27. At PSSNa M_w of 70,000, with an increasing PSSNa/LDH mass ratio from 0.125/1 to 1.000/1 (Figure 27A, B, and C), the platelets tended to aggregate and formed a rosette structure. The estimated diameter of those samples ranged from ca. 2 to 6 μm, which is similar to that of the LDH control sample. For intercalation compounds with PSSNa M_w of 200,000, when an increasing PSSNa/LDH mass ratio from 0.125/1 to 1.000/1 (Figure 27D, E, and F), the morphology all resembled rosette structure but aggregation turned to be more severe. The diameter of the samples was in the range of ca. 2-4 μm. When PSSNa M_w reached 500,000, the morphology of the intercalation compounds with various PSSNa contents (Figure 27G, H, and I) still resembled the rosette structure and aggregation turned to be even worse, especially at higher PSSNa contents. The diameter of the intercalation compounds was ca. 2-8 μm. Thus, all of the PSSNa/LDH intercalation compounds exhibited a similar dimension compared with the LDH control sample, which is consistent with our hypothesis that the polyelectrolytes only guide the growth of LDH in the Z direction, barely affecting the growth in the plane (X-Y) direction. However, the formation of the rosette structure was induced by the templating effect of PSSNa. In the reaction solution, the polyelectrolyte tends to form vesicles to which the metal cations are attracted because of the electrostatic interactions. The addition of polyelectrolyte during the formation of LDH layered structure can reduce the overall charge on the surface.[14] It is believed that the vesicles served as a template for the formation of a rosette structure.[15] During the crystal nucleation and growth, the stable interactions between the vesicles and LDH layers on the curved organic/inorganic interface induced the growth of curved LDH layers. Thus, the spherical shape from the polyelectrolyte vesicles templated the backbone of LDH rosette structure where the curved layers resembled rose petals.

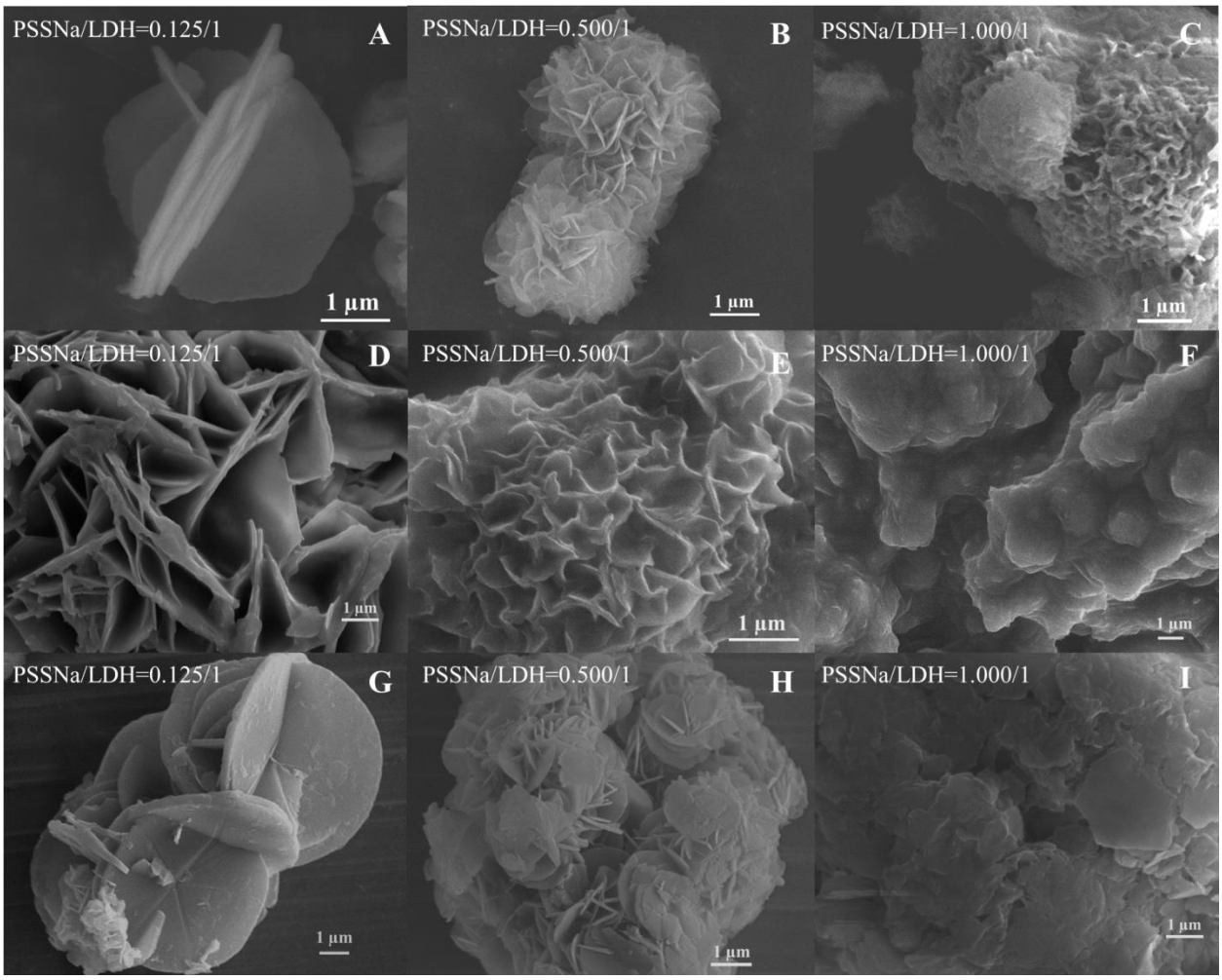

Figure 27. SEM images of selected PSSNa/LDH intercalation compounds using PSSNa with various M_w, where A, B, and C were from PSSNa with a M_w of 70,000; D, E, and F were from PSSNa with a M_w of 200,000; G, H, and I were from PSSNa with a M_w of 500,000.

3.4 Conclusion

In this chapter, PSSNa/LDH intercalation compounds were prepared in a one-pot direct synthesis process where PSSNa was examined as a layer growth coordinator. Three M_w of PSSNa were studied, where at the same PSSNa/LDH weight ratio, the intercalation efficiency declined when PSSNa M_w was increased. The PSSNa/LDH intercalation efficiency exhibited an

opposite trend compared with that of the PEG/α-ZrP intercalation compounds studied in Chapter 2, where high M_w PEG favored the growth of PEG/α-ZrP intercalation compounds.

The formation of PSSNa/LDH intercalation compounds were confirmed by XRD and FTIR. Based on the characterization results, a one-layer PSS^- structure was proposed to align in between LDH layers to maximize the electrostatic interactions. The content of PSSNa increased in the formed PSSNa/LDH intercalation compounds with an increasing PSSNa/LDH weight ratio in the formulation. Moreover, the SEM images of the intercalation compounds indicated that the presence of PSSNa guided the growth of LDH in the Z direction only but not in plane (X-Y) direction. Because of the templating effect of the PSSNa vesicles, LDH tended to grow into curved layers, which aggregated to form a rosette structure.

References

1. Oriakhi, C. O.; Farr, I. V.; Lerner, M. M., Incorporation of poly(acrylic acid), poly(vinylsulfonate) and poly(styrenesulfonate) within layered double hydroxides. *Journal of Materials Chemistry* **1996,** *6* (1), 103-107.

2. Hibino, T.; Ohya, H., Synthesis of crystalline layered double hydroxides: Precipitation by using urea hydrolysis and subsequent hydrothermal reactions in aqueous solutions. *Applied Clay Science* **2009,** *45* (3), 123-132.

3. Wilson Jr, O. C.; Olorunyolemi, T.; Jaworski, A.; Borum, L.; Young, D.; Siriwat, A.; Dickens, E.; Oriakhi, C.; Lerner, M., Surface and interfacial properties of polymer-intercalated layered double hydroxide nanocomposites. *Applied Clay Science* **1999,** *15* (1–2), 265-279.

4. Vieille, L.; Taviot-Guého, C.; Besse, J.-P.; Leroux, F., Hydrocalumite and Its Polymer Derivatives. 2. Polymer Incorporation versus in Situ Polymerization of Styrene-4-sulfonate. *Chemistry of Materials* **2003,** *15* (23), 4369-4376.

5. Prabhu, V.; Muthukumar, M.; Wignall, G.; Melnichenko, Y., Dimensions of polyelectrolyte chains and concentration fluctuations in semidilute solutions of sodium–poly (styrene sulfonate) as measured by small-angle neutron scattering. *Polymer* **2001,** *42* (21), 8935-8946.

6. Volk, N.; Vollmer, D.; Schmidt, M.; Oppermann, W.; Huber, K., Conformation and phase diagrams of flexible polyelectrolytes. In *Polyelectrolytes with Defined Molecular Architecture II*, Springer: 2004; pp 29-65.

7. Szilagyi, I.; Trefalt, G.; Tiraferri, A.; Maroni, P.; Borkovec, M., Polyelectrolyte adsorption, interparticle forces, and colloidal aggregation. *Soft Matter* **2014,** *10* (15), 2479-2502.

8. del Arco, M.; Martin, C.; Martin, I.; Rives, V.; Trujillano, R., A FTIR spectroscopic study of surface acidity and basicity of mixed Mg, Al-oxides obtained by thermal decomposition of hydrotalcite. *Spectrochimica Acta Part A: Molecular* Spectroscopy **1993,** *49* (11), 1575-1582.

9. D. H. Williams and I. Fleming, Spectroscopic Methods in organic chemistry 3rd edn. *McGraw-Hill* **1980,** *London*, 64.

10. Cavani, F.; TrifirÃ², F.; Vaccari, A., Hydrotalcite-type anionic clays: Preparation, properties and applications. *Catalysis Today* **1991,** *11* (2), 173-301.

11. Granados-Correa, F.; Corral-Capulin, N. G.; Olguín, M. T.; Acosta-León, C. E., Comparison of the Cd(II) adsorption processes between boehmite (γ-AlOOH) and goethite (α-FeOOH). *Chemical Engineering Journal* **2011,** *171* (3), 1027-1034.

12. Rey, S.; Mérida-Robles, J.; Han, K.-S.; Guerlou-Demourgues, L.; Delmas, C.; Duguet, E., Acrylate intercalation and in situ polymerization in iron substituted nickel hydroxides. *Polymer International* **1999,** *48* (4), 277-282.

13. Berber, M. R.; Hafez, I. H.; Minagawa, K.; Tanaka, M.; Mori, T., An efficient strategy of managing irrigation water based on formulating highly absorbent polymer–inorganic clay composites. *Journal of Hydrology* **2012,** *470–471* (0), 193-200.

14. Yu, J.; Fan, G.; Yang, Y.; Li, F., Multi-level three-dimensional Mg–Al layered double hydroxide hierarchical microstructures with enhanced basic catalytic property. *Journal of Colloid and Interface Science* **2014,** *432*, 1-9.

15. Li, B.; He, J., Multiple Effects of Dodecanesulfonate in the Crystal Growth Control and Morphosynthesis of Layered Double Hydroxides. *The Journal of Physical Chemistry C* **2008,** *112* (29), 10909-10917.

CHAPTER 4

DIRECT SYNTHESIS OF LDH SINGLE LAYER NANOSHEETS IN FORMAMIDE

4.1 Introduction

The objective of this chapter is to study the layer charge effect on the direct synthesis of LDH single layer nanosheets in formamide. In Chapter 2, the direct growth of LDH single layer nanosheets was described and the mechanism was proposed. However, the various effects that affect the growth process of LDH, such as LDH layer charge and formamide concentration, were not explored.

We hypothesize that formamide can absorb on the surface of LDH layers through a strong interaction formed by the carbonyl functionality of formamide.[1-5] The amine group in formamide does not form a strong interaction with counter anions (CO_3^{2-}, NO_3^-, etc.), which ultimately weakens the attraction. In this way LDH layers can be sheltered by formamide from counter anions, preventing the continuous growth of layers on top of each other. According to the proposed mechanism and the fact that formamide possess a high dielectric constant, a higher concentration of formamide should favor the formation of single layer nanosheets.

In LDH structure, it was reported that the expansion of LDH layers was related to the decrease of the net layer charge (a result of decreasing M^{3+} content), causing the electrostatic attractions between positively charged LDH layers and interlayer anions to decrease.[6-7] The interactions between the charged LDH layers and the formamide affect the amount of formamide

that can be absorbed onto LDH layers.[8] More positively charged LDH layers can absorb more formamide molecules onto the surface, diminishing the layer electrostatic interactions with anions to better facilitate the formation of single layer nanosheets.

Based on the above two assumptions, in this chapter, a detailed study of the LDH layer charge and formamide concentration effect on the direct growth of LDH single layer nanosheets is carried out.

4.2 Experimental

Chemicals

$Mg(NO_3)_2$ $6H_2O$ (98%, Alfa Aesar), formamide (99%, Alfa Aesar), $Al(NO_3)_3$ $9H_2O$ (99%, Acros Organics), sodium hydroxide pellets (Macron), and sodium nitrate (>98%, Alfa Aesar) were used as received without further purification.

Synthesis method

The detailed procedures for the growth of MgAl-LDH single layer nanosheets was developed in Chapter 2 and adopted here. Three sets of samples were prepared with Mg/Al molar ratio at 4/1, 3/1, and 2/1. The total metal salts concentration was set at 0.05 M for all three sets of experiments for comparison. A sample of 20 mL of metal salts solution ($Mg(NO_3)_2$ (0.0400 M) and $Al(NO_3)_3$ (0.0100 M) for Mg/Al=4/1, $Mg(NO_3)_2$ (0.0375 M) and $Al(NO_3)_3$ (0.0125 M) for Mg/Al=3/1, and $Mg(NO_3)_2$ (0.0333 M) and $Al(NO_3)_3$ (0.0167 M) for Mg/Al=2/1) was titrated with sodium hydroxide solution in the presence of 2.0, 5.0, 15.0, or 30.0 vol% formamide.

After reaction, all samples were centrifuged and washed with the same volumetric percentage of formamide solution (i.e., 2.0, 5.0, 15.0, or 30.0 vol% formamide solution accordingly) for three times. The freshly prepared sample was then immediately subjected for characterizations.

Characterization

X-ray diffraction (Bruker D8 with Cu Kα radiation, λ = 1.5406 Å, 40 kV, 40 mA) was conducted on both gel sample and re-stacked single layer nanosheets. The gel-like fresh sample recovered from centrifugation was covered by a Mylar® film[3] for XRD characterization. After further treatment with D.I. water and centrifugation twice, the sample was well dispersed in D.I. water. The dispersion was cast onto a silicon wafer and dried and restacked at 80 ℃ for a day for XRD characterization.

The same dispersion was then diluted into ca. 0.01 mM and cast and air dried on a clean silicon wafer for atomic force microscopy (AFM) characterization on an Asylum Research MFP-3d AFM. Tapping mode with a silicon tip coated with chromium/gold of a force constant of 40 N/m was adopted for AFM imaging. The same dilution dispersion was also cast on Cu grids for TEM imaging on a JEOL 4000EX at 200 kV for TEM imaging.

Perkin Elmer Optima 7300DV inductively coupled plasma optical emission spectrometer (ICP/OES) was used to determine the Mg and Al content. Well-mixed samples were weighed in a glass tube. A sample of 5.0 mL of concentrated nitric acid (HNO_3) was added and the glass tube was swirled. The mixed solution was covered with a watch glass and placed on a hot plate. The mixture was refluxed for 2 hours at 92-95 ℃ without boiling or drying. When the mixture was cooled to room temperature, it was diluted with D.I. water to a final volume of 50 mL for characterization.

4.3 Results and Discussion

Study of the formamide concentration and layer charge effect

LDH layer charge is originated from the substitution of M^{2+} by M^{3+} in brucite structure.[9-10] Formamide forms a strong interaction with the charged LDH sheets. We propose that a lower Mg/Al ratio, where the layer charge x^+ ($x^+ = M^{3+}/(M^{2+}+M^{3+})$) is higher, can better facilitate the formation of LDH single layer nanosheets instead of the layered structure. At a higher layer charge, the interactions between formamide and LDH layers is stronger, which in return can lead to the absorption of a higher density of formamide on the layer surface. Thus, the blocking effect of formamide should be stronger.

Three Mg/Al ratios, 2/1, 3/1, and 4/1 were investigated under 2.0, 5.0, 15.0, and 30.0 vol% formamide. The three samples prepared at 2.0 vol% formamide showed a clear trend that the stability of the samples decreased with an increasing Mg/Al molar ratio. The samples were first prepared and ultrosonicationed for 3 minutes, then they were kept motionless for 1 hour. The Mg/Al=4/1 ratio sample started to precipitate almost immediately. The Mg/Al=3/1 ratio sample precipitated slower than the Mg/Al=4/1 ratio sample. And the Mg/Al=2/1 ratio sample did not show the formation of precipitation until 2 hours later. Figure 28 shows the appearance of the samples after 1 hour.

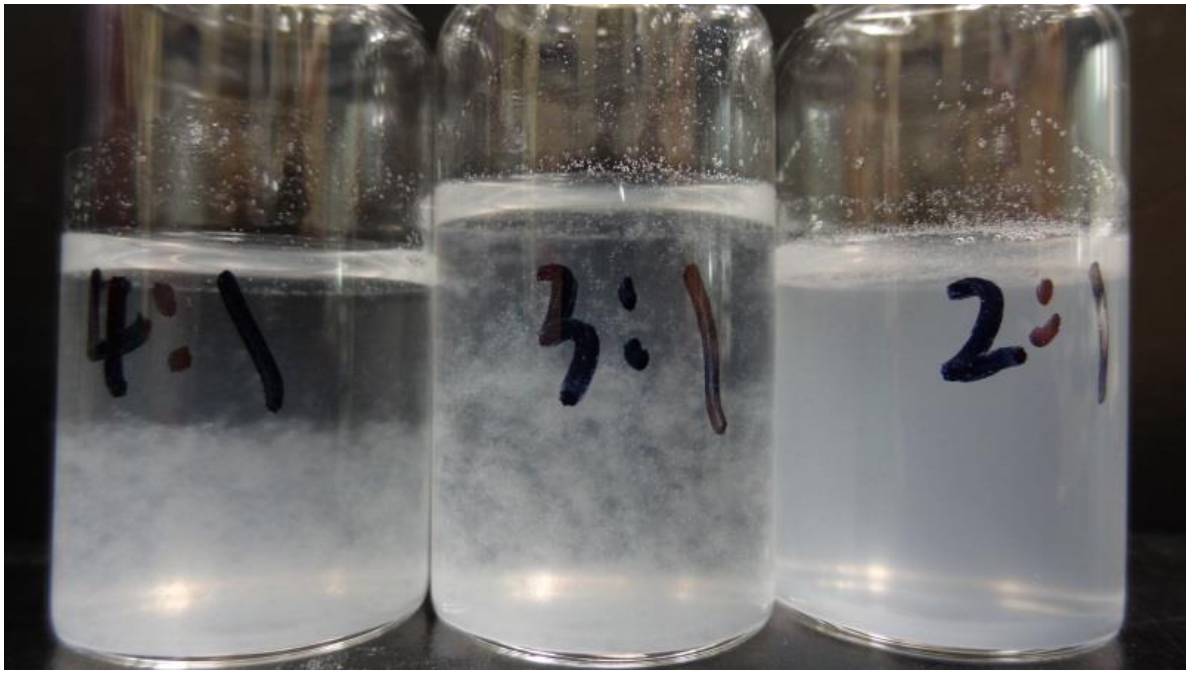

Figure 28. MgAl-LDH synthesized and washed in 2.0 vol% formamide after 1 hour of standing still.

To further study the observed phenomenon, the samples were characterized by XRD diffraction (Figures 2, 3, 4, and 5). The Mg/Al=4/1 ratio sample showed a relatively strong LDH characteristic peak at ca. $11.57\,^{d1}$ (corresponding toe LDH layered structure) at 2.0 vol% formamide (Figure 29) (the diffraction peak at ca. $25.8\,^{\circ}$ is from the Mylar® film). The peak intensity decreased with a decreasing Mg/Al molar ratio, which corresponds well with the aforementioned observation. When the three samples were prepared in the 5.0 and 15.0 vol% formamide, the same trend were observed (shown in Figures 30 and 31). At a formamide concentration of 30.0 vol%, none of the three samples exhibited the LDH characteristic peak (Figure 32), indicating the lack of a long range ordering. Thus, LDH layered structure existed at a very low concentration, below the detection limit.

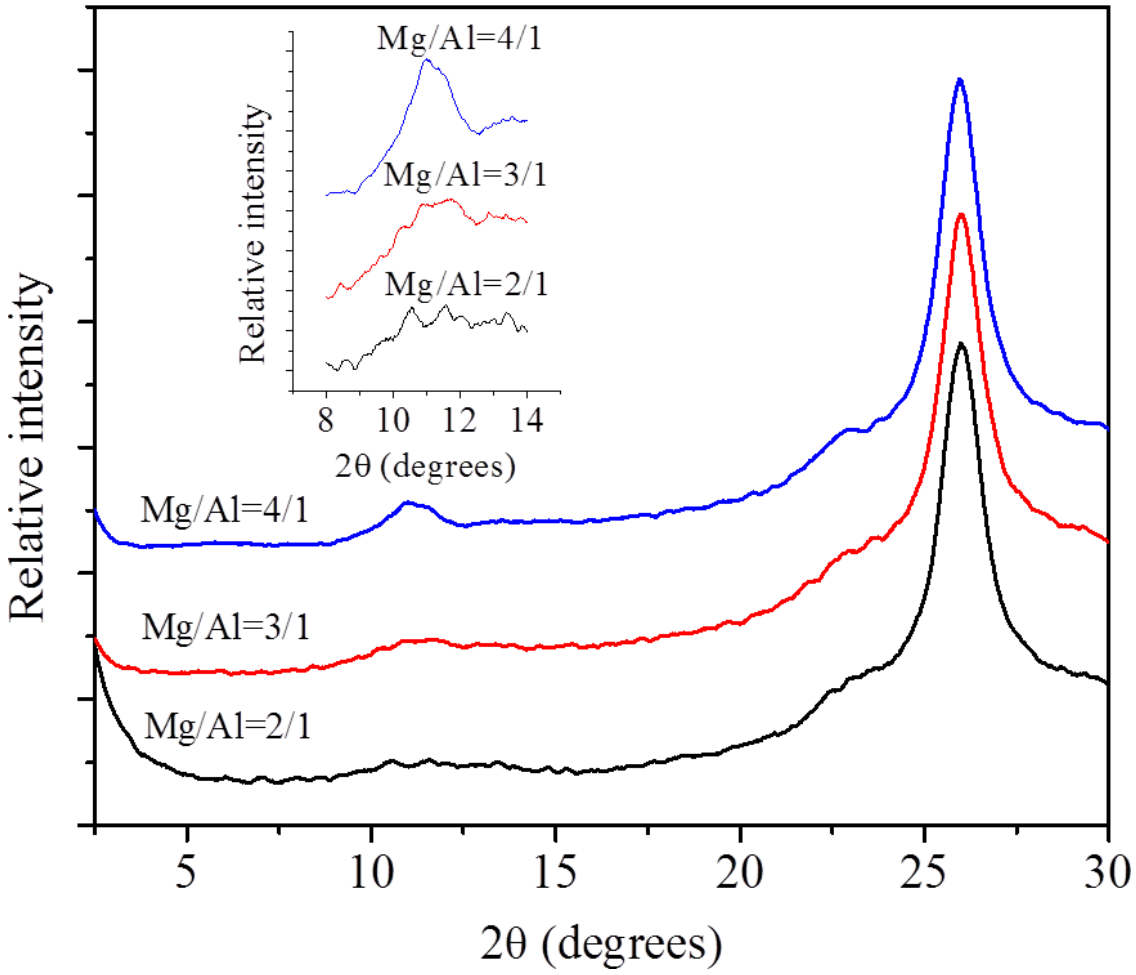

Figure 29. MgAl-LDH prepared and washed in 2.0 vol% formamide.

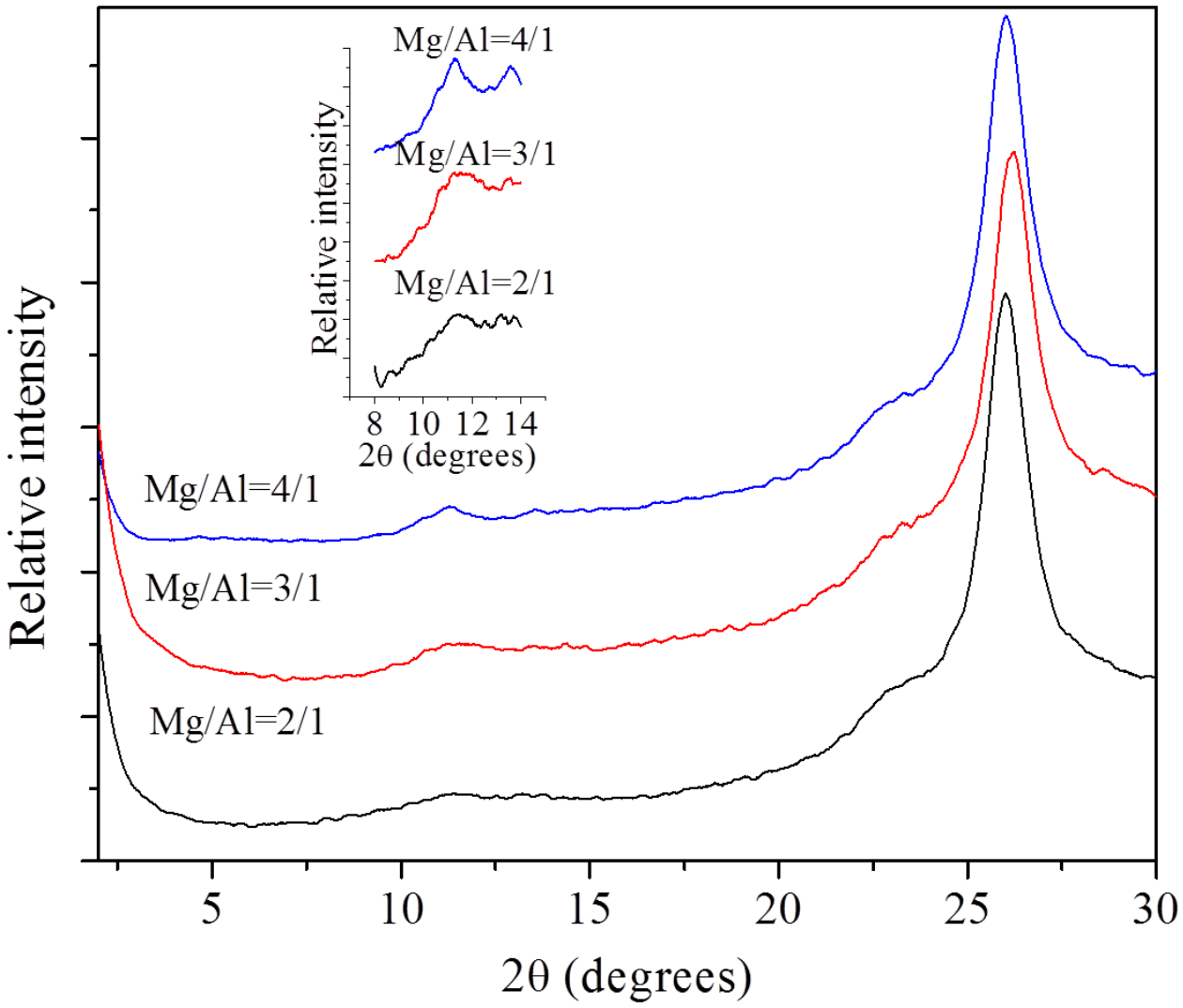

Figure 30. MgAl-LDH prepared and washed in 5.0 vol% formamide.

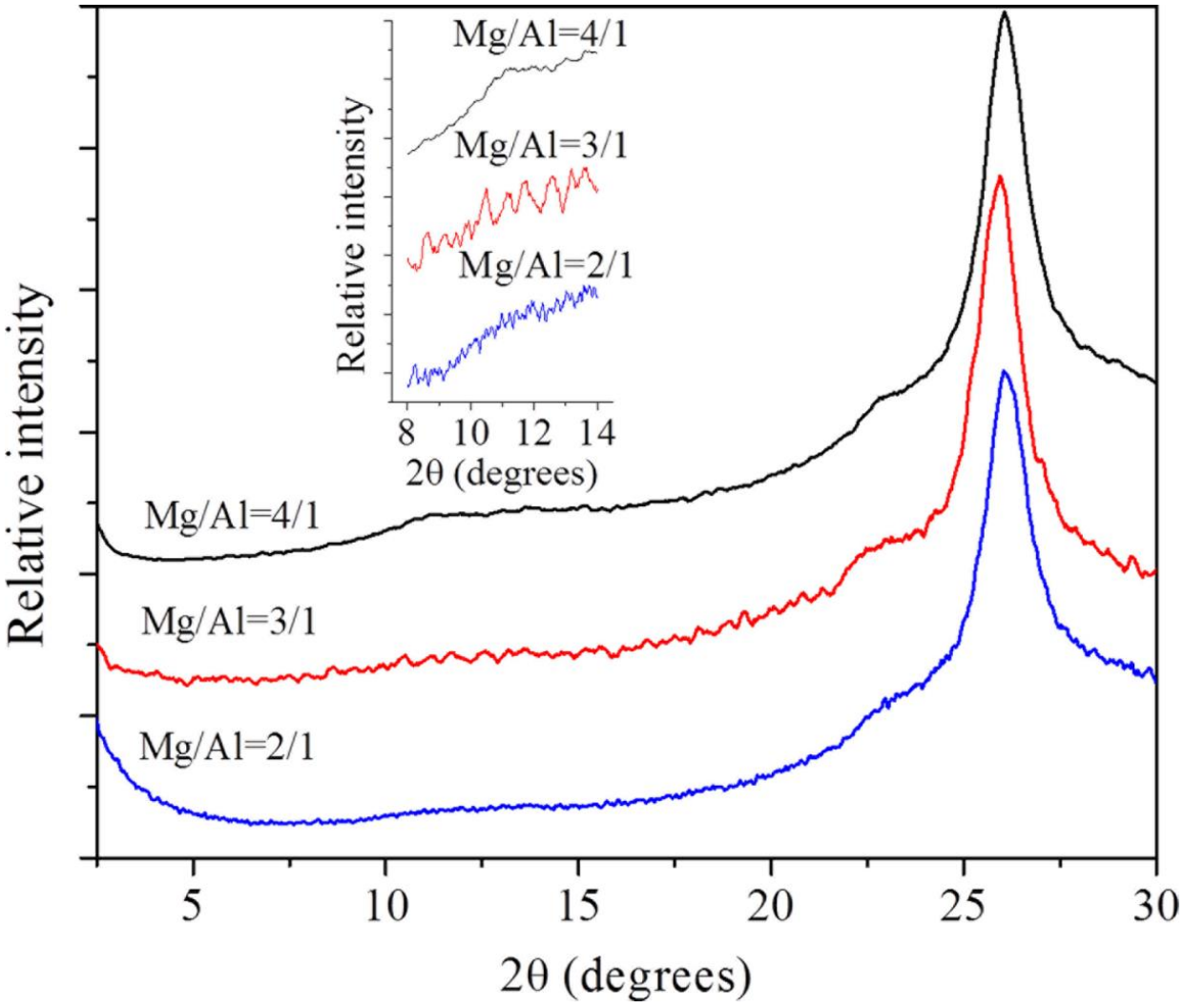

Figure 31. Mg/Al-LDH prepared and washed in 15.0 vol% formamide.

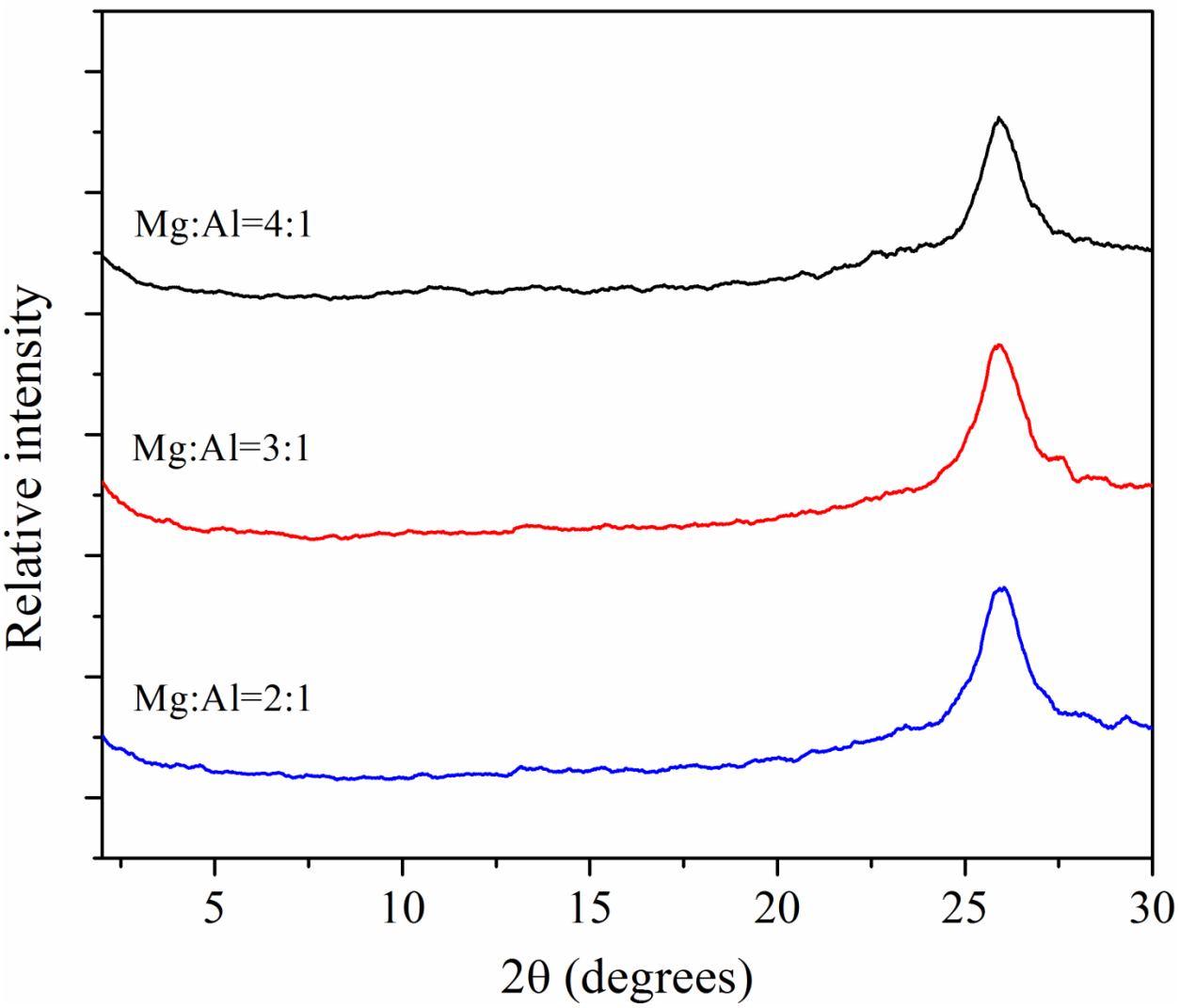

Figure 32. MgAl-LDH prepared and washed in 30.0 vol% formamide.

The diffraction peak from Mylar® film was used as an internal reference to estimate the concentration of layered LDH in the samples. As shown in Figure 33, the Y axis represents the ratio of LDH characteristic peak area to the internal reference peak area. The randomly distributed LDH single layer nanosheets could not induce X-ray diffraction peak. The LDH characteristic peak indicates the presence of LDH layered structure. Thus, the Y axis roughly represents the concentration of layered LDH in the samples. When the formamide concentration

was low (2.0 vol%, black square shown in Figure 33), the concentration of layered LDH was the highest for all three Mg/Al ratios. Increasing the formamide concentration (5.0 vol%, red sphere and 15.0 vol%, blue triangle in Figure 33), the concentration of layered LDH decreased for all of the three Mg/Al ratios. Further increasing the formamide concentration to 30.0 vol% (pink obtriangular in Figure 33), no layered LDH was detected by the X-ray for all of the three samples, indicating that the layered LDH was below detection limit. Thus, at 30.0 vol% formamide, LDH single layer nanosheets can be prepared without the presence of layered LDH regardless of Mg/Al ratio.

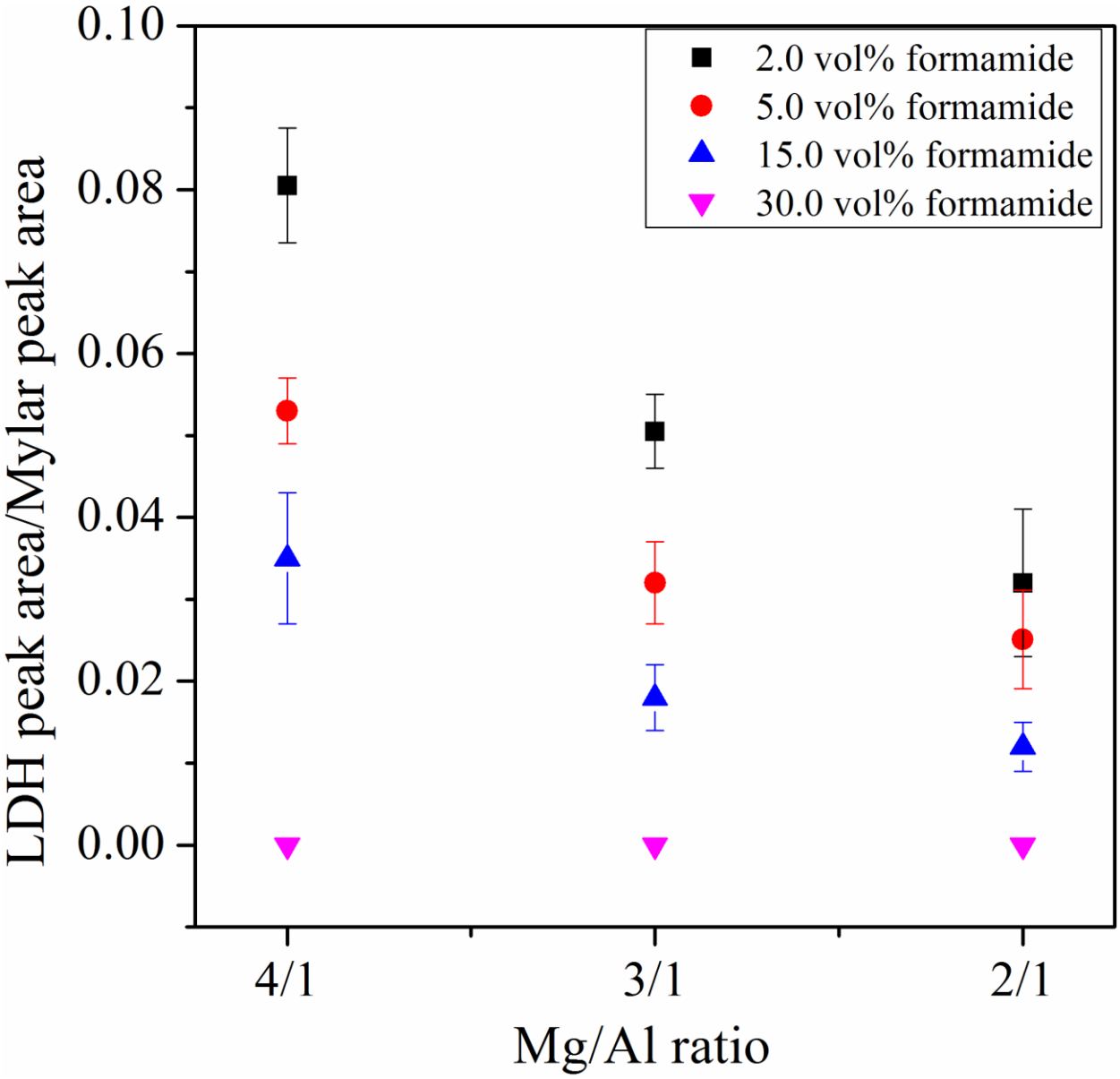

Figure 33. Summary of LDH characteristic peak to internal reference peak area ratios.

Elemental analysis was performed to determine the exact Mg and Al content in each synthesized LDH samples, as the Mg/Al ratio in the LDH product usually varies from the initial formulation ratio. The test results, and the calculated Mg/Al atomic ratio and layer charge (x) are listed in Table 2. Overall, the calculated Mg/Al ratio of all the samples agreed well with the initial Mg/Al formulation ratios. The calculation results showed that at Mg/Al formulation molar

ratio of 2/1 and 3/1, the actual Mg/Al ratio in the samples decreased (Figure 34), where the layer charge x^+ (Figure 35) increased as the formamide concentration was increased. For Mg/Al formulation molar ratio at 4, the trend was not so obvious because the result was close to each other where the difference may just come from testing error. The results agreed well with the XRD characterizations where a higher formamide concentration and a larger LDH layer charge favored the formation of LDH single layer nanosheets. It indicated that at a high LDH layer charge more formamide can be absorbed on the layer surface to enhance the blocking effect during the layer growth.

Table 2. Mg/Al ratio in different samples prepared under varied volumetric ratio of formamide.

Sample	Mg content (μg/g)	Al content (μg/g)	Mg/Al atomic ratio	Layer charge (x^+) (mol/g)
Mg2Al-LDH 0 v%	196571	103830	2.10	0.322
Mg2Al-LDH 2.0 vol%	187912	115962	1.80	0.357
Mg2Al-LDH 5.0 vol%	183505	115893	1.76	0.363
Mg2Al-LDH 15.0 vol%	162967	120673	1.50	0.400
Mg2Al-LDH 30.0 vol%	161100	130620	1.37	0.422
Mg3Al-LDH 0 vol%	210665	84569	2.76	0.266
Mg3Al-LDH 2.0 vol%	213553	89566	2.65	0.274
Mg3Al-LDH 5.0 vol%	222300	94260	2.62	0.276
Mg3Al-LDH 15.0 vol%	206289	88365	2.59	0.278
Mg3Al-LDH 30.0 vol%	203965	92198	2.46	0.289
Mg4Al-LDH 0 vol%	239967	63352	3.61	0.192
Mg4Al-LDH 2.0 vol%	224656	75103	3.32	0.231
Mg4Al-LDH 5.0 vol%	220568	73773	3.32	0.231
Mg4Al-LDH 15.0 vol%	216922	72193	3.33	0.231
Mg4Al-LDH 30.0 vol%	218917	73341	3.31	0.232

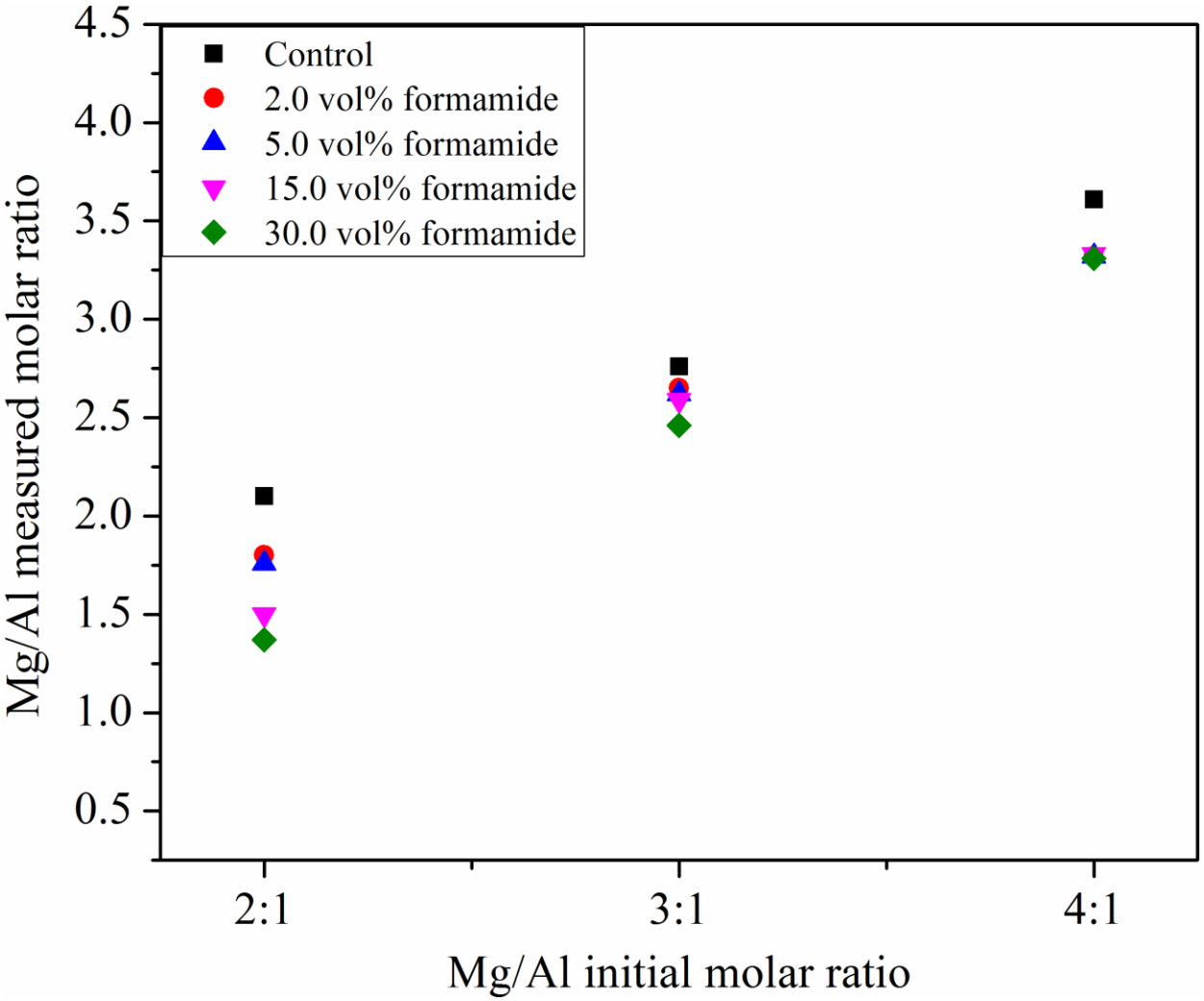

Figure 34. Summary of Mg/Al measured molar ratios.

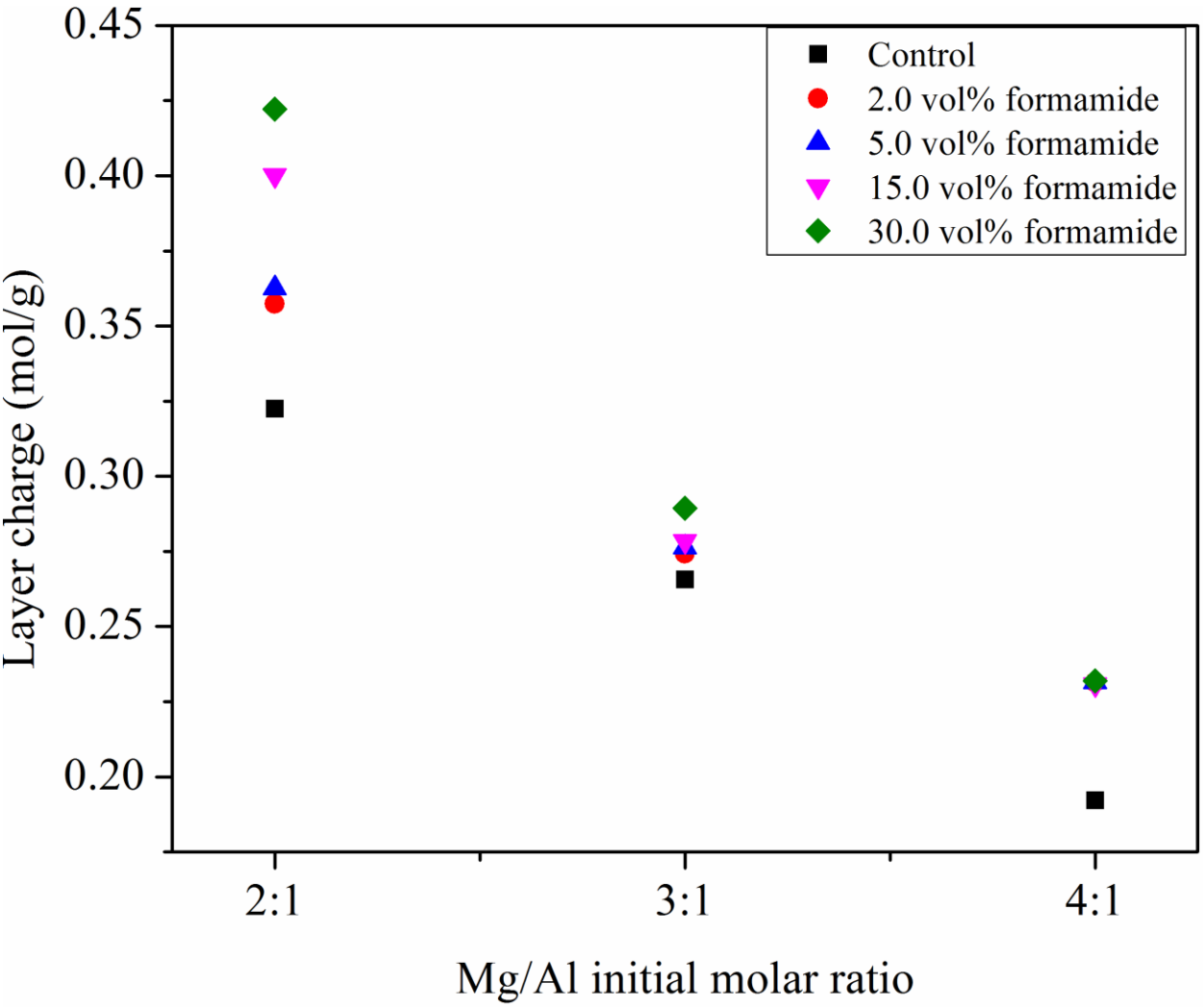

Figure 35. MgAl-LDH layer charge at different Mg/Al molar ratios and formamide concentrations.

Characterization of Mg2Al-LDH nanosheets synthesized from 30.0 vol % formamide

From the XRD results, the best sample Mg2Al-LDH nanosheets prepared at 30.0 vol% of formamide was selected for characterization. Figure 36 shows the XRD pattern of restacked Mg2Al-LDH nanosheets on a silicon wafer. The *d* spacing of 7.8 Å agreed very well with the reported interlayer distance of Mg2Al-LDH with CO_3^{2-} residing in the interlayer region.[12] TEM

images of Mg2Al-LDH nanosheets from 30.0 vol% formamide clearly show sheet like structure of LDH with a diameter ranging from ca. 40 to 150 nm.

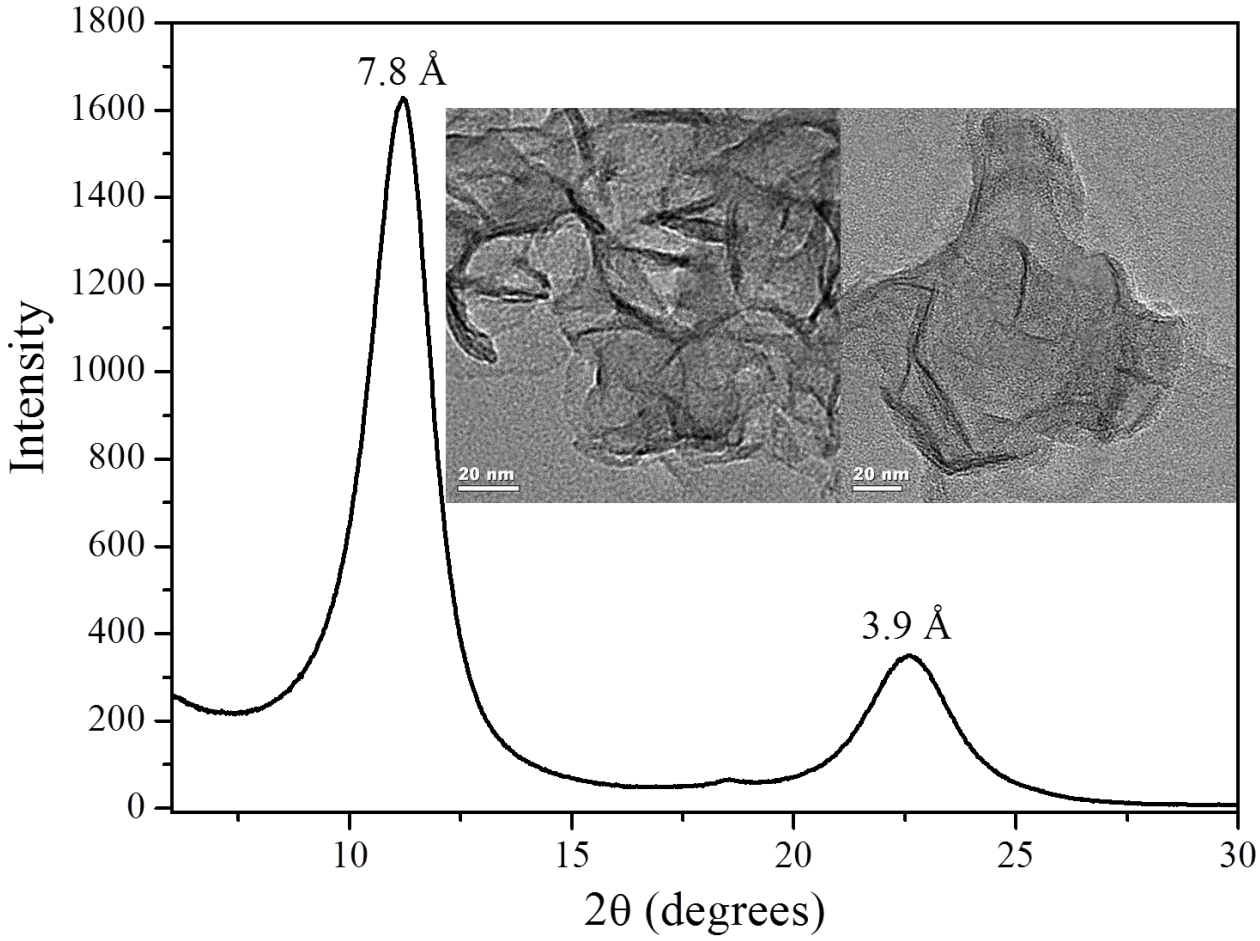

Figure 36. XRD pattern of Mg2Al-LDH nanosheets from 30.0 vol% formamide restacked on silicon wafer and the corresponding TEM images (insets).

AFM was performed to measure the thickness of the samples. Figure 37A and B showed that the diameter of the LDH nanosheets ranging from ca. 40-60 nm to ca.100-150 nm. This result agrees well with the TEM images. Regardless of the diameter of the LDH nanosheets, the average thickness was ca. 0.8 nm, which corresponds to a single LDH layer thickness.[1, 4] Figure 37B line 1 shows a configuration composed of two stacked sheets where a thickness transition

from ca. 1.6 nm to 0.8 nm, corresponding from a stack of 2 layers of a single layer LDH nanosheets. The mis-match of the sheet area indicated that the double layer was from the stacking of two individual single layers during sample preparation, instead of synthesized double-layer LDH. Overall, the XRD and AFM characterizations confirmed that the sample was composed of LDH single layer nanosheets.

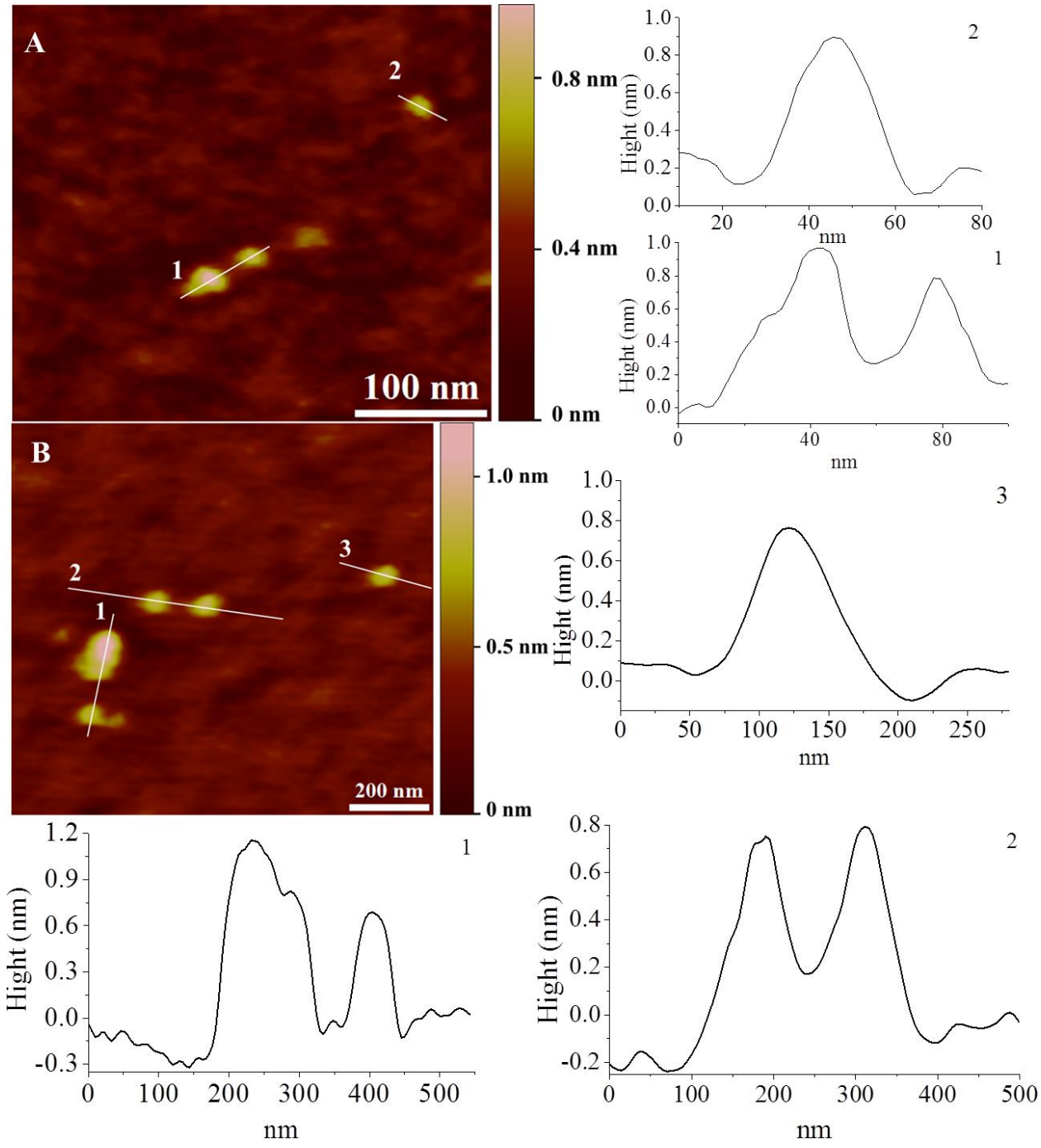

Figure 37. AFM characterization of Mg2Al-LDH prepared in 30.0 vol% formamide with a diameter of ca. 40 nm (A) and ca. 150 nm (B).

4.4 Conclusions

The results shown above indicate that a high concentration of formamide and a high LDH layer charge are beneficial for the formation of single layer LDH nanosheets, where more formamide can be absorbed on layer surface to weaken the electrostatic attractions between the anions and the positively charged LDH layers. A relatively low concentration of formamide (such as 2.0, 5.0, and 15.0 vol%) may not be sufficient to completely block the growth of LDH in the Z direction regardless of Mg/Al molar ratio, resulting in the formation of layered LDH as evidenced by the XRD characterization. On the other hand, LDH layer growth in the Z direction was effectively inhibited at a higher formamide concentration (30.0 vol%), where no layered LDH was detected by XRD. Elemental analysis was adopted to measure the Mg and Al content in each sample and the result agrees well with XRD result that at a higher LDH layer charge, LDH single layer can be better synthesized with less layered LDH present. The AFM characterization confirmed the average thickness of the Mg2Al-LDH single layer nanosheets synthesized in 30.0 vol% formamide was 0.8 nm, agreeing well with the theoretical thickness of LDH single layer nanosheets.

References

1. Ma, R.; Liu, Z.; Li, L.; Iyi, N.; Sasaki, T., Exfoliating layered double hydroxides in formamide: a method to obtain positively charged nanosheets. *Journal of Materials Chemistry* **2006,** *16* (39), 3809-3813.

2. Liu, Z.; Ma, R.; Osada, M.; Iyi, N.; Ebina, Y.; Takada, K.; Sasaki, T., Synthesis, Anion Exchange, and Delamination of Co−Al Layered Double Hydroxide: Assembly of the Exfoliated Nanosheet/Polyanion Composite Films and Magneto-Optical Studies. *Journal of the American Chemical Society* **2006,** *128* (14), 4872-4880.

3. Yu, J.; Martin, B. R.; Clearfield, A.; Luo, Z.; Sun, L., One-step direct synthesis of layered double hydroxide single-layer nanosheets. *Nanoscale* **2015,** *7* (21), 9448-9451.

4. Li, L.; Ma, R.; Ebina, Y.; Iyi, N.; Sasaki, T., Positively Charged Nanosheets Derived via Total Delamination of Layered Double Hydroxides. *Chemistry of Materials* **2005,** *17* (17), 4386-4391.

5. Alberti, G.; Dionigi, C.; Giontella, E.; Murcia-Mascarós, S.; Vivani, R., Formation of Colloidal Dispersions of Layered γ-Zirconium Phosphate in Water/Acetone Mixtures. *Journal of Colloid and Interface Science* **1997,** *188* (1), 27-31.

6. Leroux, F.; Adachi-Pagano, M.; Intissar, M.; Chauviere, S.; Forano, C.; Besse, J.-P., Delamination and restacking of layered double hydroxides. *Journal of Materials Chemistry* **2001,** *11* (1), 105-112.

7. Kooli, F.; Chisem, I. C.; Vucelic, M.; Jones, W., Synthesis and properties of terephthalate and benzoate intercalates of Mg-Al layered double hydroxides possessing varying layer charge. *Chemistry of Materials* **1996,** *8* (8), 1969-1977.

8. Hibino, T.; Jones, W., New approach to the delamination of layered double hydroxides. *Journal of Materials Chemistry* **2001,** *11* (5), 1321-1323.

9. Cavani, F.; TrifirÃ², F.; Vaccari, A., Hydrotalcite-type anionic clays: Preparation, properties and applications. *Catalysis Today* **1991,** *11* (2), 173-301.

10. Leroux, F.; Moujahid, E. M.; Taviot-Guého, C.; Besse, J.-P., Effect of layer charge modification for Co Al layered double hydroxides: study by X-ray absorption spectroscopy. *Solid State Sciences* **2001,** *3* (1–2), 81-92.

11. Yang, W.; Kim, Y.; Liu, P. K.; Sahimi, M.; Tsotsis, T. T., A study by in situ techniques of the thermal evolution of the structure of a Mg–Al–CO 3 layered double hydroxide. *Chemical Engineering Science* **2002,** *57* (15), 2945-2953.

12. Olanrewaju, J.; Newalkar, B. L.; Mancino, C.; Komarneni, S., Simplified synthesis of nitrate form of layered double hydroxide. *Materials Letters* **2000,** *45* (6), 307-310.

CHAPTER 5

COMPLEXING AGENT DIRECTED EPITAXIAL GROWTH OF α-ZIRCONIUM PHOSPHATE BASED HEXAGONAL PRISMS

5.1 Introduction

In Chapter 2, we introduced the method that uses a layer growth coordinator to assist the growth of layered compounds in the Z direction. We found that layered intercalation compounds can be prepared in a one step process, where the layer growth coordinator is incorporated in between layers.[1] The control of preferential growth of inorganic materials in one direction is a long term goal. It is viable that with the guidance of the layer growth coordinator, the growth of the layered materials in the Z direction can be enhanced. However, such a phenomenon was not observed in the PEG/α-ZrP or other related systems (BMIMCl/α-ZrP, acrylamide/α-ZrP, PVA/α-ZrP, PEI/α-ZrP).

It's known that plane-direction growth is typically faster than thickness-direction (Z direction) during crystal growth due to strong covalent or ionic bonding. Interlayer is bonded through weak Van der Waals forces,[2] electrostatic interactions,[3] or hydrogen bonds.[4] It is possible that the layer growth coordination effect in the aforementioned systems is compromised by the faster in-plane growth due to the formation of stronger bonds. Complexing agents are widely used in inorganic synthesis,[5-10] which can form complexes with the reaction ingredients and make the slow release possible. Through the use of a complexing agent, the fast in-plain

growth may be slowed down. Thus, when a complexing agent is used together with a layer growth coordinator, the effect of the layer growth coordinator may be revived.

Herein, we report our exploration of the synthesis of α-zirconium phosphate based hexagonal prisms, where the preferential growth along Z-direction was achieved. The introduction of a complexing agent and a layer growth coordinator into the reaction system appeared to be the key factor for the promotion of the growth in the Z direction. The parameters which may affect the growth of the layered compounds were discussed.

5.2 Experimental

Materials and Characterization

Formamide (99%, Acros Organics), $ZrOCl_2 \cdot 8H_2O$ (>98%, Acros Organics), $NH_4H_2PO_4$ (99%, Fisher), and phosphoric acid (85%, Fisher) were used without further treatment.

Scanning electron microscopy (SEM) was performed on a JEOL JSM-6335F. X-ray diffraction (XRD) patterns were acquired on a Bruker D5005 diffractometer with Bragg-Brentano θ-2θ geometry (40 kV and 40 mA), using a graphite monochromator with Cu Kα radiation (λ = 1.542 Å).

Synthesis method

For a typical experiment, 1.01 g of $ZrOCl_2 \cdot 8H_2O$ was dissolved in 50 mL formamide and then 10.5 mL of 6 M H_3PO_4 was added to the reaction mixture. After the reactants were fully mixed, the mixture was transferred to a hydrothermal reactor and reacted at 150 ℃ for 24 hours. After the reactor was cooled down, the reaction mixture was transferred to a flask with aluminum foil covered on the top and aged at a predetermined temperature for one week. After the reaction,

the prepared samples were washed and centrifuged three times with D.I water at 2300 G force for 5 minutes each time. All samples were dried at 60 ℃ for 24 hours before characterization.

5.3 Results and discussion

Figure 38 shows the α-ZrP structure where Zr cations coordinate with six oxygen atoms from six different phosphate groups. Each phosphate group coordinates to three different Zr cations, leaving the remaining oxygen atom protonated. The hydroxyl groups densely cover the layer surface or exist in between the layers. Its interlayer distance is 7.6 Å. α-ZrP can be easily synthesized as platelets with the dimension in thickness being much lower than those in plane directions. However, α-ZrP derivatives with elongation in the Z direction in different morphologies such as needles, rods,[11] and long prismatic morphology[12] were observed when a complexing agent and sometimes a structure directing agent were used.

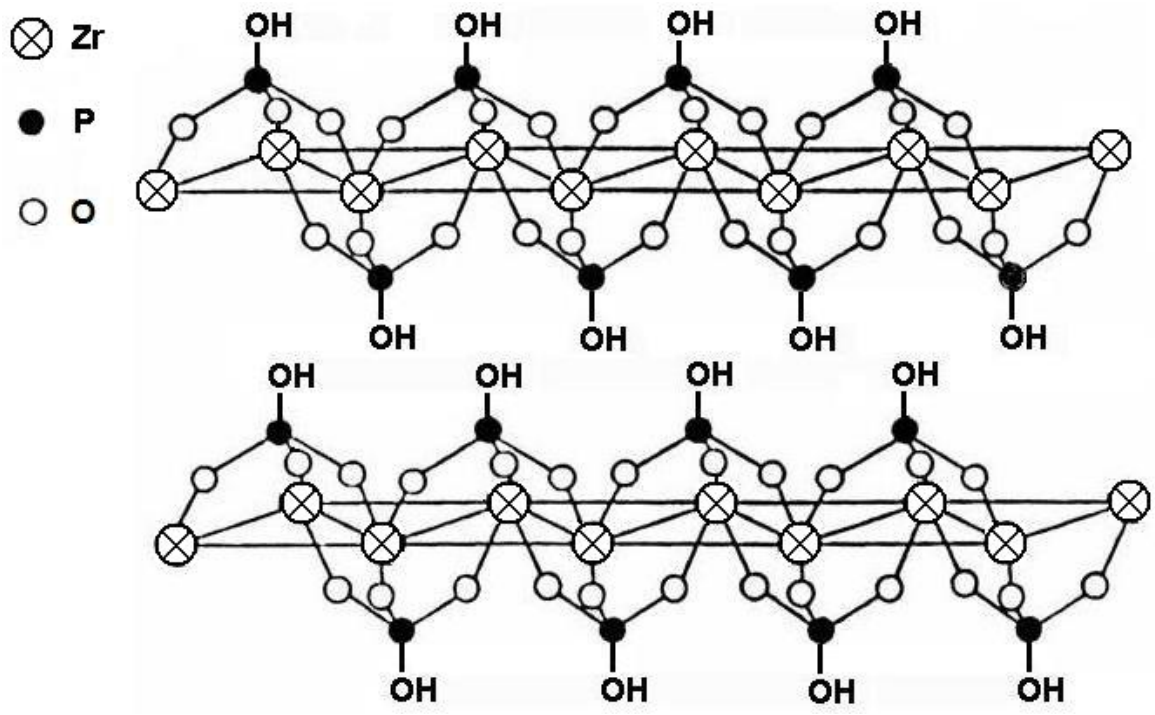

Figure 38. Structure of α-ZrP.

Hydrofluoric acid is commonly used to prepare α- and γ-ZrP through the decomposition of the flouro-zirconium complexes.[13-14] Precipitation of zirconium phosphate does not begin until the concentration of phosphoric acid reaches ca. 8-9 M.[15] The precipitation of zirconium phosphate is controlled by the elimination rate of hydrofluoric acid, which allows for the formation of large zirconium phosphate platelets at an extremely slow rate.[15-16] Free zirconium cations are in a very low concentration, which only serve as a small amount of nuclei when the elimination rate of the complexing agent is slow. Thus, the formation of large zirconium phosphate platelets is possible through the very slow decomposition of the flouro-zirconium complexes. However, manipulation of hydrofluoric acid demands high precaution. Discovery of new complexing agents with low operational demands is highly desirable.

Formamide is a common solvent which is very stable up to 180 ℃. It can coordinate with zirconium cations through its hydrogen atom with zirconyl chloride and form 4:1 ratio complexes.[17-18] Thus, formamide can be used as an ideal complexing agent. α-ZrP micro-crystals are usually prepared when a soluble zirconium salt precipitates with phosphoric acid in a prolonged reaction time. Formamide decomposes upon acid treatment.[19] Thus, when formamide is used as a complexing agent during the preparation of α-ZrP, it decomposes and forms formic acid and ammonium di-hydrogen phosphate in the presence of phosphoric acid (shown in Equation 1). Whitish whiskers are formed after the reaction which has been confirmed by XRD to be $NH_4H_2PO_4$ (XRD pattern was not shown).

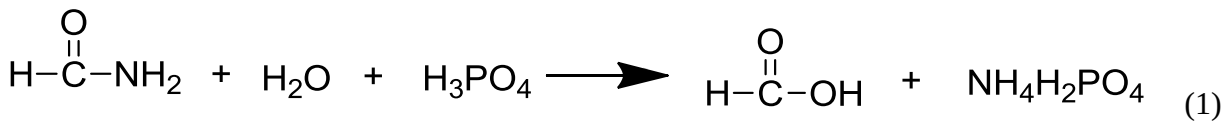

(1)

Structure directing agents,[11-12, 20-24] such as ammonia and amines,[25-26] were applied to prepare new zirconium phosphate derivatives with different structures, which often results in the incorporation of ammonium cations within their structures. It was found that the ammonium cations could serve as a binder in between the layers through a close net of hydrogen bonds with the anionic P-O groups on layer surface.[12] Thus, ammonium cation is chosen as a structure directing agent in this study. As shown in Equation 1, ammonium dihydrogen phosphate is a decomposition product of formamide. Thus formamide can serve dual purposes: (1) as the complexing agent for zirconium cations; (2) as the ammonium source. Thus, the fast in-plain growth can possibly be slowed down, allowing the layer growth coordinator to take effect.

Herein, we report the preparation of α-ZrP based hexagonal prisms in the presence of formamide. Zirconyl chloride was first dissolved in formamide and formed complexes at 1:4 molar ratio with formamide. Phosphoric acid was added to the reaction mixture and the decomposition of formamide began. Slow release of zirconium cations was started upon heating to decompose formamide, with the release speed can be controlled by the aging temperature. The formed ammonium cations can be selectively adsorbed onto layer surfaces that are parallel to the precipitated (*001*) crystal plane and coordinate the layer growth on top of each other through the formation of a close network of hydrogen bonds with surface P-OH groups.[12] Thus, the ammonium cations could work as a layer growth coordinator and direct the growth in the Z direction (Figure 39).

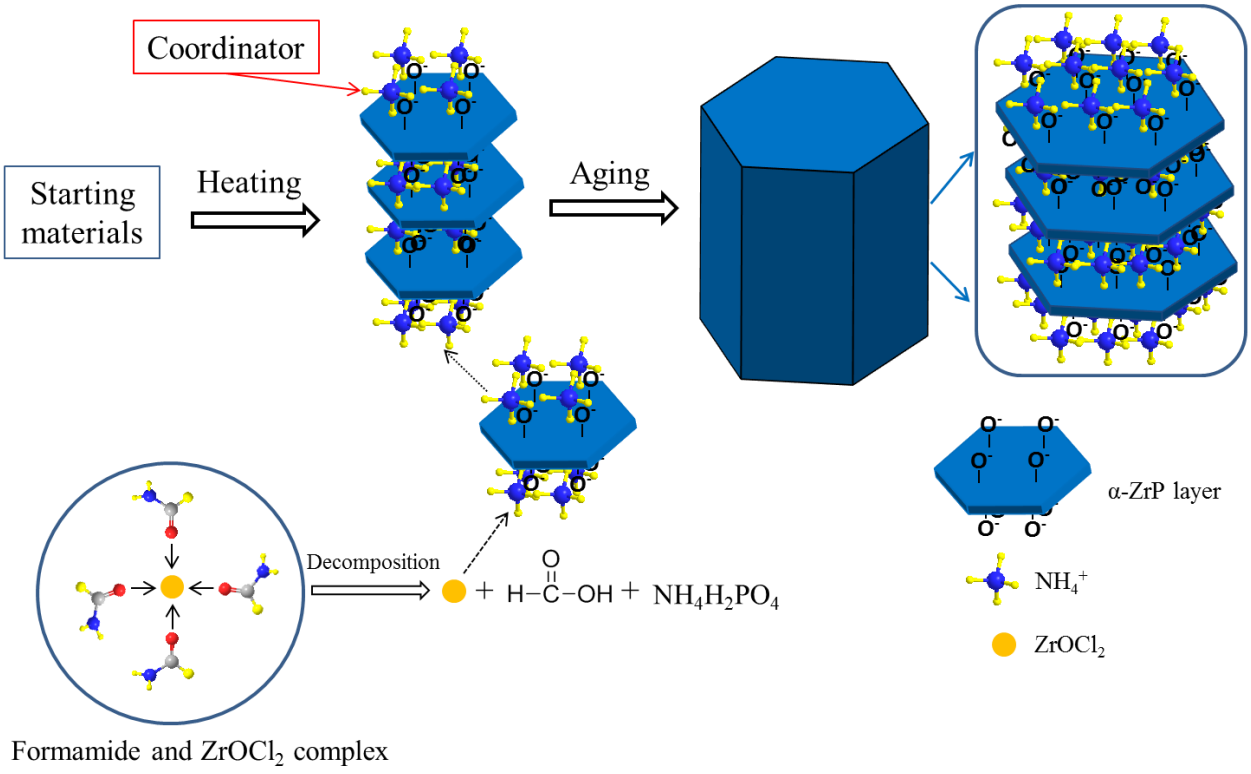

Figure 39. Schematic of the proposed mechanism.

A typical method[27] to synthesize α-ZrP was modified where formamide was included as a complexing agent. After 24 hours of treatment at 150 ℃, the reaction mixture as aged at 60 ℃ for a week for slow release of Zr^{4+}. After reaction, α-ZrP based compound was formed where a large amount of amorphous phase co-existed in the product. SEM images (Figure 40) of the product showed that the in-plain diameter is ca. 1-3 μm with a significant growth enhancement in the Z direction ranged from ca. 1 to 3 μm. Thus, the preferential growth in the Z direction was achieved and hexagonal shaped prisms were synthesized, where the elongation direction is perpendicular to the (*001*) planes.

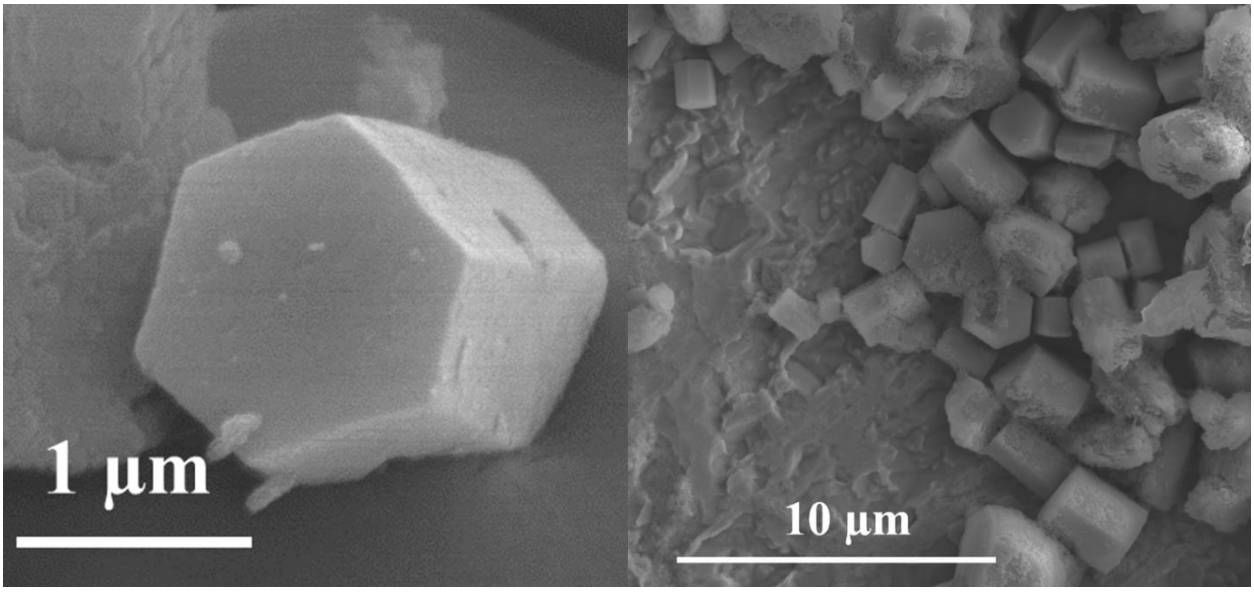

Figure 40. SEM images of as prepared α-ZrP based hexagonal prisms.

Figure 41 shows the X-ray diffraction pattern of the hexagonal prisms prepared under 60 ℃ aging, with a SEM image (Figure 41 insert) showing the hexagonal face of the prism. The diffraction peaks of the sample match very well with that of the $NH_4ZrH(PO_4)_2$ standard (PDF 35-0455). Thus, the prepared sample was identified as $NH_4ZrH(PO_4)_2$ with an interlayer distance of 11.18 Å. Thus, in this approach, ammonium acted as the layer growth coordinator, which was formed after the complexing agent, formamide, was decomposed. During aging, the decomposition of the formamide/$ZrOCl_2$ complexes in contact with phosphoric acid was controlled by the aging temperature and time, which controlled the release of Zr^{4+} cation. With the aid of the slow release of Zr^{4+} cations, the in plain growth rate of α-ZrP was slowed down, allowing the layer growth coordinator to take effect in the Z direction crystal growth. As shown in Figure 39, ammonium cations can selectively attach to the surface of α-ZrP (that parallel to

(001) planes of α-ZrP) due to the formation of a close network of hydrogen bonds with surface P-OH groups.

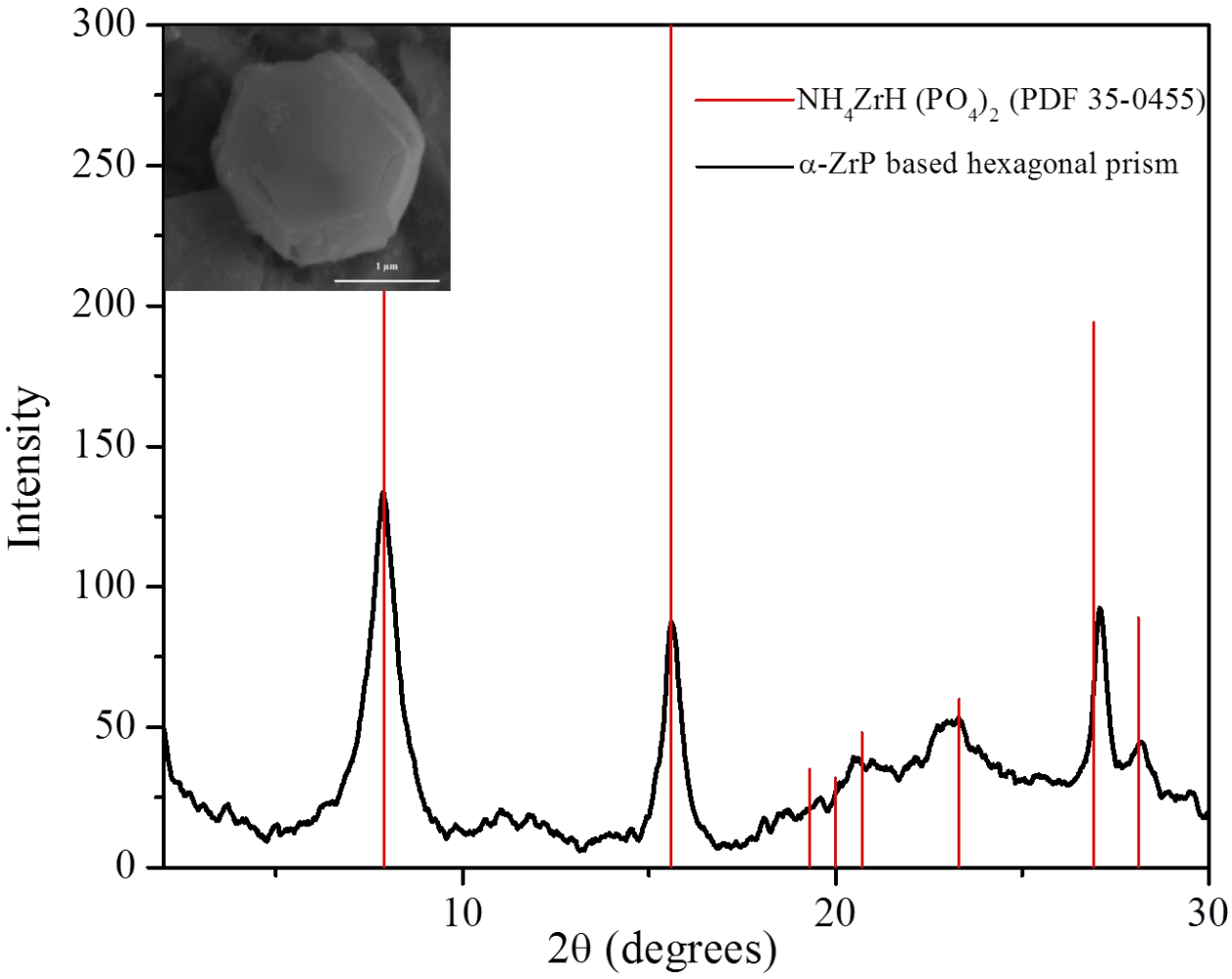

Figure 41. XRD pattern and the SEM top view image (insert) of the prepared sample aged at 60 ℃ for one week.

In order to confirm the above proposed mechanism, several control experiments were conducted. Conventional α-ZrP (Figure 42A) was synthesized as detailed in the literature[27] for

comparison. The first control experiment was conducted in the absence of formamide while $NH_4H_2PO_4$ was present in a 10:1 molar ratio to Zr^{4+} to study the coordination effect on the formation of an elongated structure in the Z direction without the complexing agent present. As expected, the morphology of the control sample (Figure 42B) was hexagonal platelets with a similar diameter and thickness as α-ZrP but without significant thickness change (Figure 42A). This control experiment showed that the presence of coordinator only cannot promote the formation of prisms. Another control sample showed no obvious elongation in the Z direction (Figure 42C) either when the prepared α-ZrP was ion exchanged with NH_4NO_3. It further confirms that in the presence of a layer growth coordinator (ammonium cations) alone, due to the intrinsic faster growth in the in-plain direction, a prismatic morphology cannot be obtained where the layer growth coordination effect is compromised. The third control experiment was conducted without the presence of phosphoric acid. The $NH_4H_2PO_4$ to Zr^{4+} molar ratio was also set at 10:1. Because formamide will decompose very slowly at an elevated temperature,[19] the release rate of Zr^{4+} was much slower than in the presence of phosphoric acid. Under a much slower release rate, the elongation in the Z direction was also slowed down (Figure 42D); where the thickness in the Z direction was increased compared with the α-ZrP control but much lower than the increment of the sample obtained in the presence of phosphoric acid. It indicates that the coordination effect is directly related to the decomposition rate of the complexes.

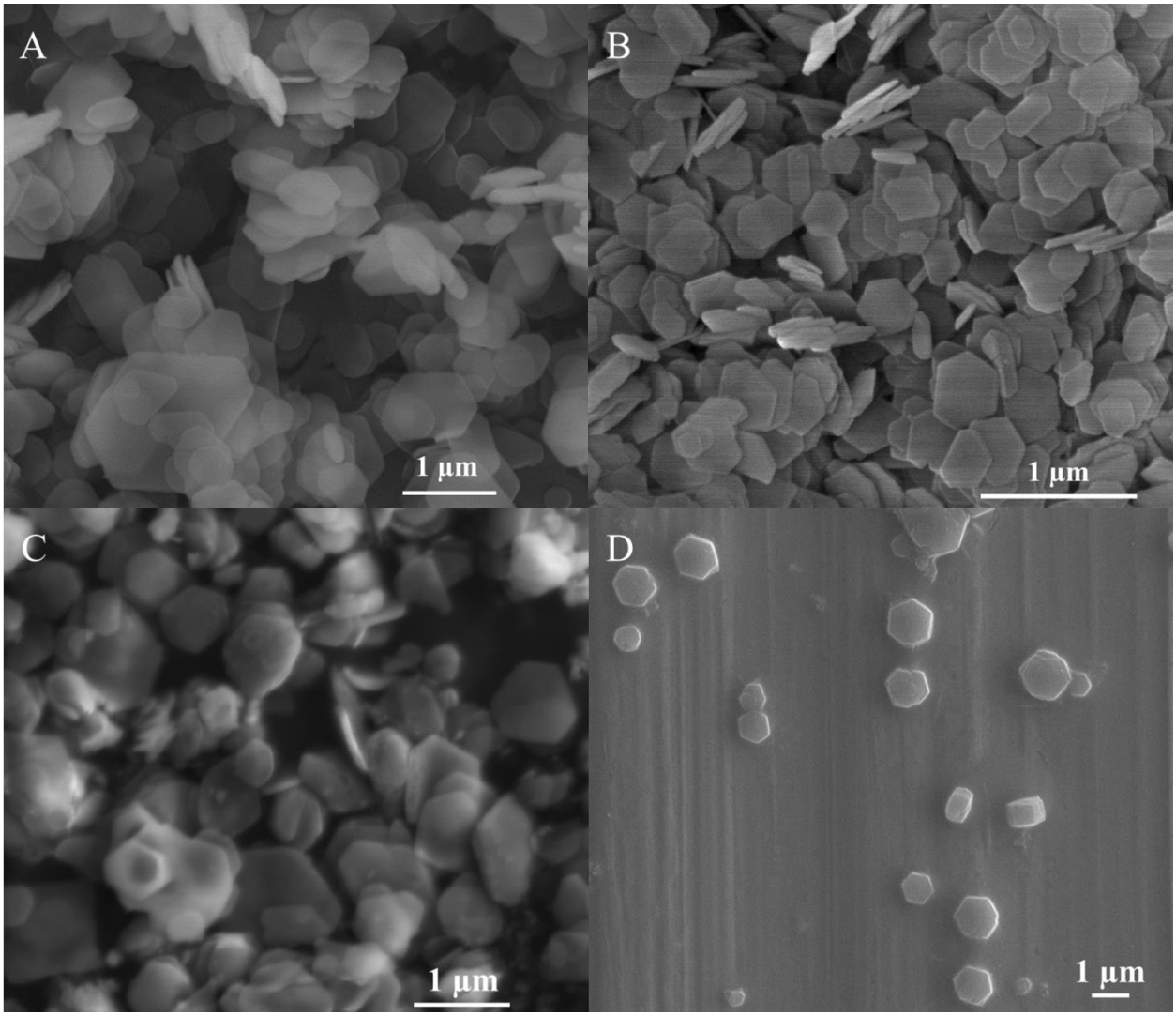

Figure 42. SEM images of α-ZrP (A), control experiment without formamide (B), α-ZrP ion exchanged with NH_4NO_3 (C), and control experiment without phosphoric acid (D).

Thus, the effect of the aging temperature on the formation of hexagonal shaped prisms was studied. As shown in Figure 43A and B, at a higher aging temperature, the growth of the prisms in the Z direction was even more significant than at relatively low temperatures. Compared with a lower aging temperature, the decomposition rate of the formamide-zirconium

complex is increased at a higher aging temperature, leading to a faster release of zirconium cations, thus a more significant growth in the Z direction. A faster release rate of zirconium cations during the precipitation stage facilitates the formation of more nuclei and thus leads to small crystals. While at the same time, the faster decomposition of formamide releases more NH_4^+ ions. Thus, the growth of zirconium phosphate crystals is more prominent in the Z direction when combining the following two factors: (1) an increased amount of zirconium phosphate nuclei which will result in smaller crystal size at in plain direction; (2) an increased supply of binding agent, NH_4^+, which will further assist the growth in the Z direction. Thus, the coordination effect is more prominent in the Z direction at high aging temperatures.

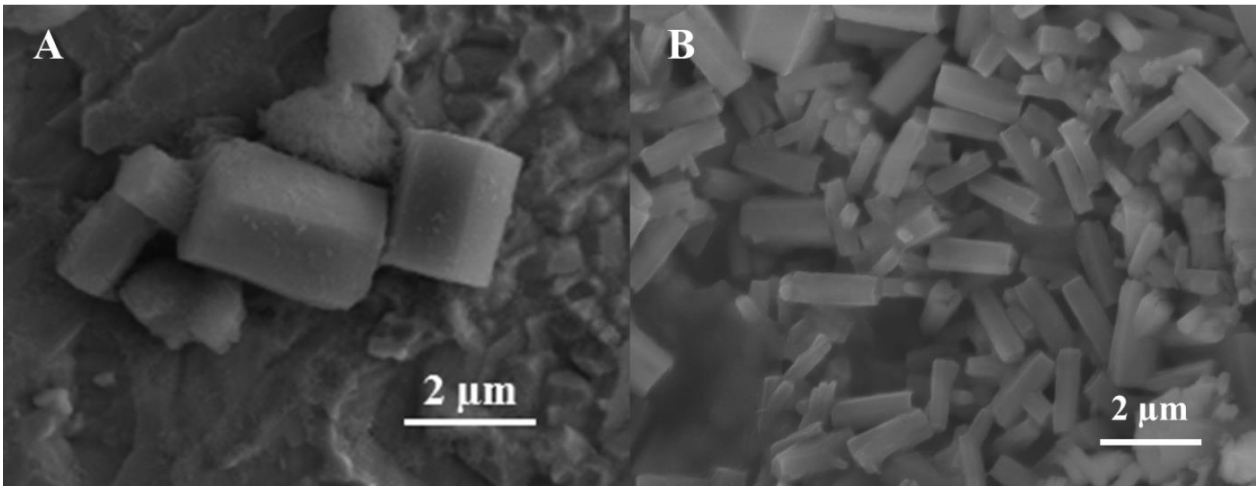

Figure 43. α-ZrP based hexagonal prisms prepared at different aging temperatures of 60 ℃ (A) and 100 ℃ (B).

It was also found that by an acid treatment (Figure 44), the interlayer distance of the prepared α-ZrP based hexagonal prism was shifted from 11.18 Å to 7.6 Å, indicating the

elimination of ammonium cations. Nevertheless, further research is needed to determine the structure transformation during the acid treatment.

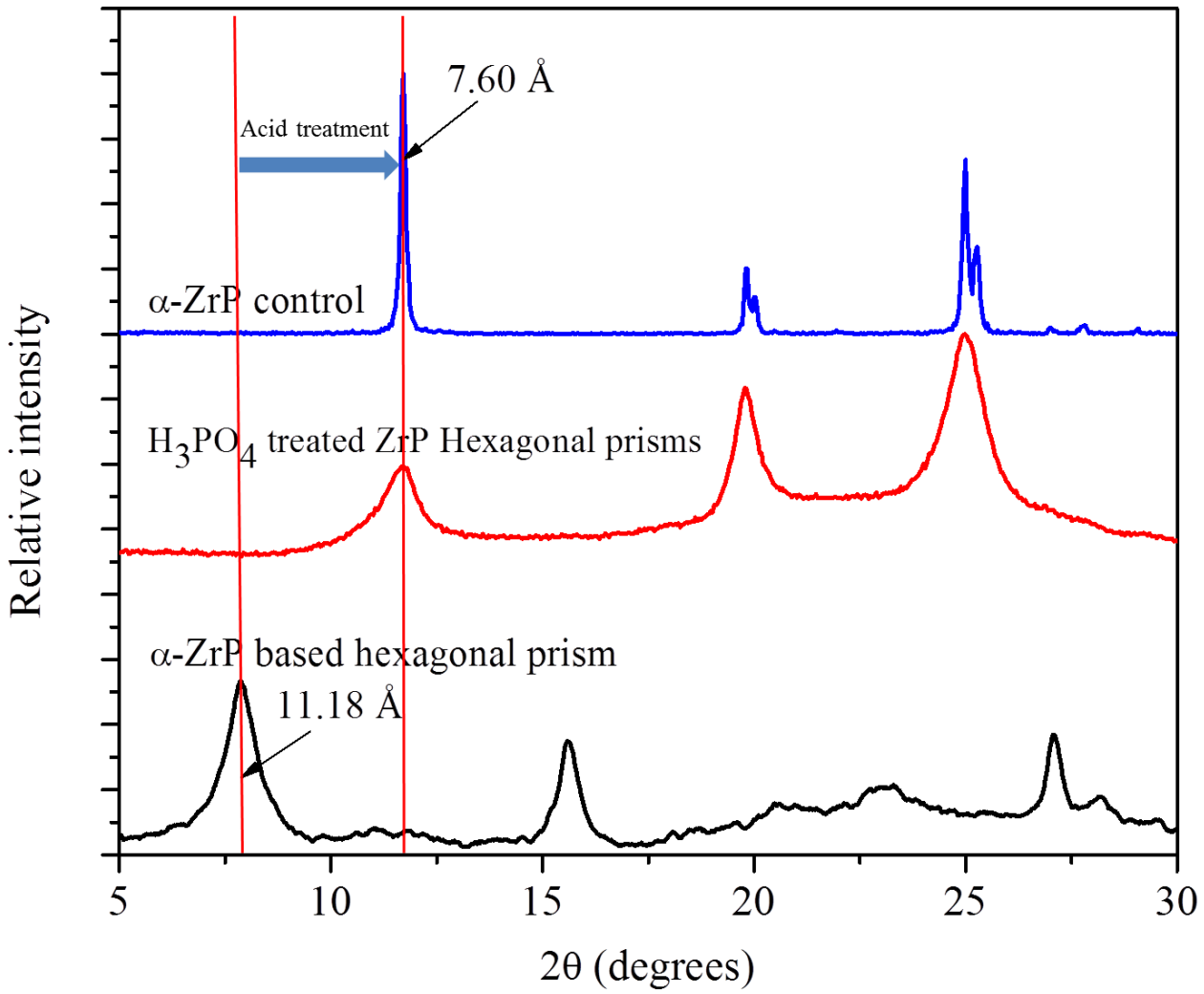

Figure 44. Structure transfer upon acid treatment.

5.4 Conclusion

In this chapter, the preparation of α-ZrP based hexagonal prism was studied. The formation mechanism was proposed where formamide acting as the complexing agent allowing Zr^{4+} to slowly release and react with phosphoric acid while the decomposition product of

formamide, ammonium can be selectively adsorbed on the formed α-ZrP surface [(*001*) plane]. Thus, the crystal growth perpendicular to the (001) surface was enhanced to form a prismatic morphology. The layer growth coordinator effect on the morphology, which was usually compromised by the intrinsically faster growth in the in-plain direction due to the formation of stronger chemical bonds, was now revived. It agrees well with the mechanism proposed in Chapter 2, where a layer growth coordinator can guide the growth of the layered material in the Z direction during which the coordinator was incorporated in between the layers (in this chapter, NH_4^+ functioned as the layer growth coordinator).

References

1. Yu, J.; Xiang, L.; Martin, B. R.; Clearfield, A.; Sun, L., Direct growth of layered intercalation compounds via single step one-pot in situ synthesis. *Chemical Communications* **2015,** *51* (57), 11398-11400.

2. Gabriella, G.; Jiří, K.; Felix, F.-A.; Angelos, M., Improved description of soft layered materials with van der Waals density functional theory. *Journal of Physics: Condensed Matter* **2012,** *24* (42), 424216.

3. Grégoire, B.; Ruby, C.; Carteret, C., Structural Cohesion of MII-MIII Layered Double Hydroxides Crystals: Electrostatic Forces and Cationic Polarizing Power. *Crystal Growth & Design* **2012,** *12* (9), 4324-4333.

4. Tosoni, S.; Doll, K.; Ugliengo, P., Hydrogen Bond in Layered Materials: Structural and Vibrational Properties of Kaolinite by a Periodic B3LYP Approach. *Chemistry of Materials* **2006,** *18* (8), 2135-2143.

5. Cushing, B. L.; Kolesnichenko, V. L.; O'Connor, C. J., Recent advances in the liquid-phase syntheses of inorganic nanoparticles. *Chemical Reviews* **2004,** *104* (9), 3893-3946.

6. DiLeo, L.; Romano, D.; Schaeffer, L.; Gersten, B.; Foster, C.; Gelabert, M. C., Effect of complexing agent on hydrothermal growth of ZnO crystals. *Journal of crystal growth* **2004,** *271* (1), 65-73.

7. Kimling, J.; Maier, M.; Okenve, B.; Kotaidis, V.; Ballot, H.; Plech, A., Turkevich method for gold nanoparticle synthesis revisited. *The Journal of Physical Chemistry B* **2006,** *110* (32), 15700-15707.

8. Laurent, S.; Forge, D.; Port, M.; Roch, A.; Robic, C.; Vander Elst, L.; Muller, R. N., Magnetic iron oxide nanoparticles: synthesis, stabilization, vectorization, physicochemical characterizations, and biological applications. *Chemical Reviews* **2008,** *108* (6), 2064-2110.

9. Panáček, A.; Kvitek, L.; Prucek, R.; Kolar, M.; Vecerova, R.; Pizurova, N.; Sharma, V. K.; Nevečná, T. j.; Zboril, R., Silver colloid nanoparticles: synthesis, characterization, and their antibacterial activity. *The Journal of Physical Chemistry B* **2006,** *110* (33), 16248-16253.

10. Chen, D.-H.; He, X.-R., Synthesis of nickel ferrite nanoparticles by sol-gel method. *Materials Research Bulletin* **2001,** *36* (7), 1369-1377.

11. Sung, H. H. Y.; Yu, J.; Williams, I. D., Zirconium Phosphates of Variable Dimension Templated by Ethylene Diamine: Crystal Structures of 1-D [enH2][Zr(HPO4)3] and 2-D [enH2]0.5[Zr(PO4)(HPO4)]. *Journal of Solid State Chemistry* **1998,** *140* (1), 46-55.

12. Gatta, G. D.; Masci, S.; Vivani, R., Dimensional reduction in zirconium phosphate; from layers to ribbons to chains. *Journal of Materials Chemistry* **2003,** *13* (5), 1215-1222.

13. Alberti, G.; Torracca, E., Crystalline insoluble salts of polybasic metals - II. Synthesis of crystalline zirconium or titanium phosphate by direct precipitation. *Journal of Inorganic and Nuclear Chemistry* **1968,** *30* (1), 317-318.

14. Alberti, G.; Bernasconi, M. G.; Casciola, M., Preparation of γ-zirconium phosphate microcrystals with high degree of crystallinity and proton conductivity of their hydrogen and ammonium forms. *Reactive Polymers* **1989,** *11* (0), 245-252.

15. Inoue, Y.; Yamada, Y., The Synthesis of Crystalline Zirconium Phosphate with Large Particle Size by the Direct-precipitation Method. *Bulletin of the Chemical Society of Japan* **1979,** *52* (12), 3528-3531.

16. Alberti, G.; Costantino, U.; Giulietti, R., Preparation of large crystals of α-Zr(HPO4)2 ·H2O. *Journal of Inorganic and Nuclear Chemistry* **1980,** *42* (7), 1062-1063.

17. Paul, R. C.; Chadha, S. L.; Vasisht, S. K., Addition compounds of zirconyl(IV) chloride. *Journal of the Less Common Metals* **1968,** *16* (3), 288-289.

18. R. C. Paul, A. K. M., S. L. Chadha & S. K. Vasisht, Addition Compounds of Zirconyl Chloride with Amines & Amides. *Indian Journal of Chemistry* **1970**, 1017.

19. Wang, B.; Cao, Z., Mechanism of Acid-Catalyzed Hydrolysis of Formamide from Cluster-Continuum Model Calculations: Concerted versus Stepwise Pathway. *The Journal of Physical Chemistry A* **2010,** *114* (49), 12918-12927.

20. Wang, D.; Yu, R.; Kumada, N.; Kinomura, N.; Yanagisawa, K.; Matsumura, Y.; Yashima, T., A Novel Layered Zirconium Phosphate $[NH_4]_2[Zr(OH)_3(PO_4)]$ Synthesized through Non-aqueous Route. *Chemistry Letters* **2002,** *31* (8), 804-805.

21. Wang, D.; Yu, R.; Takei, T.; Kumada, N.; Kinomura, N.; Onda, A.; Kajiyoshi, K.; Yanagisawa, K., Non-aqueous Synthesis and Structure of a Novel Monodimensional Zirconium Phosphate: $[NH_4]_3[Zr(OH)_2(PO_4)(HPO_4)]$. *Chemistry Letters* **2002,** *31* (3), 398-399.

22. Wang, D.; Yu, R.; Kumada, N.; Kinomura, N., Nonaqueous Synthesis and Characterization of a Novel Layered Zirconium Phosphate Templated with Mixed Organic and Inorganic Cations. *Chemistry of Materials* **2000,** *12* (4), 956-960.

23. Serre, C.; Taulelle, F.; Ferey, G., Synthesis and characterisation of MIL-43 and MIL-44, two new layered templated tetravalent phosphates: Zr(PO4)2 ·N2C2H10 and Ti2(PO4)2(HPO4)2 ·N2C2H10. *Solid State Sciences* **2001,** *3* (5), 623-632.

24. Kumada, N.; Nakatani, T.; Yonesaki, Y.; Takei, T.; Kinomura, N., Preparation of new zirconium phosphates by solvothermal reaction. *Journal of Materials Science* **2008,** *43* (7), 2206-2212.

25. Zhang, H.; Ma, X.; Yang, D., Effects of complexing agent on CdS thin films prepared by chemical bath deposition. *Materials Letters* **2004,** *58* (1), 5-9.

26. Kaufman, V. B.; Kistler, R. C., Alumina abrasive; oxidizer, complexing agent such as ammonium oxalate, benzotriazole. Google Patents: 1999.

27. Sun, L.; Boo, W. J.; Sue, H.-J.; Clearfield, A., Preparation of [small alpha]-zirconium phosphate nanoplatelets with wide variations in aspect ratios. *New Journal of Chemistry* **2007,** *31* (1), 39-43.

CHAPTER 6

NANOCOATINGS CONTAINING LAYERED DOUBLE HYDROXIDE SINGLE LAYER NANOSHETS TO IMPROVE BARRIER PROPERTIES

6.1 Introduction

The application of LDH single layer nanosheets prepared in Chapter 6 was studied in this chapter. The prepared LDH nanosheets were aligned and bonded with poly(vinyl alcohol) (PVA) to prepare nanocoatings on polymer film substrates aiming at improving their barrier properties.

It is desirable to have a thin, transparent, and flexible film for food packaging and medical devices to protect them from gas and water vapor. Biomimetic polymer/inorganic nanosheet nanocomposites with structures similar to nacre[1-4] and abalone shell[5] have been intensively studied because of their great potentials in improving gas barriers,[6-10] mechanical properties,[11-12] and other functionalities.[13-14] The brick and wall structure where inorganic nanosheets are arranged like bricks in a wall and polymers acting like the mortar is the key to achieve such enhancements.[3, 10, 15-18] Multiple methods have been developed to align inorganic nanosheets to achieve such a desired structure. Layer by layer (LBL)[19-23] was the most extensively developed process, where a substrate is dipped in a polymer solution and a nanosheets dispersion repeatedly to achieve alternated organic/inorganic layers.

However, LBL is a tedious and time consuming process. Herein we propose a method where uniformly mixed PVA and LDH nanosheets were coated onto polylactic acid (PLA) and polyethylene terephthalate (PET) film surface through a facile dip coating process. The Mg2Al-

LDH nanosheets were synthesized using the method reported in Chapter 4 where the starting Mg/Al molar ratio was set at 2 and 30 vol% formamide was used. PVA was selected as organic "glue" because of its water soluble nature and densely packed -OH groups which may form weak interactions with LDH nanosheets, as well as its good film formability. Crosslinking agent was used to incorporate the aligned nanosheets well into the PVA matrix to form a highly integrated system.

6.2 Experimental

Materials

$Mg(NO_3)_2$ $6H_2O$(98%, Alfa Aesar), formamide (99%, Alfa Aesar), $Al(NO_3)_3$ $9H_2O$ (99%, Acros Organics), sodium hydroxide (98%, Macron), and sodium nitrate (>98%, Alfa Aesar) were used as received without further purification to prepare LDH single layer nanosheets.

Poly(vinyl alcohol) (PVA) (Mowiol® 8-88, M_w: 67,000, 86.7-88.7 mol% hydrolysis, Kuraray, Japan), glutaraldehyde (GA) (50% aqueous solution, Aldrich), and HCl (37%, Aldrich) were used without further purification. Polylactic acid (PLA) films (20 μm in thickness of, BI-AX International Inc.) and polyethylene terephthalate (PET) films (22 μm in thickness, Toray Plastics (America), Inc.) were used as the substrates.

Coating process

Mg2Al-LDH single layer nanosheet were prepared and purified as described in Chapter 6. In this study, LDH single layer nanosheets aqueous dispersion at a concentration of ca. 0.025

g/mL was prepared as a stock solution. PVA stock solution (10.0 wt%) was prepared by dissolving PVA resin in D.I. water under heat treatment.

The PVA/LDH nanocoating dispersion was prepared by mixing PVA solution and LDH single layer aqueous dispersion to reach a concentration of 3.0 wt% LDH, 3.0 wt% PVA, and 94.0 wt% water. In a typical coating process, approximately 50 g of nanocoating dispersion is needed to coat polymer films. The nanocoating dispersion was fully mixed after one hour of magnetic stirring and one hour of ultrasonication treatment (Branson 8510R-MT, 250 W, 44 kHz).

Crosslinking agent GA solution was prepared and HCl was added in a molar ratio of 5/1 (GA/HCl) as the catalyst for the crosslinking reaction. The molar ratio of GA and PVA hydroxyl groups was set at 1:20, which is equivalent to a mass ratio of 1:5 for GA and PVA. The GA solution was cooled down to 0 ℃ before being added to the nanocoating dispersion in an ice bath.

Immediately before the coating process, the GA solution was added into the nanocoating dispersion, followed by stirring and ultrasonication for 5 minutes each in an ice bath. The substrate (ca. 9 cm × 13 cm) was immersed into the nanocoating dispersion and then being vertically hung in an oven at 60 ℃ for 30 minutes to dry and crosslink. The coating process was repeated four times for each substrate.

Characterization

X-ray diffraction (Bruker D8 Advance with Cu Kα radiation, λ = 1.5406 Å, 40 kV, 40 mA) was conducted on the coated films. TEM images of the cross-section of the coated films were recorded on an FEI Tecnai T12 microscope. The film samples were first embedded into

epoxy and then microtomed into thin slices with a thickness of 80-100 nm on a Reichert-Jung Ultracut E. ultramicrotome.

Oxygen transmission rates (OTRs) were measured on a MOCON (Minneapolis, MN) OX-TRAN 1/50 OTR tester (ASTM D-3985) at 23 ℃ and 0% relative humidity (RH). Water vapor transmission rates (WVTRs) were tested on a MOCON PERMATRAN-W 1/50 WVTR tester (ASTM F-1249) at 23 ℃ and 50% RH.

6.3 Results and discussion

Lowering gas permeability in composite containing well aligned inorganic nanosheets is simply because of the formation of tortuous pathway,[18, 24-25] as shown in Figure 45. We assume polymers are permeable but inorganic LDH nanosheets are not permeable, gas molecules are forced to circle around such inorganic nanosheets to diffuse through the film, which results in a much longer pathway. Thus, a high concentration of well aligned LDH nanosheets is the key to achieve an enhanced barrier property.

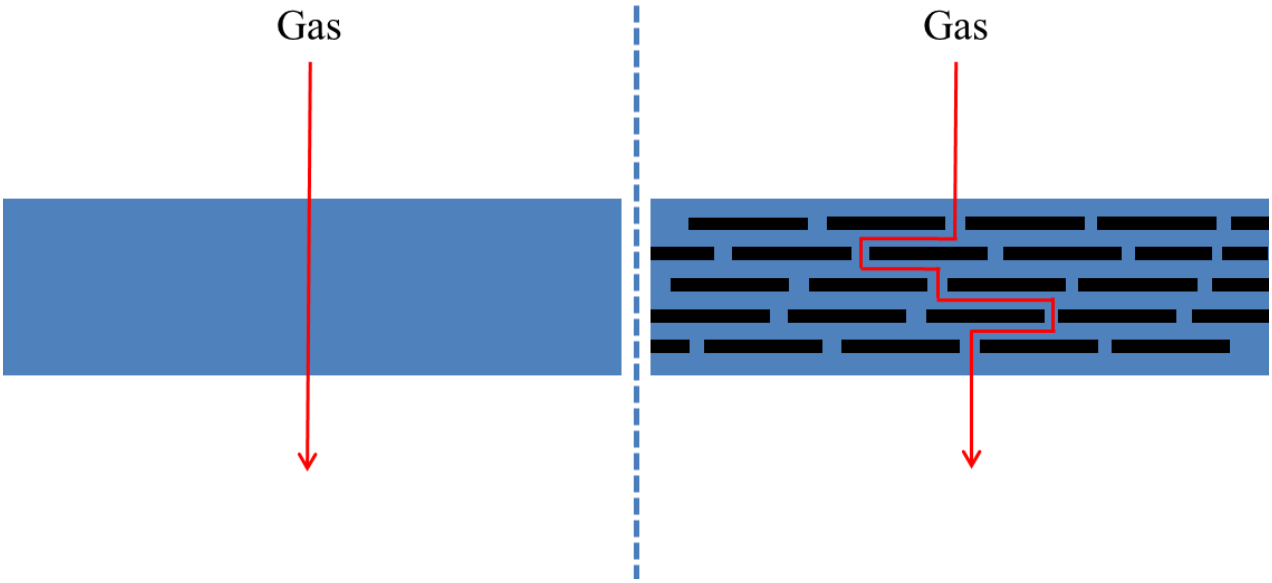

Figure 45. Comparison of gas molecule passing through a neat polymer film (left) and a polymer film containing a high concentration of well aligned impermeable inorganic nanosheets.

During the coating process, the gravity drives the coating dispersion to flow on the polymer substrates when the dipped film was vertically hung. The liquid flow generates stress, which in turn helps to align LDH nanosheets along the polymer substrate surface. The XRD pattern of the coated PET film (Figure 46) and PLA film (Figure 47) showed an obvious diffraction peak at 2.85 ° and 2.80 °, (corresponding to an interlayer distance of 31.1 and 31.5 Å), respectively. Such intensive first order diffraction peaks, together with the presence of a second order diffraction peak, indicated that the LDH single layer nanosheets were well aligned on the substrates. In addition, the very low interlayer distance suggested that the nanosheets were closely packed. Both the high level orientation and dense packing are very beneficial for achieving excellent barrier properties. The two strong diffraction peaks at 26.00 ° and 16.50 ° are from the semi-crystalline structure of PET and PLA, respectively.

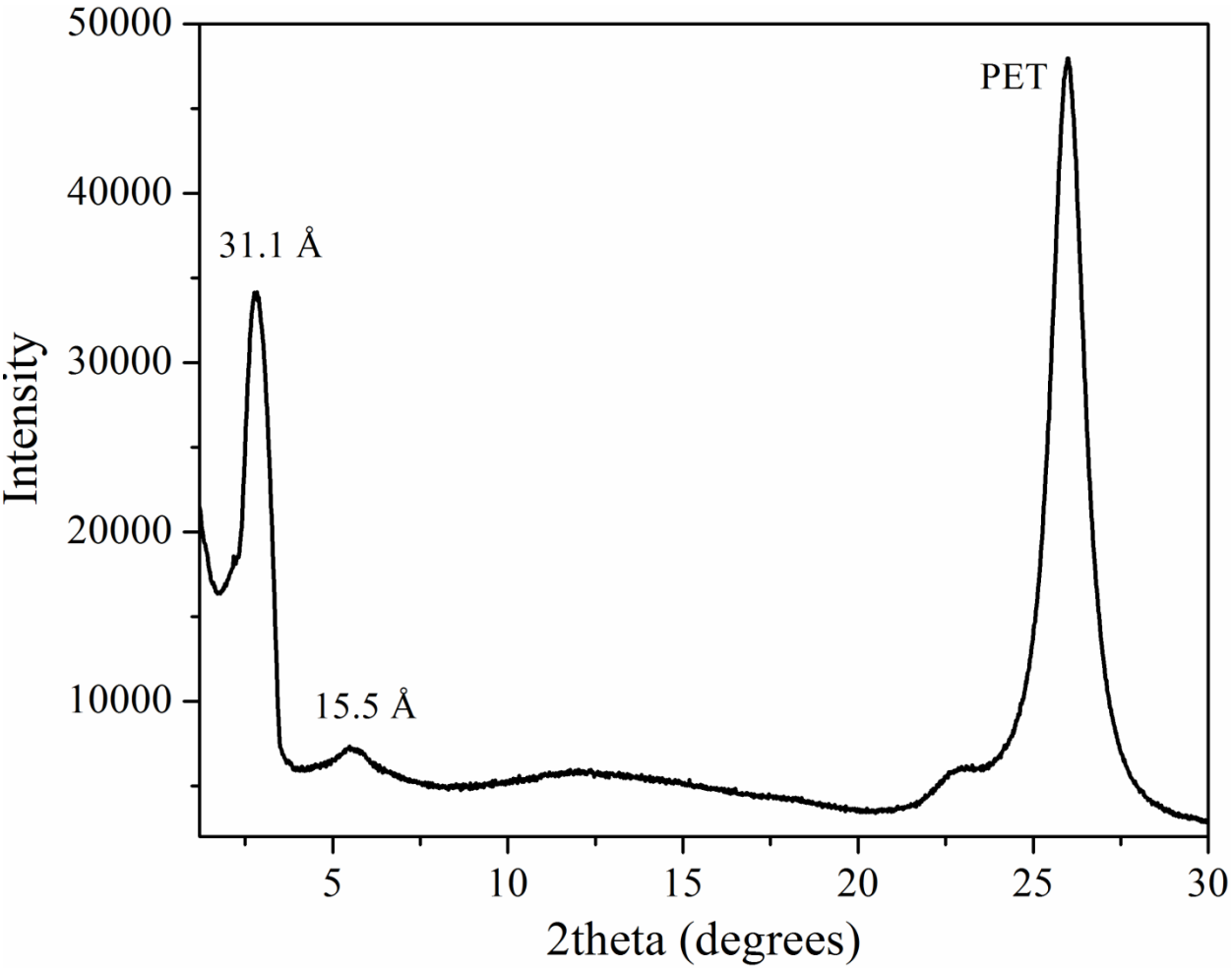

Figure 46. XRD pattern of the coated PET film.

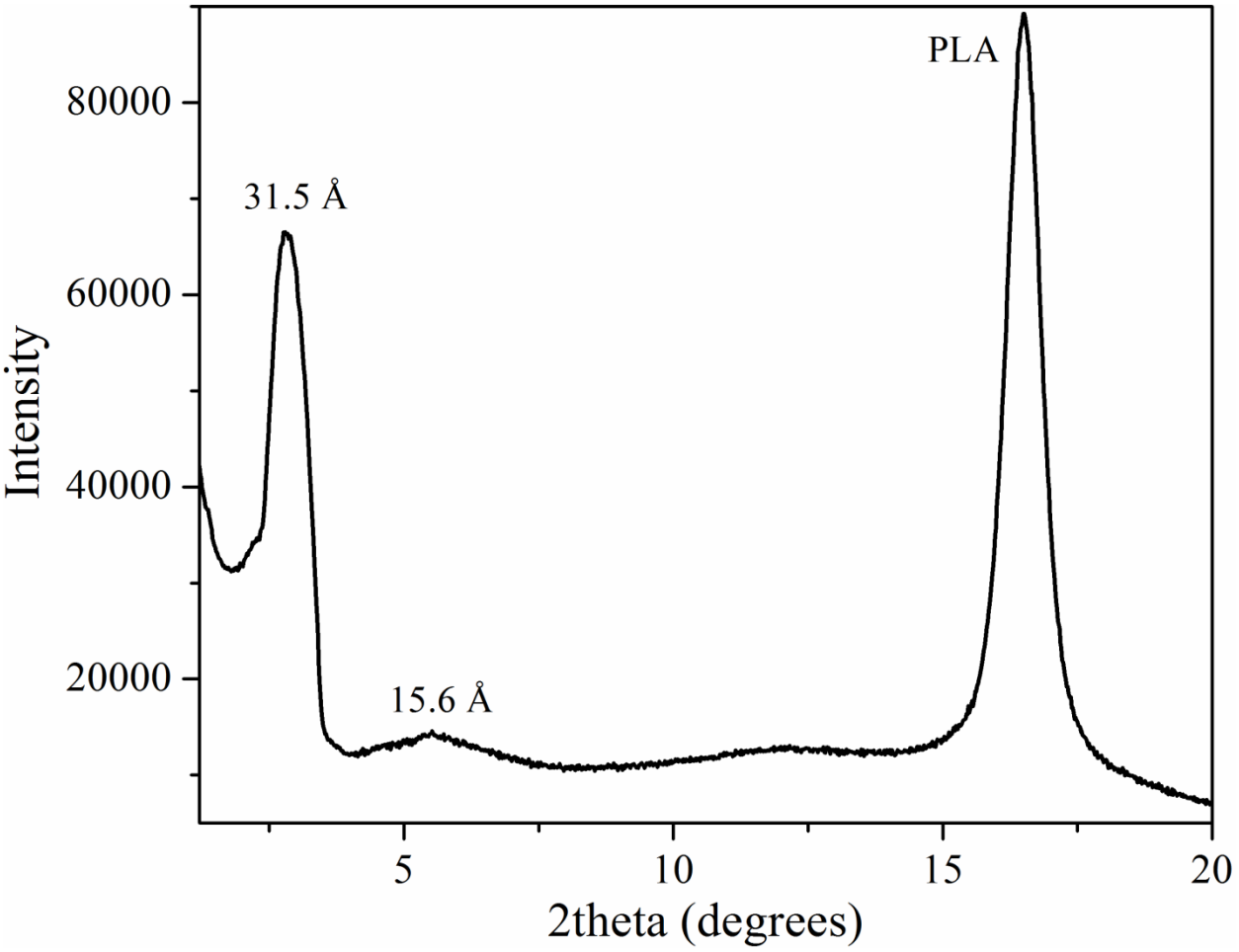

Figure 47. XRD pattern of the coated PLA film.

TEM images were obtained to assess the alignment of LDH single layer nanosheets in the nanocoatings. As shown in Figure 48A and B, LDH single layer nanosheets were well aligned on the substrate. The nanocoating was ca. 80-100 nm in thickness. Overall, the TEM observation was consistent with the XRD results, both of which suggested an ordered alignment of LDH single layer nanosheets on the polymer substrates.

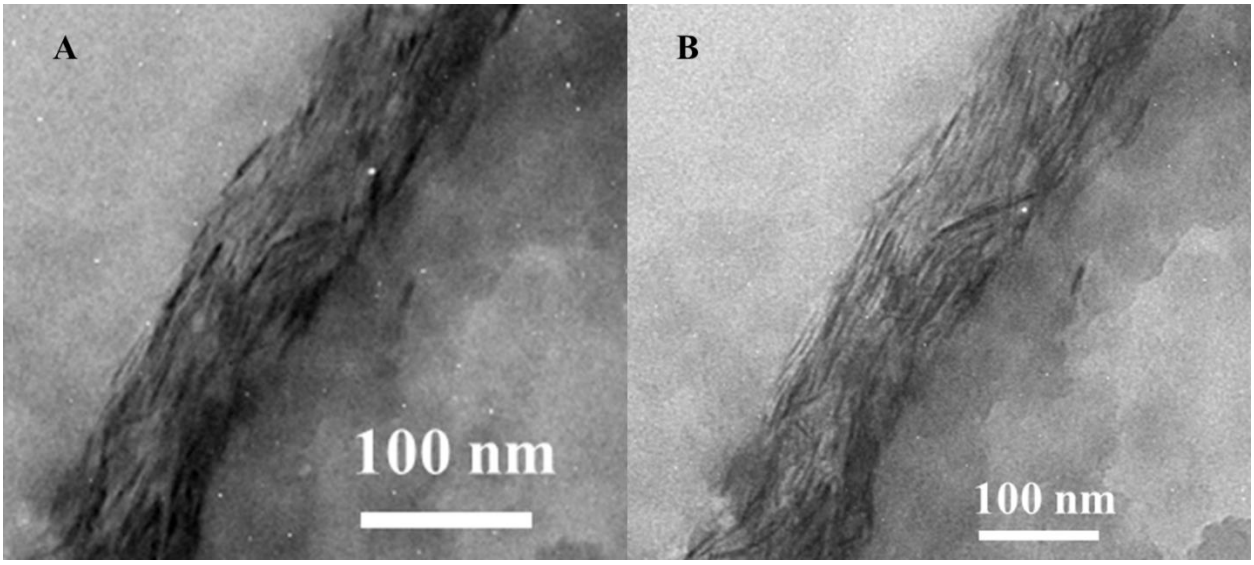

Figure 48. TEM images of the nanocoating on PET film.

The coated PET and PLA films were tested at 1 atm for oxygen and water vapor permeability. The testing results are summarized in Table 3. The OTR of neat PET film was 64.1 cc/(m^2 day), which dropped significantly to 5.3 mL/(m^2 day) after the PET film was coated with a thin layer of nanocoating. Similarly, the OTR of the coated PLA film was 3.3 mL/(m^2 day), which decreased from 846.6 mL/(m^2 day) of the uncoated PLA film. The oxygen barrier property of the PET and PLA was improved by ca. 11 and 256 times, respectively, after coated by LDH/PVA nanocoating. At the same time, the WVTR of the coated PET was decreased to 2.6 g/(m^2 day) from 4.1 g/(m^2 day) of the uncoated PET film. The WVTR of the coated PLA was decreased to 22.1 g/(m^2 day) from 210.0 g/(m^2 day) of the uncoated PLA film. The water vapor barrier property was increased by ca. 1.5 and 10 times for PET and PLA films, respectively. PVA is very hydrophilic, which might be one of the key reasons that the water vapor barrier performance improvement was not as impressive as the oxygen barrier.

Table 3. Barrier properties of the coated PET and PLA films.

	OTR ($mL/(m^2\ day)$)	WVTR ($g/(m^2\ day)$)
PET	64.1	4.1
Coated PET	5.3	2.6
PLA	846.6	210.0
Coated PLA	3.3	22.1

6.4 Conclusion

In this chapter, we reported the application of Mg2Al-LDH single layer nanosheets synthesized in Chapter 4 to prepare LDH/PVA hybrid nanocoatings. Two substrates, PET and PLA films were coated by the LDH/PVA nanocoatings, and their barrier properties (especially the oxygen barrier) were significantly improved.

The enhanced barrier properties are ascribed to the formation of a well aligned and closely packed inorganic LDH nanosheets induced by the liquid flow driven by the gravity during the coating process. Both the XRD and TEM characterizations results supported such morphology.

References

1. Huang, S.; Phua, S. L.; Liu, W.; Ding, G.; Lu, X., Nacre-like composite films based on mussel-inspired 'glue' and nanoclay. *RSC Advances* **2014,** *4* (3), 1425-1431.

2. Currey, J. D., *Mechanical Properties of Mother of Pearl in Tension*. 1977; Vol. 196, p 443-463.

3. Ebina, T.; Mizukami, F., Flexible Transparent Clay Films with Heat-Resistant and High Gas-Barrier Properties. *Advanced Materials* **2007,** *19* (18), 2450-2453.

4. Liu, A.; Berglund, L. A., Clay nanopaper composites of nacre-like structure based on montmorrilonite and cellulose nanofibers—improvements due to chitosan addition. *Carbohydrate Polymers* **2012,** *87* (1), 53-60.

5. Cook, R.; Chen, Y.; Beall, G. W., Highly Ordered Self-Assembling Polymer/Clay Nanocomposite Barrier Film. *ACS Applied Materials & Interfaces* **2015,** *7* (20), 10915-10919.

6. Inagaki, N.; Tasaka, S.; Hiramatsu, H., Preparation of oxygen gas barrier poly(ethylene terephthalate) films by deposition of silicon oxide films plasma-polymerized from a mixture of tetramethoxysilane and oxygen. *Journal of Applied Polymer Science* **1999,** *71* (12), 2091-2100.

7. Triantafyllidis, K. S.; LeBaron, P. C.; Park, I.; Pinnavaia, T. J., Epoxy−Clay Fabric Film Composites with Unprecedented Oxygen-Barrier Properties. *Chemistry of Materials* **2006,** *18* (18), 4393-4398.

8. Priolo, M. A.; Gamboa, D.; Holder, K. M.; Grunlan, J. C., Super Gas Barrier of Transparent Polymer−Clay Multilayer Ultrathin Films. *Nano Letters* **2010,** *10* (12), 4970-4974.

9. Möller, M. W.; Kunz, D. A.; Lunkenbein, T.; Sommer, S.; Nennemann, A.; Breu, J., UV-Cured, Flexible, and Transparent Nanocomposite Coating with Remarkable Oxygen Barrier. *Advanced Materials* **2012,** *24* (16), 2142-2147.

10. Wu, C.-N.; Saito, T.; Fujisawa, S.; Fukuzumi, H.; Isogai, A., Ultrastrong and high gas-barrier nanocellulose/clay-layered composites. *Biomacromolecules* **2012,** *13* (6), 1927-1932.

11. Li, P.; White, K. L.; Lin, C.-H.; Kim, D.; Muliana, A.; Krishnamoorti, R.; Nishimura, R.; Sue, H.-J., Mechanical Reinforcement of Epoxy with Self-Assembled Synthetic Clay in Smectic Order. *ACS Applied Materials & Interfaces* **2014,** *6* (13), 10188-10195.

12. Bodaghi, H.; Mostofi, Y.; Oromiehie, A.; Ghanbarzadeh, B.; Hagh, Z. G., Synthesis of clay–TiO2 nanocomposite thin films with barrier and photocatalytic properties for food packaging application. *Journal of Applied Polymer Science* **2015,** *132* (14), n/a-n/a.

13. Walther, A.; Bjurhager, I.; Malho, J.-M.; Ruokolainen, J.; Berglund, L.; Ikkala, O., Supramolecular Control of Stiffness and Strength in Lightweight High-Performance Nacre-Mimetic Paper with Fire-Shielding Properties. *Angewandte Chemie International Edition* **2010,** *49* (36), 6448-6453.

14. Kovacs, J. R.; Liu, C.; Hammond, P. T., Spray Layer-by-Layer Assembled Clay Composite Thin Films as Selective Layers in Reverse Osmosis Membranes. *ACS Applied Materials & Interfaces* **2015,** *7* (24), 13375-13383.

15. Dou, Y.; Xu, S.; Liu, X.; Han, J.; Yan, H.; Wei, M.; Evans, D. G.; Duan, X., Transparent, Flexible Films Based on Layered Double Hydroxide/Cellulose Acetate with Excellent Oxygen Barrier Property. *Advanced Functional Materials* **2014,** *24* (4), 514-521.

16. Priolo, M. A.; Gamboa, D.; Grunlan, J. C., Transparent clay− polymer nano brick wall assemblies with tailorable oxygen barrier. *ACS Applied Materials & Interfaces* **2009,** *2* (1), 312-320.

17. Bai, H.; Huang, C.; Xiu, H.; Zhang, Q.; Deng, H.; Wang, K.; Chen, F.; Fu, Q., Significantly improving oxygen barrier properties of polylactide via constructing parallel-aligned shish-kebab-like crystals with well-interlocked boundaries. *Biomacromolecules* **2014,** *15* (4), 1507-1514.

18. Osman, M. A.; Mittal, V.; Morbidelli, M.; Suter, U. W., Polyurethane adhesive nanocomposites as gas permeation barrier. Macromolecules **2003,** *36* (26), 9851-9858.

19. Decher, G.; Schlenoff, J. B., Multilayer Thin Films: Sequential Assembly of Nanocomposite Materials. *Wiley-VCH Verlag GmbH & Co.* **2012,** *Weinheim, Germany*.

20. Kovtyukhova, N. I.; Ollivier, P. J.; Martin, B. R.; Mallouk, T. E.; Chizhik, S. A.; Buzaneva, E. V.; Gorchinskiy, A. D., Layer-by-layer assembly of ultrathin composite films from micron-sized graphite oxide sheets and polycations. *Chemistry of Materials* **1999,** *11* (3), 771-778.

21. Lvov, Y.; Ariga, K.; Ichinose, I.; Kunitake, T., Assembly of multicomponent protein films by means of electrostatic layer-by-layer adsorption. *Journal of the American Chemical Society* **1995,** *117* (22), 6117-6123.

22. Sukhorukov, G. B.; Donath, E.; Lichtenfeld, H.; Knippel, E.; Knippel, M.; Budde, A.; Möhwald, H., Layer-by-layer self assembly of polyelectrolytes on colloidal particles. *Colloids and Surfaces A: Physicochemical and Engineering Aspects* **1998,** *137* (1), 253-266.

23. Jang, W.-S.; Rawson, I.; Grunlan, J. C., Layer-by-layer assembly of thin film oxygen barrier. *Thin Solid Films* **2008,** *516* (15), 4819-4825.

24. Choudalakis, G.; Gotsis, A., Permeability of polymer/clay nanocomposites: a review. *European Polymer Journal* **2009,** *45* (4), 967-984.

25. Yang, Y. H.; Bolling, L.; Priolo, M. A.; Grunlan, J. C., Super Gas Barrier and Selectivity of Graphene Oxide-Polymer Multilayer Thin Films. *Advanced Materials* **2013,** *25* (4), 503-508.

CHAPTER 7

ONE STEP DIRECT SYNTHESIS OF α-ZIRCONIUM PHOSPHATE/IONIC LIQUID INTERCALATION COMPOUNDS AS HETEROGENEOUS CATALYSTS FOR THE BIGINELLI REACTIONS

7.1 Introduction

In this chapter, α-Zirconium phosphate (α-ZrP)/ionic liquid (IL) intercalation compounds were synthesized by the method reported in Chapter 2, with an aim to immobilize ionic liquids in α-ZrP as heterogeneous catalysts for various reactions. 1-Butyl-3-methylimidazolium chloride (BMIMCl) is chosen as the representative IL because of its high catalytic activity for various reactions.[1] As proposed in Chapter 2, BMIMCl functions as the layer growth coordinator to guide the growth of α-ZrP, during which BMIMCl was sandwiched in between the layers to form α-ZrP/BMIMCl intercalation compounds, which were subsequently evaluated for the Biginelli reactions.[2-4]

Immobilization of ionic liquids (ILs) on a solid support[5] by covalent bonding or non-covalent interactions can be achieved to improve their catalytic activities. Another alternative to provide recyclability is to intercalate ILs into the interlayer region of a layered material. Graphite,[6] layered metal dichalcogenides,[7] and clays[8-9] have been evaluated as the layered matrix. Studies on using α-ZrP as an inorganic matrix have also been reported. Ionic liquids cannot be directly intercalated into zirconium phosphates

because of the size mismatch.[10] Ion exchange with pre-intercalated[10-11] α-ZrP is a general method to introduce ionic liquid into α-ZrP interlayer region. Attempt of mechanical intercalation of ionic liquid into α-ZrP gallery developed in our group[12-13] is an efficient alternative. However, the one-step direct synthesis method described earlier is obviously more desirable in terms of efficiency.

Recently, BMIMCl has been found active to catalyze the Biginelli reactions in solvent-less condition with high yield and high efficiency.[2-4, 14] The Biginelli reaction[15] is the condensation of three components including an aldehyde, a β-ketoester and urea (or thiourea) to synthesis dihydropyrimidones catalyzes by acidic materials. It is first discovered in 1893[16] by a Italian chemist. Since its discovery, a lot of attention was drawn to improve the yield because of its prominent potentials in preparing pharmacological active materials including calcium channel blockers, anti-hypertensive agents, and α-1a-antagonists.[17-19] The reaction is traditionally conducted in ethanol or THF solvent and catalyzed by strong protic acids.[20] However, the traditional method is suffered from low yield, high reaction temperature and time, and toxic byproducts. Recently, various efforts, such as conducting the reaction under microwave heating in different solvent[21] (alcohol, glycol, and poly phosphate esters) or in solvent-less condition; apply homogeneous or heterogeneous catalysts to modify the reaction have been reported. Solid catalysts such as clay,[22] zeolite,[23] ion exchange resin, and lanthanide triflate[24] have been evaluated. However, it is difficult to reach a protocol where the catalyst can be recycled, recycling yield stays high and the product can be obtained with low toxicity. Thus, it is required that a method to be developed to achieve the ultimate goal.

Thus, we prepared α-ZrP/BMIMCl intercalation compounds through the one-step direct synthesis method. Their catalytic activity and recyclability were evaluated by the Biginelli reaction between benzaldehyde, urea and ethyl acetoacetate as a probe reaction. X-ray diffraction and TGA were performed to characterize the prepared intercalation compounds. DSC was performed to measure the melting point of the isolated product. NMR and IR were performed to identify the product.

7.2 Experimental

Chemicals

$ZrOCl_2 \cdot 8H_2O$ (98%, Sigma-Aldrich), phosphoric acid (85%, Sigma-Aldrich), and 1-butyl-3-methylimidazolium chloride (BMIMCl) (>98.0%, Sigma-Aldrich), ethanol (99.99%, Pharmco-AAPER), ethyl acetoacetate (98%, Sigma-Aldrich), benzaldehyde (≥99.5%, Sigma-Aldrich), and urea (99.0-100.5%, J.T. Baker) were used as received without further purification. Potassium bromide (99+%, FTIR grade, Sigma-Aldrich) was used to prepare pallet for FT-IR.

Synthesis of α-ZrP/BMIMCl intercalation compounds

α-ZrP/BMIMCl intercalation compounds were prepared through a hydrothermal reaction. A predetermined amount of $ZrOCl_2$ aqueous solution (20 wt%) was first mixed with BMIMCl. Then, a predetermined amount of concentrated H_3PO_4 aqueous solution was added into the mixture to achieve a molar ratio of $ZrOCl_2$ to H_3PO_4 at 1:10. Deionized water was then added into the reaction mixture to dilute the concentration of H_3PO_4 to reach 5.0 M. The reaction mixture was fully mixed before subject to a treatment

at 90 °C for 24 h. The mass ratio of α-ZrP (assuming all the Zr^{4+} cations were completely converted to α-ZrP) to BMIMCl was varied from 1/0.5 to 1/4.0 to study the intercalation process. After reaction, the products were centrifuged and washed with deionized water and ethanol for three times. Then the products were dried at 70 ℃ for 24 h and were grinded into fine powders for various characterizations. The control α-ZrP sample was prepared under the same condition without the addition of BMIMCl.

Catalyst evaluation and recycling

The Biginelli reaction of benzaldehyde, urea, and ethyl acetoacetate was chosen to evaluate the catalytic activity of α-ZrP/BMIMCl intercalation compounds (Scheme 1). Typically, a mixture of 5 mmol of benzaldehyde, 7.5 mmol of ethyl acetoacetate, 7.5 mmol of urea, and 250 mg of α-ZrP/BMIMCl intercalation compound were charged into a 25 mL round bottomed flask equipped with a magnetic stirrer. Before reaction, the reactants were treated with ultra-sonification for 5 minutes to disperse the catalyst. Reaction temperature was set at 130 ℃ and the duration was 4 h. A condensation system was attached to the reaction flask to prevent the reactant from evaporation. After the reaction, the crude product was first washed with 30 mL icy water and then filtered. After that, the filtered solid was partially dissolved in 150 ml ethanol at a heated temperature for 15 minutes. The separated catalyst was then dried in an oven overnight at 70 ℃ for the next catalytic run. Overall, the catalyst can be easily separated and recycled from the products. The product was obtained by further recrystallization of the primary product from ethanol. Rotary evaporator was used to evaporate and recycle ethanol. Ethyl acetoacetate and urea were in excess to promote the conversion of benzaldehyde.

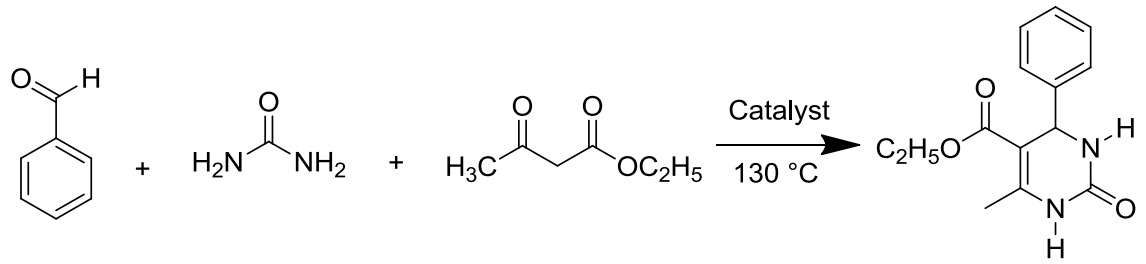

Scheme 1. The Biginelli reaction.

Characterization

The samples were characterized by X-ray diffraction (Brucker D5 with Cu Kα radiation, λ = 1.5406 Å, 40 kV, 40 mA), thermal gravimetric analysis (TGA) (TA Instruments Q-500), differential scanning calorimetry (DSC) (TA Instruments Q-100), nuclear magnetic resonance (NMR) spectroscopy (Bruker DMX 500 MHz), and Fourier transform infrared spectroscopy (FT-IR) (Nicolet Magna 560).

7.3 Results and Discussion

The α-ZrP/BMIMCl intercalation compounds were characterized by X-ray diffraction and the results are presented in Figure 49. The interlayer distance of the control α-ZrP prepared without BMIMCl is 7.6 Å, agreeing well with the literature data.[25] When BMIMCl was added into the reaction mixture, the interlayer distance of the formed intercalation compounds expanded to ca. 10.8 Å, regardless of the amount added (Figure 50). All the samples showed a ca. 3.2 Å interlayer space increase compared to the control α-ZrP, which indicated that the intercalation process was successful. This observation is highly consistent with the proposed mechanism as described in Chapter 2 that the layer growth coordinators tend to position themselves parallel to α-ZrP layers. It is reported

that the thickness of $BMIM^+$ is ca. 2.9 Å.[13] Thus, the increase of the interlayer distance can be counted on a single layer of $BMIM^+$ parallel to the α-ZrP layers. When the amount of BMIMCl was increased in the formulated mixture (from α-ZrP/BMIMCl=1/0.5 to 1/2.0), the diffraction peak of the α-ZrP/BMIMCl intercalation compounds turned to be more and more intense, while the diffraction peak of α-ZrP almost disappeared. The degree of intercalation reached the maximum at α-ZrP/BMIMCl=1/2.0. Further increasing the ratio between BMIMCl and α-ZrP (from 1/2.0 to 1/4.0) did not change lead to a more favorable intercalation. The result is very similar to that of α-ZrP/PEG intercalation compounds reported in Chapter 2.

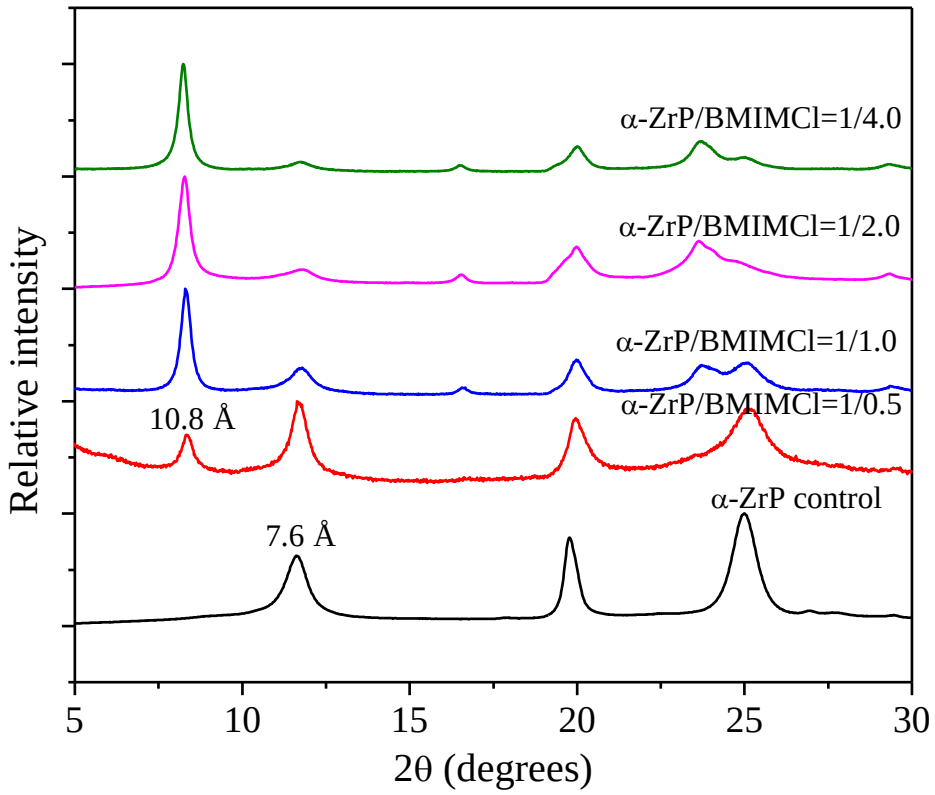

Figure 49. XRD characterization of α-ZrP/BMIMCl intercalation compounds.

Thermal analysis (Figure 50) was performed to investigate the thermal stability and BMIMCl content of the prepared intercalation compounds. All the samples were first isothermally heated at 90 ℃ for 30 min to remove the physically absorbed water prior to the thermal analysis at a heating rate of 10 °C/min. The control α-ZrP and BMIMCl were also analyzed by TGA for comparison. The control α-ZrP sample showed two major weight loses at 100-180 ℃ and 380-560 ℃, corresponding to hydration water and condensation water loss, respectively.[12-13] BMIMCl experienced a virtually 100% weight loss in the range of 180-360 ℃.

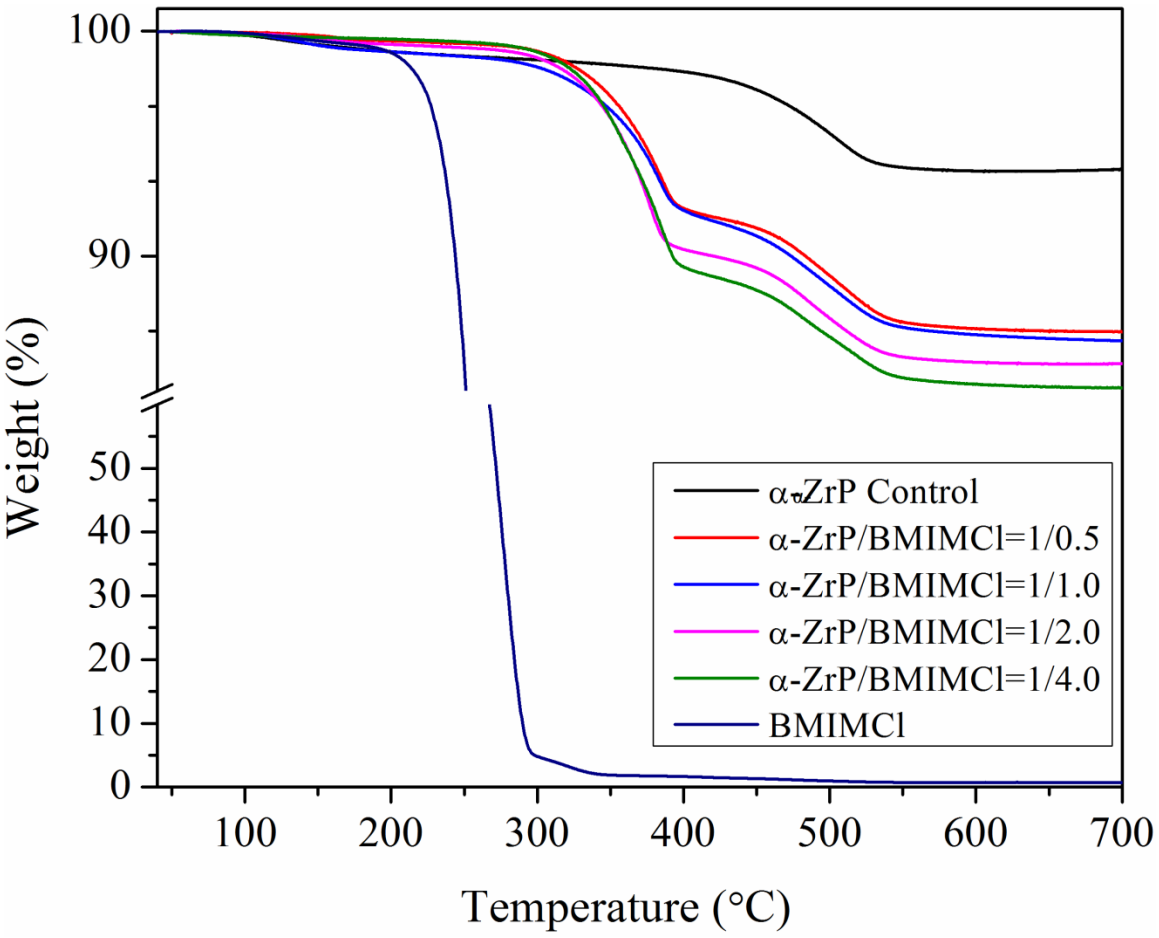

Figure 50. TGA analysis of α-ZrP/BMIMCl intercalation compounds.

The α-ZrP/BMIMCl intercalation compounds exhibited three major weight losses. The first one was at ca. 100-180 ℃, which corresponded to the loss of hydration water in α-ZrP. The second weight loss at ca. 310-390 °C was due to the loss of BMIMCl in the α-ZrP/BMIMCl intercalation compounds. As shown in Figure 50, BMIMCl completely decomposes at ca. 180-360 °C. After being intercalated into α-ZrP, the decomposition temperature of BMIMCl is shifted to ca. 270-410 ℃, which is due to the protection of the inorganic layers. The third weight loss at ca. 420-530 ℃ is from the loss of condensation water in α-ZrP. Based on the second weight loss at ca. 310-390 °C of the α-ZrP/BMIMCl intercalation compounds α-ZrP/BMIMCl at 1/0.5, 1/1.0, 1/2.0, and 1/4.0, the BMIMCl contents were estimated to be ca. 7.0%, 7.5%, 9.4%, and 10.6% respectively.

As described above, the Biginelli reaction was selected to evaluate the catalytic activity of the α-ZrP/BMIMCl intercalation compounds. Various ionic liquids, including $BMIMBF_4$,[2] BMIMCl,[1] 1,1,3,3-tetrmethylguanidinium trifluoroacetate,[3] BMIMBr,[26] and $BMIMClO_4$[3] have been found to be effective to catalyze the Biginelli reactions under a solvent-free condition. However, it is very difficult to recycle the ionic liquids when they are homogeneously mixed with the reaction system. Other recyclable solid acid catalysts often result in longer reaction time and a lower yield.[22, 27]

Considering the Biginelli reaction has been well investigated, only some basic characterizations were conducted to verify the product. At each catalytic run, the melting point of the product 5-ethoxycarbonyl-4-phenyl-6-methyl-3, 4-dihydropyridin-2(1H)-one was measured by DSC at a heating rate of 2 ℃/min. The result (Figure 51) showed a melting point range of 203-206 ℃, where the literature data are 202-204 ℃.[28]

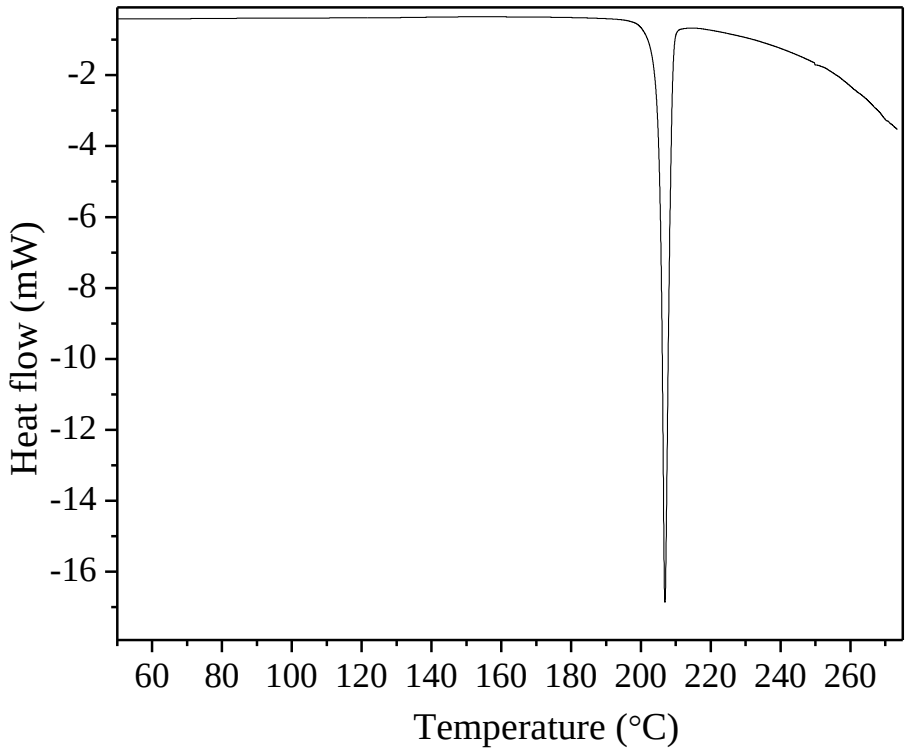

Figure 51. DSC of the Biginelli reaction product of the first run.

Nuclear magnetic resonance (NMR) was performed to characterize the product, where DMSO-d_6 was used as solvent. The result for the product 5-ethoxycarbonyl-4-phenyl-6-methyl-3, 4-dihydropyridin-2(1H)-one is shown below. ^{1}H NMR (Figure 52): δ =9.17 (s, 1H, NH); 7.72 (s, 1H, NH); 7.35-7.20 (m, 5H, C_6H_5); 5.14 (s, 1H, CH); 4.0 (q, 2H, OCH_2CH_3); 2.24 (s, 3H, CH_3); 1.11 (t, 3H, OCH_2CH_3).

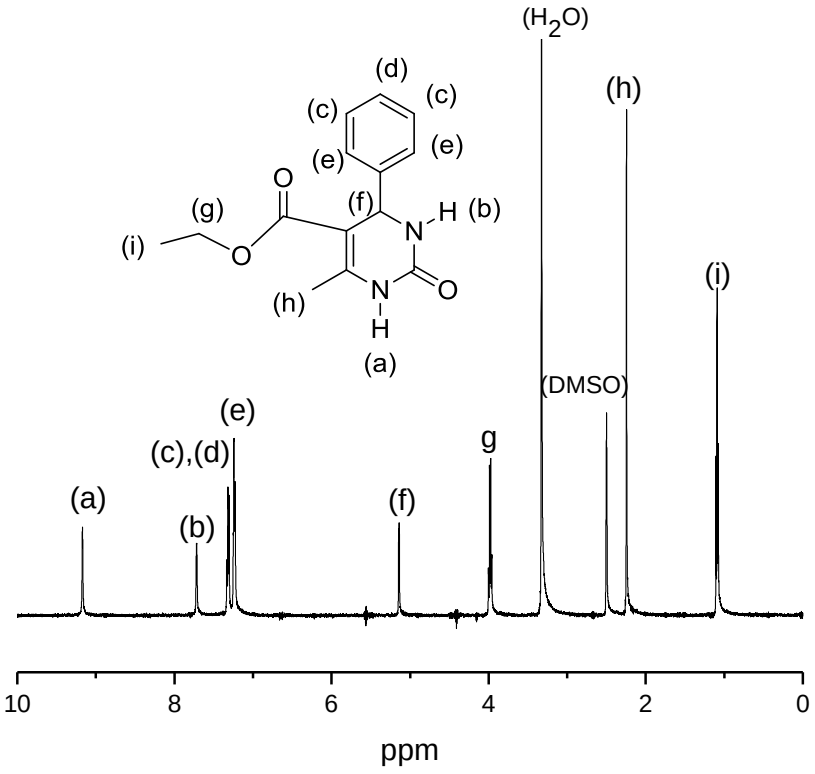

Figure 52. ^{1}H-NMR of the product in DMSO-d_6.

FT-IR was also performed to further characterize the product. The sample was compressed with KBr into a pallet. Figure 53 shows the result: v_{max}= 3436, 3247, 3118, 2956, 1726, 1702, 1648, 1463, 1222, 1093, 778 cm^{-1}.

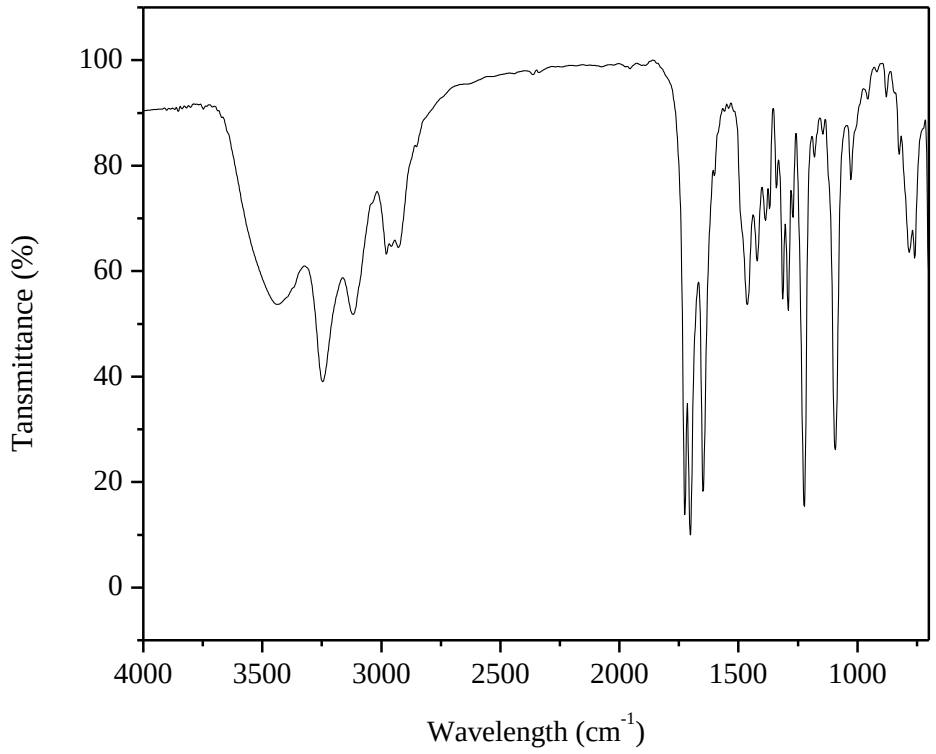

Figure 53. Typical FT-IR of the Biginelli reaction product.

In this study, BMIMCl was immobilized within α-ZrP as a heterogeneous catalyst for the Biginelli reaction. At the first catalytic run, the yield reached 97%. After reach cycle of reaction, the catalyst α-ZrP/BMIMCl intercalation compound was separated by centrifugation and collected for the next run. After 5 cycles of reaction, the yield was still above 93% (Figure 54). The lowered yield was probably because of the marginal catalyst loss during every cycle of separation.

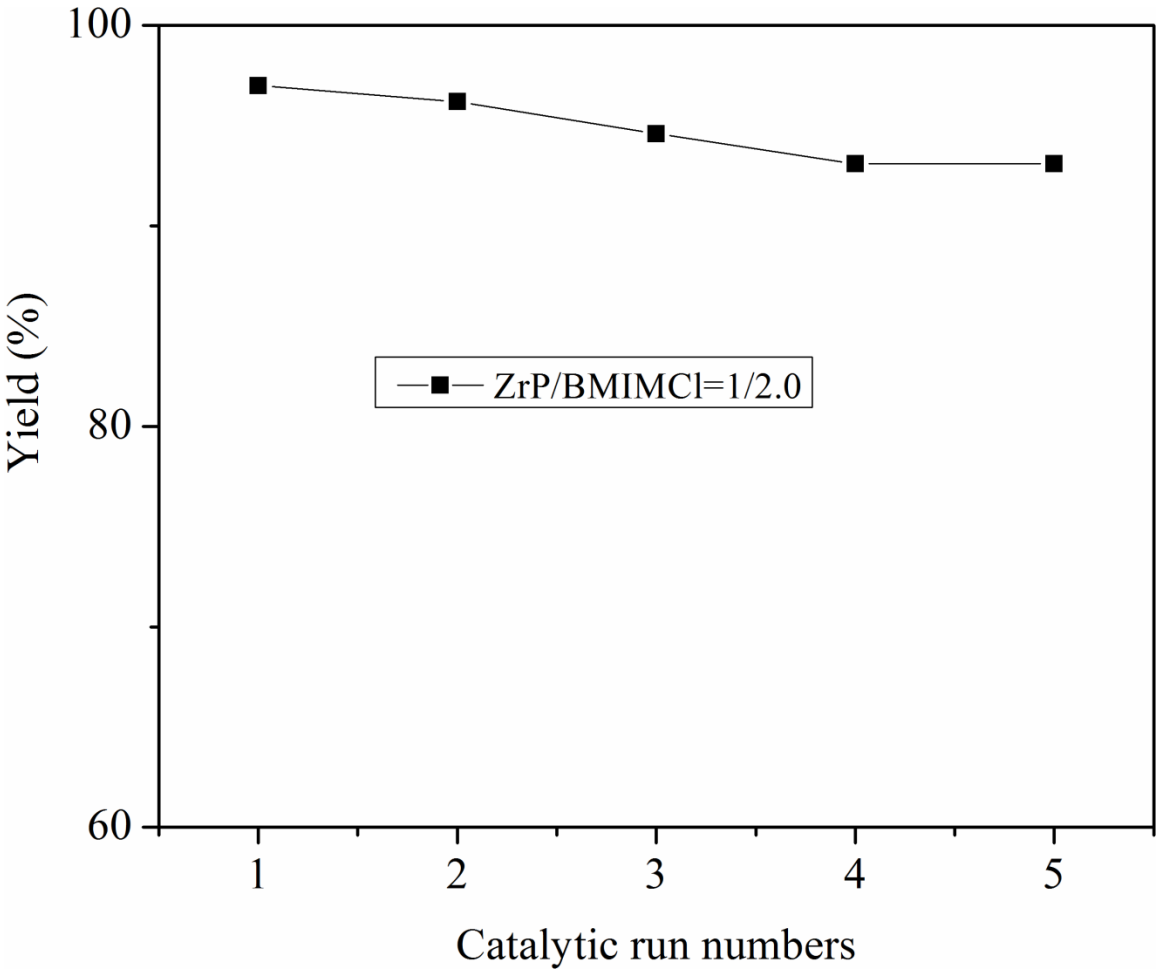

Figure 54. Yield of the product at each recycle run.

7.4 Conclusions

BMIMCl/α-ZrP intercalation compounds were prepared through the one-step direct synthesis method. The intercalation compound was tested as the heterogeneous catalyst for the Biginelli reactions due to the recent report of the high catalytic activities of ionic liquid towards the reactions. Results showed that even after 4 times of recycle, the yield of the product maintained at 93%.

References

1. Zhang, Q.; Zhang, S.; Deng, Y., Recent advances in ionic liquid catalysis. *Green Chemistry* **2011,** *13* (10), 2619-2637.

2. Peng, J.; Deng, Y., Ionic liquids catalyzed Biginelli reaction under solvent-free conditions. *Tetrahedron Letters* **2001,** *42* (34), 5917-5919.

3. Gholap, A. R.; Venkatesan, K.; Daniel, T.; Lahoti, R. J.; Srinivasan, K. V., Ionic liquid promoted novel and efficient one pot synthesis of 3,4-dihydropyrimidin-2-(1H)-ones at ambient temperature under ultrasound irradiation. *Green Chemistry* **2004,** *6* (3), 147-150.

4. Shaabani, A.; Rahmati, A., Ionic liquid promoted efficient synthesis of 3,4-dihydropyrimidin-2-(1H)-ones. *Catalysis Letters* **2005,** *100* (3-4), 177-179.

5. Valkenberg, M. H.; deCastro, C.; Holderich, W. F., Immobilisation of ionic liquids on solid supports. *Green Chemistry* **2002,** *4* (2), 88-93.

6. Placke, T.; Fromm, O.; Lux, S. F.; Bieker, P.; Rothermel, S.; Meyer, H.-W.; Passerini, S.; Winter, M., Reversible Intercalation of Bis(trifluoromethanesulfonyl)imide Anions from an Ionic Liquid Electrolyte into Graphite for High Performance Dual-Ion Cells. *Journal of the Electrochemical Society* **2012,** *159* (11), A1755-A1765.

7. Sutto, T. E.; Duncan, T. T., The intercalation behavior of ionic liquids in the layered metal dichalcogenide TiS2. *Electrochimica Acta* **2012,** *77*, 204-211.

8. Wu, L.; Liao, L.; Lv, G.; Qin, F.; Li, Z., Microstructure and process of intercalation of imidazolium ionic liquids into montmorillonite. *Chemical Engineering Journal* **2014,** *236*, 306-313.

9. Aftafa, C.; Pelit, F. O.; Yalçinkaya, E. E.; Turkmen, H.; Kapdan, İ.; Nil Ertaş, F., Ionic liquid intercalated clay sorbents for micro solid phase extraction of steroid hormones from water samples with analysis by liquid chromatography–tandem mass spectrometry. *Journal of Chromatography A* **2014,** *1361*, 43-52.

10. Wang, H.; Zou, M.; Li, N.; Li, K., Preparation and characterization of ionic liquid intercalation compounds into layered zirconium phosphates. *Journal of Materials Science* **2007,** *42* (18), 7738-7744.

11. Wang, H. Y.; Han, D. X., A new method of immobilizing ionic liquids into layered zirconium phosphates. *Chinese Chemical Letters* **2007,** *18* (6), 764-767.

12. Hu, H.; Martin, J. C.; Zhang, M.; Southworth, C. S.; Xiao, M.; Meng, Y.; Sun, L., Immobilization of ionic liquids in [small theta]-zirconium phosphate for catalyzing the coupling of CO2 and epoxides. *RSC Advances* **2012,** *2* (9), 3810-3815.

13. Hu, H.; Martin, J. C.; Xiao, M.; Southworth, C. S.; Meng, Y.; Sun, L., Immobilization of Ionic Liquids in Layered Compounds via Mechanochemical Intercalation. *The Journal of Physical Chemistry C* **2011,** *115* (13), 5509-5514.

14. Salim, S. D.; Akamanchi, K. G., Sulfated tungstate: An alternative, eco-friendly catalyst for Biginelli reaction. *Catalysis Communications* **2011,** *12* (12), 1153-1156.

15. Wang, Z., Biginelli Reaction. In *Comprehensive Organic Name Reactions and Reagents*, John Wiley & Sons, Inc.: 2010.

16. Biginelli, P. G., Synthesis of 3,4-Dihydropyrimidin-2(1H)-Ones. *Chim. Ital.* **1893,** *23*, 360-416.

17. Atwal, K. S.; Rovnyak, G. C.; Kimball, S. D.; Floyd, D. M.; Moreland, S.; Swanson, B. N.; Gougoutas, J. Z.; Schwartz, J.; Smillie, K. M.; Malley, M. F., Dihydropyrimidine calcium channel blockers. II. 3-Substituted-4-aryl-1,4-dihydro-6-methyl-5-pyrimidinecarboxylic acid esters as potent mimics of dihydropyridines. *Journal of Medicinal Chemistry* **1990,** *33* (9), 2629-2635.

18. Atwal, K. S.; Swanson, B. N.; Unger, S. E.; Floyd, D. M.; Moreland, S.; Hedberg, A.; O'Reilly, B. C., Dihydropyrimidine calcium channel blockers. 3. 3-Carbamoyl-4-aryl-1,2,3,4-tetrahydro-6-methyl-5-pyrimidinecarboxylic acid esters as orally effective antihypertensive agents. *Journal of Medicinal Chemistry* **1991,** *34* (2), 806-811.

19. Kappe, C. O., Biologically active dihydropyrimidones of the Biginelli-type—a literature survey. *European journal of medicinal chemistry* **2000,** *35* (12), 1043-1052.

20. Oliver Kappe, C., 100 years of the biginelli dihydropyrimidine synthesis. *Tetrahedron* **1993,** *49* (32), 6937-6963.

21. Kappe, C. O.; Kumar, D.; Varma, R. S., Microwave-assisted high-speed parallel synthesis of 4-aryl-3, 4-dihydropyrimidin-2 (1H)-ones using a solventless Biginelli condensation protocol. *Synthesis* **1999,** (10), 1799-1803.

22. Bigi, F.; Carloni, S.; Frullanti, B.; Maggi, R.; Sartori, G., A revision of the Biginelli reaction under solid acid catalysis. Solvent-free synthesis of dihydropyrimidines over montmorillonite KSF. *Tetrahedron Letters* **1999,** *40* (17), 3465-3468.

23. Kulkarni, M. G.; Chavhan, S. W.; Shinde, M. P.; Gaikwad, D. D.; Borhade, A. S.; Dhondge, A. P.; Shaikh, Y. B.; Ningdale, V. B.; Desai, M. P.; Birhade, D. R., Zeolite catalyzed solvent-free one-pot synthesis of dihydropyrimidin-2(1H)-ones – A practical synthesis of monastrol. *Beilstein Journal of Organic Chemistry* **2009,** *5*, 4.

24. Ma, Y.; Qian, C.; Wang, L.; Yang, M., Lanthanide Triflate Catalyzed Biginelli Reaction. One-Pot Synthesis of Dihydropyrimidinones under Solvent-Free Conditions. *The Journal of Organic Chemistry* **2000,** *65* (12), 3864-3868.

25. Sun, L.; Boo, W. J.; Sue, H.-J.; Clearfield, A., Preparation of [small alpha]-zirconium phosphate nanoplatelets with wide variations in aspect ratios. *New Journal of Chemistry* **2007,** *31* (1), 39-43.

26. Shi, D.-Q.; Zhou, Y.; Rong, S.-F., Ionic Liquid, [bmim]Br, as an Efficient Promoting Medium for Synthesis of 3-Acetoacetylcoumarin Derivatives Without the Use of Any Catalyst. *Synthetic Communications* **2009,** *39* (19), 3500-3508.

27. Mondal, J.; Sen, T.; Bhaumik, A., Fe3O4@mesoporous SBA-15: a robust and magnetically recoverable catalyst for one-pot synthesis of 3,4-dihydropyrimidin-2(1H)-ones via the Biginelli reaction. *Dalton Transactions* **2012,** *41* (20), 6173-6181.

28. Folkers, K.; Harwood, H. J.; Johnson, T. B., RESEARCHES ON PYRIMIDINES. CXXX. SYNTHESIS OF 2-KETO-1,2,3,4-TETRAHYDROPYRIMIDINES. *Journal of the American Chemical Society* **1932,** *54* (9), 3751-3758.

CHAPTER 8

SUMMARY

8.1 Summary

For decades, researches in layered materials have been focused on two aspects: (1) preparation of layered intercalation compounds and (2) exfoliation of layered materials to obtain single layer nanosheets. Traditional methods to prepare layered intercalation compounds and single layer nanosheets involve the pre-synthesis of layered materials and the subsequent intercalation/exfoliation treatments. In this dissertation, we introduced a new methodology to directly synthesis α-ZrP layered intercalation compounds and LDH single layer nanosheets. A layer growth coordinator was proposed to guide the growth of the layered materials in the Z direction, during which the coordinators were embedded within the layers to form the layered intercalation compounds. Various polymers (PEG, PEI, and PVA), small molecules (acrylamide), and ion ($BMIM^+$) can act as layer growth coordinators to guide the direct synthesis of layered intercalation compounds. Alternatively, when a layer growth inhibitor (such as formamide) was used, the growth of layered compounds in the Z direction can be effectively blocked, leading to the formation of LDH single layer nanosheets.

The direct intercalation method based on another layered material: positively charged LDH was explored. It was found that at a higher PSSNa MW, the intercalation

efficiency was lower, and at a higher PSSNa/LDH mass ratio, the intercalation efficiency is higher. Systematical examination of the layer charge and formamide concentration effect on the direct synthesis of LDH single layer nanosheets was also conducted. It was confirmed that at a higher LDH layer charge and a higher formamide concentration, LDH single layer nanosheets can be favorably synthesized. Based on the above methodology, a further control of layered compound growth for the formation of hexagonal prisms was explored. Assisted by a complexing agent, the layer growth coordination effect of ammonium cation was revived, resulting in the preferential growth of α-ZrP/NH_4^+ intercalation compound in the Z direction to form a prismatic morphology. Potential applications of the above methodology were also explored and demonstrated using two examples. BMIMCl/α-ZrP intercalation compounds prepared through the one-step direct synthesis method served as effective heterogeneous catalyst for Biginelli reactions. LDH single layer nanosheets obtained through the one-step direct synthesis method were applied to prepare transparent nanocoatings on polymer substrates (PET and PLA), leading to significantly improved barrier properties.

8.2 Outlook

Besides adopting different layered materials as the matrix, study of various layer growth coordinators is also very important to further understand the reaction mechanism. PEG derivatives with various end groups (methoxy PEG-COOH and HOOC-PEG-COOH) and with different side groups (polypropylene glycol (PPG), PEG-b-PPG, and PPG-b-PEG-b-PPG block copolymer with a similar number of repeating units) are examples to study the structure effect of layer growth coordinators on the formation of

layered intercalation compounds. Also, it has been a long term goal to grow layered materials with a specific thickness. We achieved the preferential growth of layered materials in the Z direction where the thickness was greatly increased. Since complexing agents can slow down the growth rate of layered materials, it is possible by controlling the amount of layer growth coordinator to tune the thickness of the layered materials.

The efficient one-step direct synthesis method to LDH single layer nanosheets was achieved. It is of practical importance to be able to prepare such nanosheets with a larger lateral dimension. Urea hydrolyzes at elevated temperatures, which allows for a slow release of OH^-. This process ensures a homogeneous pH distribution throughout the reaction, possibly leading to the formation of LDH nanosheets with a relatively large size compared with conventional titration method. Reaction time is another factor that can be controlled to prepare LDH single layer nanosheets with a larger lateral dimension. After the initial reaction, the reaction time can be prolonged by aging the reaction mixture for varied time periods so that nanosheets with various lateral dimensions can possibly be synthesized.

Various other applications of the prepared intercalation compounds can be explored to prepare energy storage devices, supercapacitors, and so on. It is also of great interest to apply the prepared LDH single layer nanosheets to catalyze the oxygen evaluation reactions.